A co-rotational Discrete Macro-Element Method (DMEM) for large displacement analysis of masonry structures

A thesis submitted in fulfilment of the requirements for the degree of Doctor of Philosophy

Domenico D'Urso

Supervisor:
Prof.Ivo Caliò - University of Catania

Co-Supervisors:
Prof. Bassam Izzuddin - Imperial College of London
Prof. Salvatore Caddemi - University of Catania

Coordinator:
Prof. Massimo Cuomo - University of Catania

«Assessment and Mitigation of Urban and Territorial Risks»
XXXII Study Cycle

Department of Civil Engineering and Architecture

University of Catania

Declaration

This submission is my own work. Any quotation from, or description of, the work of others is acknowledged herein by reference to the sources, whether published or unpublished.

Domenico D'Urso
May 2020

Abstract

The simulation of the nonlinear behaviour of masonry structures subjected to earthquake excitations or extreme loadings represents a complex computational issue for which many numerical strategies, characterised by different level of accuracy and efficiency, have been proposed so far. A great effort is made today in the link between the micro- and macro-modelling approaches using homogenization techniques which allow the use of continuum based approaches as the nonlinear FEM simulation and simplified strategies at macro-scale.

Nonlinear FEM modelling approaches require the adoption of sophisticated constitutive laws, huge computational cost as well as advanced skills in the model implementation and in the interpretations of the numerical results. On the other hand, practitioners need simple and efficient numerical tools, whose complexity and computational demand should be appropriate for engineering practise. For these reasons, in the last decades, some research groups proposed alternative efficient numerical methodologies for predicting the nonlinear seismic behaviour of unreinforced masonry (URM) structures. A common limitation of the existing simplified numerical strategies for URM structures, currently used by practitioners, is the basic strong assumption of in-plane behaviour of masonry walls, making these approaches unsuitable for the historical masonry structures whose out-of-plane behaviour strongly influences the nonlinear seismic response. More recently new alternative macro-modelling strategy for the simulation of the nonlinear behaviour of URM structures has been proposed in the context of finite or discrete element strategies.

The original research performed within this thesis is based on a Discrete Macro-Element Method (DMEM) approach recently proposed with the aim of capturing the nonlinear behaviour of an entire structure through an assemblage of discrete macro-elements characterized by different levels of complexity according to the role played in the global model. One of the advantages of the adopted macro-element strategy is related to the strongly reduced computational cost compared to a traditional nonlinear finite element modelling or DEM simulations. Another benefit relies on the adopted mechanical homogenization/calibration strategy that, being based on a straightforward fiber discretization, allows the use of simple uniaxial constitutive laws and leads to an easy interpretation of the numerical results although maintaining efficiency and good accuracy. Based on the above issues, the proposed discrete macro-element method has been applied not only as an efficient and reliable numerical tool for practitioners but also for academic research applications.

This thesis represents a further nontrivial contribution in the context of the DMEM. Namely, a new solid discrete macro-element, able to exhibit large rotations and small deformations, is proposed. The element enriches the DMEM with the introduction of the following significant novelties:

i) The previously introduced macro-elements were formulated under the assumption of linearized kinematics. The solid element here formulated can exhibit large rotations and large displacements assuming kinematics that allows small shear deformations within each element and small deformations at the interfaces between adjacent elements.

ii) The previously proposed spatial elements possess shear deformability only in one plane while the solid element here proposed is characterized by a uniform shear linearized strain tensor.

iii) Differently from the previous spatial discrete macro-elements, the zero-thickness two-dimensional cohesive interfaces, inheriting the masonry properties, are continuously distributed.

The large displacement capabilities are taken into account by considering an original co-rotational strategy, based on local reference systems accounting for the small deformations at the interfaces between adjacent macro-elements. This new solid macro-element will allow the investigation of structures both at macro or meso- scale accounting for geometric and constitutive nonlinearities.

The kinematics is described according to a DMEM strategy that allows to consider the minimum required degrees of freedom with a significant computational advantage with respect to macro-modelling strategies based within a Finite Element context.

The adopted co-rotational formulation is based on a two-node interface element whose degrees of freedom are directly related to the independent degrees of freedom of the corresponding adjacent elements.

The proposed macro-element strategy has been validated considering some benchmarks already investigated in the literature. The results obtained so far seem to demonstrate the capability of the proposed approach to be used, as an efficient numerical strategy, for the nonlinear assessment of masonry structures accounting for constitutive and geometrical nonlinearities.

Table of Contents

List of Tables

List of Figures

Introduction

The numerical simulation of the nonlinear behaviour of masonry structures subjected to earthquake excitations, extreme loadings, or loading distributions that cause failure or instability conditions represents a very complex computational issue that is the subject of many researches. Several nonlinear numerical strategies characterised by different level of accuracy and efficiency and often based on specific purposes have been proposed so far. This research topic is of particular importance for many reasons.

Masonry itself constitutes the most ancient construction material and nowadays represents a large part of existing and new structures and the greater part of historical monumental structures.

With the term ‘masonry’ is intended a composite material obtained by the assemblage of individual units and mortars whose property is different by the property of its components [1]. According to this definition, the word 'masonry' itself refers to a great variability of masonry materials characterised by different constituents, different geometrical layouts and diverse construction techniques. This huge variability makes difficult to define reliable numerical models and general constitutive laws suitable for all the different masonry typologies [2], [3], [4].

Many significant examples of applications of nonlinear finite element simulations to historical masonry buildings and monumental historical structures are reported in the scientific literature. Some of these studies consider the masonry walls as a homogenised continuum at the macro-scale [5], [6], [7], [8], [9], [10], [11], other refined FE approaches are based

on detailed simulations of units and mortar according to a micro-modelling approach [12], [13], [14], [15], [16], [17]. A great effort is made today for realizing a link between the micro- and macro-modelling approaches using homogenization techniques in continuum based approaches generally based on nonlinear FEM simulation and discrete element methods [18]. On the other hand, nonlinear FEM modelling approaches require the adoption of sophisticated three-dimensional constitutive laws, huge computational cost as well as advanced skills in the model implementation and in the interpretations of the numerical results. For these reasons, in the last two decades, many researchers proposed alternative simplified numerical methodologies for predicting the nonlinear seismic behaviour of unreinforced masonry (URM) structures [19], [20], [21], [22], [23] [24] [25], [26]. In [24] the authors report a comparison between different simplified approaches, currently used in engineering practice for the seismic assessment of URM leading to the conclusion that for masonry buildings the analysed simplified methods lead to a satisfactory prediction of the global response. However, a common limitation of these simplified numerical strategies, for URM structures, is the assumption of in-plane behaviour of masonry walls, limiting their applicability to those cases for which the out-of-plane behaviour is prevented. An original alternative approach is represented by the 'rigid-body spring model', and some valuable applications of this strategy to historical masonry buildings are reported in the literature [27], [28], [29].

Among the simplified methods, the equivalent frame modelling approach currently represents the most adopted strategy and has been implemented in many software largely used in engineering practise. Recently, an alternative macro-modelling approach for the simulation of

the nonlinear behaviour of URM structures has been proposed. The approach is based on the concept of macro-element discretization [30] and has been conceived with the aim of capturing the nonlinear behaviour of an entire structure through an assemblage of discrete macro-elements characterized by different levels of complexity according to the role played in the global model. The basic element has been firstly proposed in 2004 [31], [22] specifically developed for the simulation of the in-plane response of masonry walls. The element can be regarded as an articulated quadrilateral interacting with other elements by nonlinear interface along its edges. This discrete macro-element approach received several numerical and experimental validations [24], [30], [32]. This novel approach has been also successfully applied for infilled frame structures [33], [34], [35], [36]. In this latter case, the infills are modelled by the macro-elements, while the reinforced concrete frames are modelled by inelastic beam columns. However, the 2D macro-element has been conceived for the simulation of the non-linear response of masonry walls in their own plane only. To overcome this significant restriction a third dimension and the relevant needed additional degrees of freedom have been introduced in a 3D macro-element [37], [38], [39] allowing an efficient simulation of both the in-plane and the out-of-plane response of masonry walls. However, many masonry monumental constructions are characterized by the presence of structural elements with curved geometry, such as arches, vaults, domes which require an efficient reliable simulation. For this reason, a further enrichment of the proposed 3D macro-element, towards a more general macro-shell-element, has been subsequently introduced [40], [41], [42], [43]. This shell macro-element was conceived as an extension of the spatial element and represented the first proposed macro-element for curved masonry structures. Its nucleus is still

constituted by an irregular articulated quadrilateral whose orientation and size are now related to the shape of the element and to the thickness of the modelled masonry portion. One of the advantages of the proposed DMEM is related to the strongly reduced computational cost if compared to the traditional nonlinear finite element modelling. However, another benefit relies on the adopted simplified mechanical calibration strategy that, being based on a straightforward fiber discretization, allows the use of simple uniaxial constitutive laws and leads to an easy interpretation of the numerical results.

Based on the above issues, the proposed discrete macro-element method has been applied not only as an efficient and reliable numerical tool for practitioners but also for academic research applications.

This thesis represents a further significant contribution to the DMEM. Namely a new solid discrete macro-element able to exhibit large rotations and small deformations is proposed. The element enriches the DMEM with the introduction of the following significant novelties:

i) The previously introduced macro-elements were formulated under the assumption of linearized kinematics. The solid element here formulated can exhibit large rotations and large displacements assuming kinematics that allows small shear deformations within each element and small deformations at the interfaces between adjacent elements.

ii) The previously proposed spatial elements possess shear deformability only in one plane while the solid element here proposed is characterised by a uniform shear linearized strain tensor.

iii) Differently from the previous spatial discrete macro-elements, zero-thickness two-dimensional cohesive interfaces, inheriting the masonry properties, are continuously distributed.

The large displacement capabilities are taken into account by considering an original co-rotational strategy, based on local reference systems accounting for the small deformations at the interfaces between adjacent macro-elements. This new solid macro-element will allow the investigation of structures both at macro or meso scale accounting for geometric and constitutive nonlinearities

The kinematics is described according to a DMEM that allows considering the minimum required degrees of freedom with a significant computational advantage with respect to macro-modelling strategy based within a Finite Element context.

The adopted co-rotational formulation, detailed described in chapter 3, is based on a two-node interface element whose degrees of freedom are related to the independent degrees of freedom of the corresponding adjacent elements.

The mechanical calibration of the solid element, following a straightforward fiber discretization approach provides very accurate results.

The thesis is divided into five main chapters.

The first Chapter reports a review on numerical modelling of masonry structure with emphasis to the methods accounting for the in-plane and out-of plane behaviour.

The second Chapter is focused on the description of the DMEM approach focusing on the different macro-elements already introduced with some examples of applications and experimental and numerical validations.

The third Chapter, that contains the original contribution of the present study, reports the theoretical formulation of the proposed solid

co-rotational macro-element within the framework of the DMEM and the two-node co-rotational interface.

The fourth Chapter provides some numerical and experimental validation of the solid co-rotational macro-element with reference to some significant benchmarks.

The last conclusive Chapter reports a summary of the present research highlighting the applicability of the proposed strategy and the possible future developments.

Some theoretical details, related to the adopted co-rotational frameworks, are reported in Appendix.

1 NUMERICAL MODELLING STRATEGIES FOR MASONRY STRUCTURES

1.1 Prominent modelling strategies for masonry structures

The numerical modelling of the nonlinear behaviour of masonry structures represents a complex research topic in which many different strategies have been proposed. Simplified and highly accurate approach are the subject of several academic researches. Many simplified approaches are still used in the context of engineering practice and recommended by engineering code although their reliability is questioned by several scientific researches. On the other hand, more sophisticated numerical strategies, although allowing high fidelity simulations requires a huge computational cost and expert judgement. At the same time, it has to be considered that any numerical simulation is based on uncertain assumptions on the actual geometry, material characteristics of the structural elements, loading history (as for the case of earthquake actions) as well as the properties of the underlying soil. This latter consideration is particularly true for masonry monumental structural for which the actual structural geometry, the complex and not uniform properties of masonry material do not always justify the use of high-fidelity modelling strategy for a real structure that is not possible to accurately characterise.

Masonry is a very complex material, exhibits a non-linear behaviour for very low level of loads particularly when subjected to earthquake loadings.

The anisotropic nature of masonry, strictly related to the masonry typology, represents a further problem in the definition of masonry constitutive laws.

Masonry monumental structures are often characterised by uncertainties in the definition of the actual structural geometry being not clear the distinction between structures and decorations.

In view of the above considerations, different modelling strategies characterised by different capabilities, computational costs and accuracies have been proposed for their use in different contexts of engineering applications and academic researches.

In the subsequent paragraphs a brief review of the main modelling strategies for masonry monumental structures is reported, only the approaches able to account for the in-plane and out-of-plane behaviour are considered.

1.1.1 Finite element method – FEM

The finite element method is the most adopted numerical method in structural analysis, and it is also widely used for modelling masonry structures. Two different modelling approaches are generally used in FEM applications for masonry structures. Detailed approaches at the micro or meso-scale [15] in which a discretization brick by brick is needed, and all the structural components are properly characterized. A macro-modelling strategy in which the structure is modelled as assemblage of elements identifying macro-portions of the structure according to a homogenization approach.

The following figure shows the classification of FEM approach.

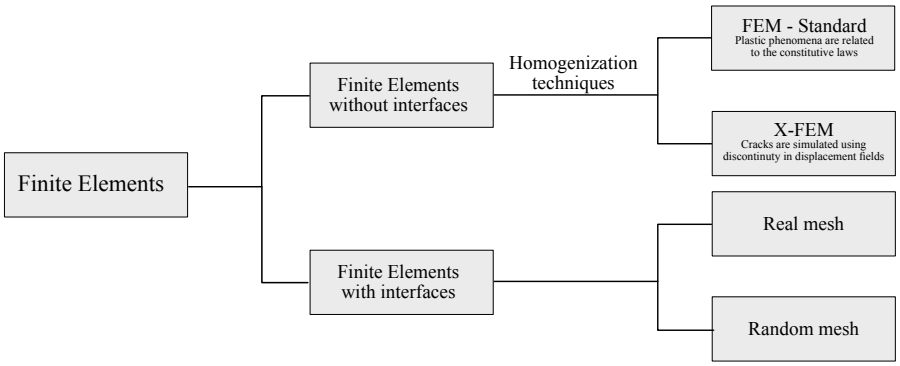

Figure 1 - FEM classification

Finite element methods incorporating generalised functions in the displacement field (X-FEM) allow to consider discontinuities simulating concentration of damage and fracture phenomena without the need of introducing interface elements. Pietruszczak e Ushaksaraei [44] element's embed a critical plane for each element that have a variable orientation. The correct orientation is obtained maximizing the collapse function.

FEM Micro-Modelling is based on a detailed mesh reproducing the real texture of the masonry element and can be considered as the most advanced method developed until now. For example, using this approach, in a masonry panel each brick and each mortar layer have to be modelled in explicit way using 3d solid elements. One of the most realistic model recently developed is that reported into the Macorini and Izzuddin paper [17]. In this paper, authors model bricks using a 3d solid element with 16 nodes and three degrees of freedom for each node, and interfaces with a 2d surface that is evaluated starting from the nodes of the adjacent elements. Interfaces connect the elements that don't share any nodes. So, the kinematic compatibility is allowed by interfaces. The particularity of this model is that a co-rotational reference system rigidly connected to

the interface is used and in this way the model is capable to grasp second order phenomena. Each interface is considered continuous and it is integrated using gauss quadrature.

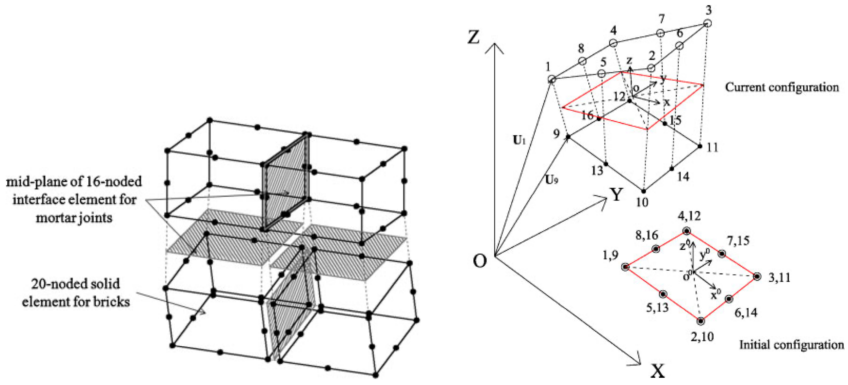

Figure 2 - FEM - micro modelling using co-rotational interfaces

The same model was applied from Chisari et al. [18] in comparison with laboratory tests confirming the accuracy of the approach.

Another interesting FEM model is the one's proposed by Milani et al [45]. They used a macro-scale approach to reproduce the non-linear behaviour of masonry wall in presence of second order effects. The masonry structure is divided into rigid triangles and interfaces where all the deformations occurs. The non-liner curvature bending moment is obtained from a simplified homogenization model.

1.1.2 Distinct element method – DEM

The distinct element method was introduced by Cundall [46] in 1971. At the beginning it was implemented in order to study the rocks motion and their interaction. Later on, it was extended for structures with particular reference to masonry structures due to their heterogeneous nature and the low tensile resistance. Blocks are connected by interfaces

and the contact forces and displacement at the interfaces are found through a series of calculation that take into account the movement of blocks, and their material. The method works in terms of forces and displacement and each block can exhibit unlimited translation and rotations. At each contact between blocks, normal and shear forces are calculated in relation to the displacements. These relationships can be linear or non-linear. Usually this method is used in systems in which there are rigid part and interfaces, but it is also possible to model pseudo deformable blocks that are discretized as finite elements. Figure 3.

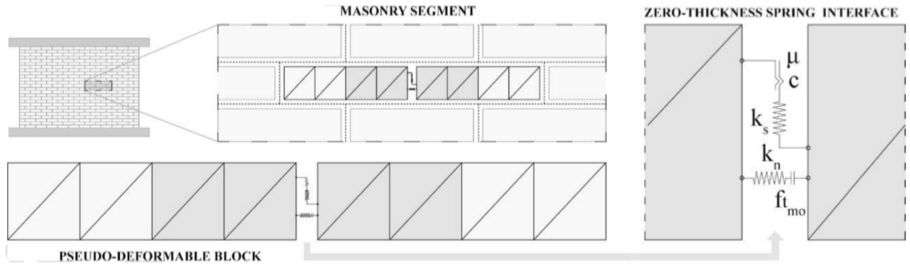

Figure 3 – Distinct element method [47]

Finite displacement and rotations can be taken into account and also the complete detachment between blocks; Also new contact interfaces are automatically created during the analysis. Figure 4 reports the calculation cycle of 3DEC [48], a commercial software that implements the distinct element method.

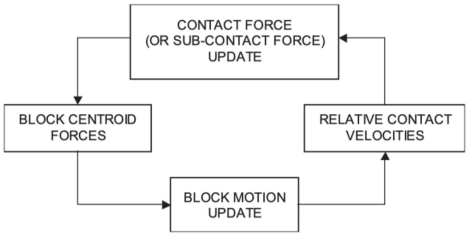

Figure 4 – Calculation cycle of distinct element method [48]

Also, dynamic analysis using a time stepping algorithm is allowed. A lot of studies were performed during the years, for example Papantonopoulos [49] tried to predict the displacement time history of an ancient Greek column. He found that this kind of phenomena is strictly dependent on the initial condition or trivial changes in the loading sequence, but all the essential characteristics of the earthquake response of the column model were very well captured. Dejong et al. [50] modelled the spire of St. Mary Magdalene church in Waltham-on-the-Wolds, in the UK, which was damaged in the 2008 Lincolnshire Earthquake. They evaluated the minimum possible acceleration as well as the minimum impulse which could cause collapse. They also created a scale model and compared numerical and experimental results. Malomo et al. [47] studied the damage propagation in a URM panel and compared the numerical result with an experimental in-plane cyclic shear compression test. Çaktı et al. [51] modelled "Mustafa Pasha Mosque" in Skopje using the DEM and they also realized a 1:10 scale model in order to study the earthquake response of the structure using the shake table. Based on the comparison of numerical and experimental results they calibrated the DEM model and they obtained good agreement between data.

The main problem related to DEM model is that the calibration of springs is generally obtained with experimental data. This problem is overcome with the rigid body spring model described in the following paragraph.

1.1.3 Rigid body spring model – RBSM

The rigid body spring model RBSM was introduced by Kawai in 1978 [52]. He started from the following idea: when a structure reaches his ultimate state of loading it crush into pieces. After that each part

moves as a rigid body. According to the RBSM the structure is divided into large but finite number of parts that are mutually connected by springs system distributed over the contact boundary surfaces. The deformation of each interface can be obtained from the centroid movement of adjacent rigid bodies. Consequently, the size of the stiffness matrix of each element is 6x6 with a considerably reduction in computing time. In 2007 Casolo et all. [27] studied the in-plane dynamics of masonry walls having a hysteretic constitutive law.

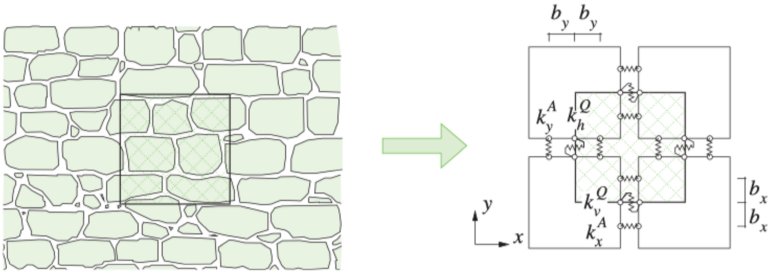

Figure 5 – Scheme of an irregular masonry discretised in RBSM [27]

Figure 5 reports the discretisation scheme, the number of springs for each interface are three, one is needed to catch slide mechanism, the other two are needed to catch flexural and axial behaviour. Springs are defined by a relationship with a corresponding continuum. After that in 2013 Casolo et all [53] studied with the same approach the out of plane behaviour of a masonry façade. The main problem related to the RBSM is that large displacements and rotations are not allowed. This limit is overcome by Applied Element Method described in the following.

1.1.4 Applied Element Method – AEM

The name Applied element method was introduced in 2002 by Meguro et al. [54]. It is very similar to the RBSM but it allows large displacements analyses and it can follow structural behaviour from the

initial loading stages until complete collapse. Even in this case, the structure is divided into rigid parts connected by springs. A finite point number of the interface has two springs, one to catch the slide behaviour and the other to rule flexural and axial behaviour.

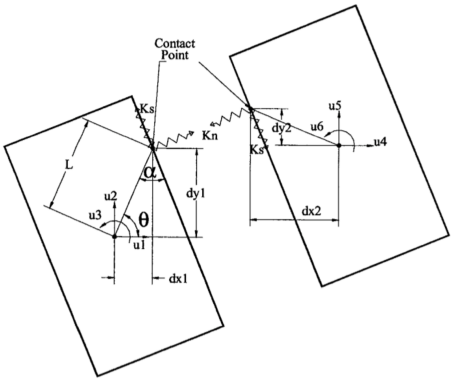

Figure 6 - Element shape, contact point, and degree of freedom [54]

The in-plane stiffness matrix of each element has 3x3 components and the contribution of each contact point is reported in the following formula:

$$\boldsymbol{K} = \begin{bmatrix} s_{\theta\alpha}^2 K_n + c_{\theta\alpha}^2 K_s & (K_s - K_n) s_{\theta\alpha} c_{\theta\alpha} & L(K_s s_\alpha c_{\theta\alpha} - K_n s_{\theta\alpha} c_\alpha) \\ (K_s - K_n) s_{\theta\alpha} c_{\theta\alpha} & s_{\theta\alpha}^2 K_s + c_{\theta\alpha}^2 K_n & L(K_n c_\alpha c_{\theta\alpha} + K_s s_{\theta\alpha} s_\alpha) \\ L(K_s s_\alpha c_{\theta\alpha} - K_n s_{\theta\alpha} c_\alpha) & L(K_n c_\alpha c_{\theta\alpha} + K_s s_{\theta\alpha} s_\alpha) & L^2\left(s_{\theta\alpha}^2 K_n + c_{\theta\alpha}^2 K_s\right) \end{bmatrix} \quad (1.1)$$

Where:

$$\mathrm{K_n} = \frac{EdT}{a} \quad \mathrm{K}_s = \frac{GdT}{a} \quad s_{\theta\alpha} = \sin(\theta + \alpha) \quad c_{\theta\alpha} = \cos(\theta + \alpha) \quad s_\alpha \quad (1.2)$$

Where d is the distance between springs, T the element thickness, a the length of the relative area, E is the Young's modulus and G the material shear modulus. So, each spring of the interface represent the stiffness of a volume with the dimension d, T, a. The AEM has been further developed over the year. It allows linear and non-linear, static and dynamic, small and large displacement analyses and also many kinds of material constitutive laws.

The large displacement procedure is based on the following formula:

$$\boldsymbol{K}\Delta\boldsymbol{U} = \Delta\boldsymbol{F} + \boldsymbol{R_m} + \boldsymbol{R_G} \tag{1.3}$$

Where:

- $\boldsymbol{K}$ is the tangent stiffness matrix;
- $\Delta\boldsymbol{U}$ is the increment of the Lagrangian parameters;
- $\Delta\boldsymbol{F}$ is the incremental load vector;
- $\boldsymbol{R_m}$ is the residual force vector due to cracking or incompatibility between spring strains and stresses;
- $\boldsymbol{R_G}$ is the residual force vector due to geometrical changes in the structure during loading;

In the [54] the application of AEM in large displacement is explained, in particular it follows the following steps:

1. Assume that $\boldsymbol{R_m}$ and $\boldsymbol{R_G}$ are null and solve (1.3) to get $\Delta\boldsymbol{u}$.
2. Modify the structural geometry according to the calculated incremental displacements;
3. Modify the direction of the spring force vectors according to the new element configuration. The geometrical changes generate incompatibility between the applied forces and internal stresses.
4. Verify whether cracking occurred and calculate $\boldsymbol{R_m}$. In elastic analysis $\boldsymbol{R_m}$ is zero.
5. Calculate the element force vector, $\boldsymbol{F_m}$, by summing the forces of the springs around each element.
6. Calculate the geometrical residuals around each element with the following formula:

$$\boldsymbol{R_G} = \boldsymbol{f} - \boldsymbol{F_m} \tag{1.4}$$

7. Calculate the stiffness matrix for the structure with the new configuration considering stiffness changes due to cracking or yielding.
8. Repeat the process.

A commercial software called “Extreme loadings for structures” is based on this method. Although its simplicity the method, if well calibrated, provides reasonable results. However, it needs a lot of elements to provide good solutions leading to a significant computational cost.

1.1.5 Limit Analisys

The limit analysis was one of the first methods used for the safety assessment of masonry structures. The father of modern limit analysis is Jacques Heyman, who used clear hypotheses for the evaluation of the ultimate load of arch structures. His work represented a decisive impulse towards modern limit analysis theories.

The limit analysis consists in the evaluation of the ultimate load of a structure subjected to certain load and under certain boundary conditions. In its classical formulation, it is based on the assumption that the mechanical behaviour of the materials is rigid-plastic with no tensile resistance. As for the FEM modelling also for limit analysis methods distinction is made between a *macroblocks method* and the *detailed limit analysis*. The first approach consists in assuming a reasonable number of collapse mechanisms involving the entire structure or parts of it, and in deriving the relative kinematic multipliers in order to identify the minimum value corresponding to the collapse multiplier. *Macroblock methods* are currently very popular in professional practice. The study of

the crack patterns gives useful information on the collapse mechanisms that can occur. The *detailed limit analysis* consists in discretizing the structure through a mesh of elements using discrete elements or finite elements and evaluating the ultimate multiplier of the loads and the relative collapse mechanism solving a problem of mathematical optimization (linear programming). Using distinct elements, the structure is discretized into rigid blocks connected by interfaces in which the possibility of having a finite sliding resistance can be contemplated or not. The presence of a sliding resistance means that the normality rule of the classical theory of limit analysis is no longer satisfied (non-associated law). The consequence is that there is no longer a unique solution to the problem. Casapulla et al. [55], have shown that for some types of structures the uniqueness of the solution is guaranteed even in the case of the presence of an non-associated flow rule. The solution is however obtained through linear programming procedures.

Limit analysis can be also conducted using finite elements connected by interfaces. At the macro-scale the elements are calibrated by homogenization techniques. The collapse mechanism is identified, even in this case, using linear programming techniques [56].

1.1.6 Discrete Macro element method – DMEM

Since this thesis is focused on the DMEM, this method is properly discussed in the next chapter.

2 The Discrete Macro Element Method

2.1 A discrete macro-element strategy

Starting from a pioneering work in 2004 [31] a research team of the University of Catania proposed an original macro-element method defined in the context of the discrete element strategy. This approach is based on the subdivision of the structure in several macro-portions, each represented by corresponding macro-elements. After a homogenization of the mechanical properties of the components (mortar and units), each macro-portion is regarded as an equivalent continuum whose mechanical properties can be assumed as isotropic or orthotropic depending on the masonry texture. The next step is the discretization by means of a mesh of macro-elements chosen according to the macro-portion that has to be modelled.

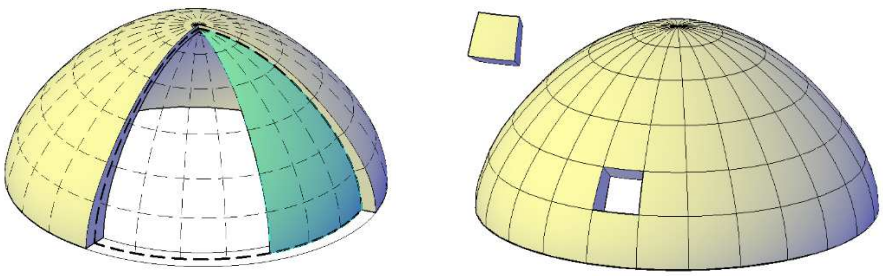

Figure 7 - Subdivision of a dome in macro-portion to be represented by macro-elements

Figure 7 reports a qualitatively subdivision of a dome by means of several macro-portions that, according to this macro-element strategy,

will be represented by shell macro-elements conceived for modelling curved masonry structures.

In this Discrete Macro Element Method (DMEM) each macro-element, that is not rigid (like in the classical formulation of DEM), interacts with the adjacent elements through nonlinear distributed zero-thickness interfaces.

The nonlinear behaviour of the structure is captured through an assemblage of macro-elements, characterized by different level of complexity according to the role played in the global model which incorporate both the in-plane and out-of-plane behaviour.

The degrees of freedom needed to describe the macro-elements' kinematics are those strictly related to the rigid body motion of each element plus a further degree of freedom governing the in-plane element deformability. This allows to obtain a very efficient model characterised by a low computational burden compared to those required by nonlinear FEM simulations.

In the following subsections a brief description of the different macro-elements introduced so far, in the context of the DMEM, is reported.

2.2 The basic 2D macro-element

The basic 2D macro-element is a plane quadrangular element endowed by four degrees of freedom only, Figure 8a

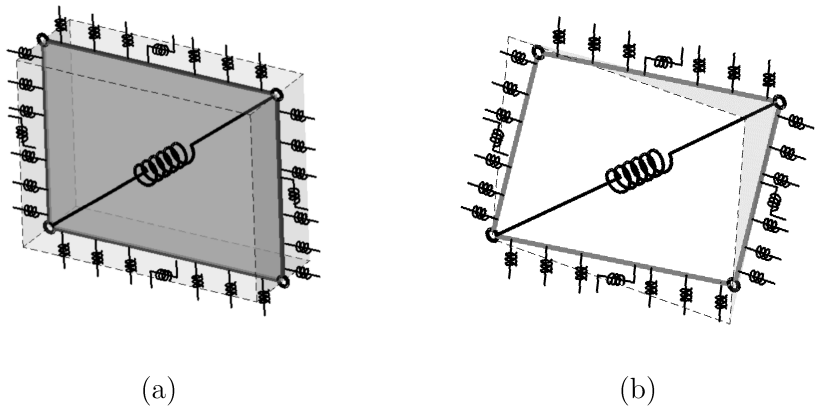

(a) (b)

Figure 8 - The 2D macro-element and its mechanical scheme. (a) initial undeformed configuration (b) deformed configuration.

The 2D macro-element, firstly proposed in 2004 [31], has been conceived for the simulation of the nonlinear response of masonry walls in their own plane, Figure 8a. The element can be regarded as an articulated quadrilateral of rigid beams connected by four hinges, leading to a kinematics governed by four degrees of freedom. Zero-thickness interfaces govern the interaction with the adjacent elements, while the element deformability is conveniently ruled by a single diagonal nonlinear link, being related to a single Lagrangian parameter.

The kinematics of the mechanical scheme, after a proper calibration procedure of the nonlinear links, is capable of simulating the main in-plane collapse failure modes of a masonry panel: flexural failure, diagonal shear failure and sliding shear failure [30].

In spite of its simplicity, the assemblage of these elements allows the simulation of the global nonlinear response of masonry buildings also in presence of irregular openings distribution allowing a geometric consistent [57] simulation of the masonry walls in their own plane.

The deformations of the interfaces are related to the relative motion between corresponding macro-elements; therefore, no further Lagrangian

parameter has to be introduced to describe the relative motion at the interfaces.

The adopted model has the advantage of interacting with the adjacent elements along the whole perimeter, thus allowing the possibility of using different mesh discretization as highlighted in the following paragraphs.

The numerical approach has been validated by several researches [24] and it has been implemented in the software 3DMacro [58] currently used for research and practical applications.

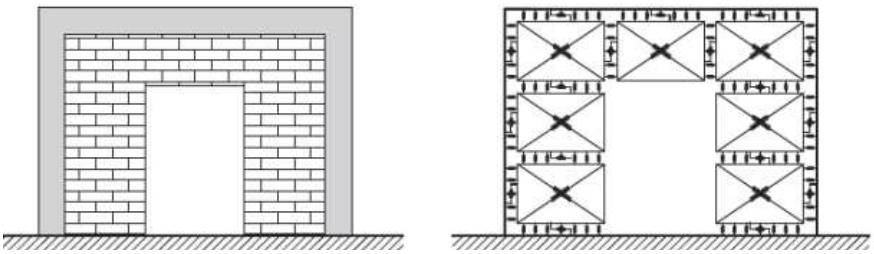

Figure 9 - Typical macro-element discretization of an infilled frame in presence of a central door opening.

The geometric consistency of the elements also allows an efficient simulation of infilled frame structures, Figure 9 reports an example of infilled frame model by means of a hybrid approach in which the beams are modelled as inelastic frame elements and the infill is modelled by means of a mesh of plane macro-elements.

2.3 The 3D macro-element

The 2D macro-element allows the simulation of a masonry wall in its own plane but ignore the out-of-plane response, therefore its use is recommended only for buildings or structures exhibiting a box behaviour. To overcome this significant restriction a third dimension and the relevant

needed additional degrees of freedom have been introduced in a spatial macro-element.

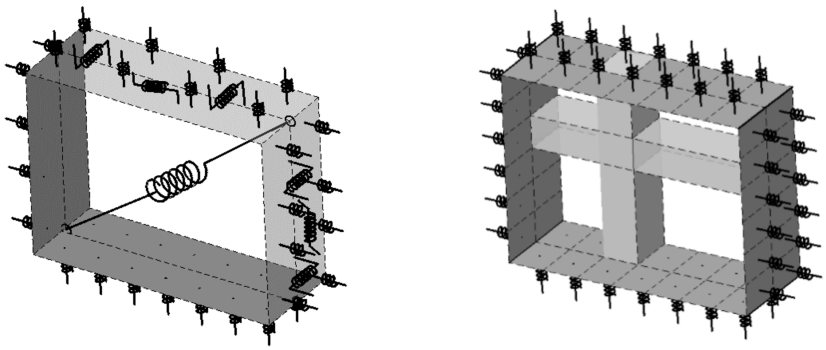

(a) (b)

Figure 10 -3D macro-element. (a) simplified mechanical scheme; (b) a typical fiber discretization of the element.

The 3D macro-element is represented in Figure 10 [59] , [39], its kinematics is governed by 7 degrees-of-freedom, able to describe the in- and out-of-plane rigid body motions and the in-plane shear deformability.

The interaction of the spatial macro-element with the adjacent elements or the external supports is ruled by 3D-interfaces. Following a fiber discretization strategy, each interface possesses m rows of n orthogonal (i.e. perpendicular to the planes of the interface) nonlinear links, Figure 10b.

The 3D interfaces are endowed with additional shear-sliding springs Figure 10a, required to control the in-plane and out-of-plane sliding mechanisms as well as the torsion around the axis perpendicular to the plane of the interface. The number of NLinks adopted in the 3D-interfaces is selected according to the desired level of accuracy of the nonlinear response.

A detailed description of the mechanical calibration of the spatial macro-element and some validation examples are reported in [59]. This model has also been applied for the complex nonlinear simulation of infilled frame structures accounting for the in- and the out-of-plane behaviour of infills [60].

2.4 The shell macro-element for modelling curved geometry

The 3D macro-element [59] allows the simulation of the in-plane and out-of-plane behaviour plane masonry walls. However Historical monumental structures are often characterised by the presence of curved geometry structures, like arches, vaults, domes, etc. whose role in the global and local nonlinear static or dynamic response cannot be ignored.

In order to model curved geometry masonry structures a more general shell macro-element has been introduced. This is characterised by four rigid layer edges, connected by hinges, whose orientation and dimension is related to the shape of the element and to the thickness of the portion of structure to be modelled, Figure 11.

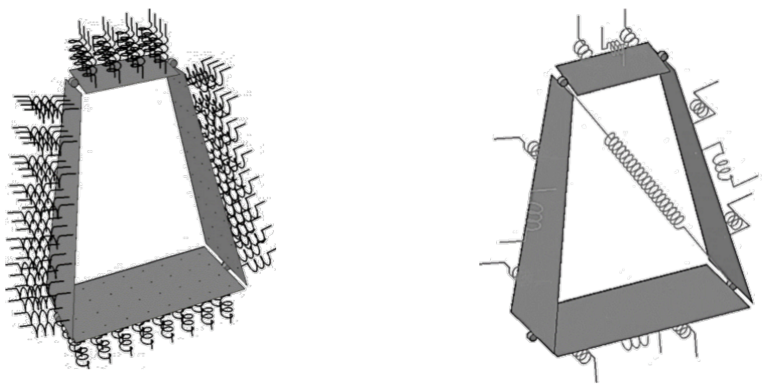

(a) (b)

Figure 11 - Shell macro-element. (a) the orthogonal links of the interfaces; (b) the longitudinal and the diagonal links.

The generalised in-plane shear deformability is still governed by a single degree of freedom that can still related to a diagonal spring placed along one of the diagonals of the quadrilateral.

The plane interfaces rule the interaction with the adjacent elements or the external supports. Due to the irregular geometry these interfaces are in general skew with respect to the medium plane of the element. Curved surfaces are therefore modelled under the assumption that the behaviour of a curved surfaces can be satisfactorily represented by flat macro-elements. The geometry of the macro-element is defined by the coordinates of its vertices, the four normal vectors to the surface and the thicknesses in these points, Figure 12.

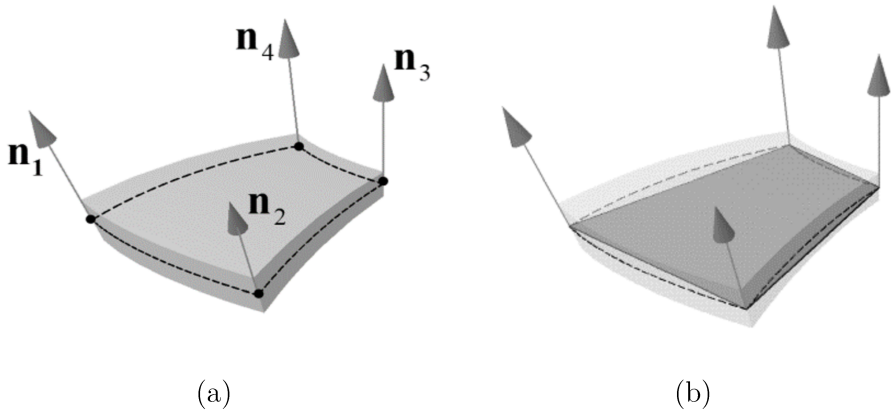

Figure 12 - Curved portion of masonry structures and (b) its flat discrete element representation

The most significant novelties introduced in the shell macro-element can be summarized in the following features:

- interfaces are no longer orthogonal to the principal plane of the element, thus allowing to follow the curved geometry of the structure;
- the thickness can be linearly variable at each interface;

- the shape of the element can be represented by a generic quadrangular element.

In spite of the difficulties related to the curved geometry, the model keeps the original simplicity and low computational cost. Its kinematics is still ruled by seven degrees of freedom only (six rigid body motion degrees of freedom and one associated with the in-plane generalised shear deformability). The irregular geometry implies that each link corresponds to a prismatic fiber, whose cross-sectional area varies with a parabolic trend, Figure 13.

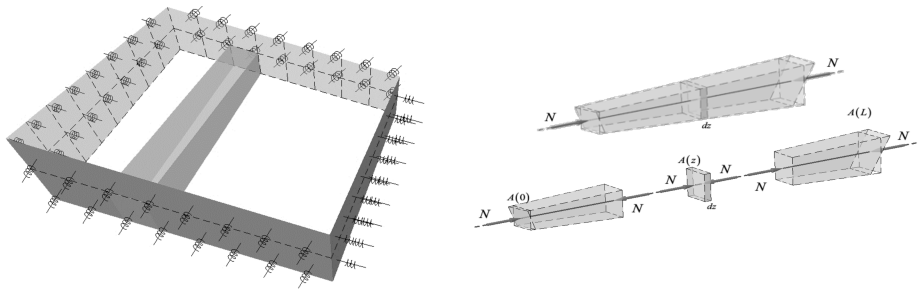

(a) (b)

Figure 13 - Fiber discretization of the shell macro-element.

The calibration strategy follows the same approach adopted for the spatial regular model. Since those links have to simulate also the occurrence of sliding along the bed joints, their nonlinear behaviour is closely affected by friction phenomena and the yielding domain accounts for the influence of the normal force acting on the interface.

2.5 The mechanical characterization strategy of the macro-element

According to the proposed strategy each macro-element must be representative of the corresponding finite portion of masonry wall. The

mechanical characterization strategy follows an intuitive phenomenological description of the mechanical behaviour of a masonry portion in which, the zero-thickness interfaces rule the membrane-flexural response and the shear-sliding behaviour of adjacent elements, while the in-plane shear element deformability is related to the angular distortion of the articulated rigid quadrilateral. The mechanical characterization of the zero-thickness interfaces is here performed following a straightforward fiber calibration procedure while the shear element deformability is calibrated through a mechanical equivalence with a reference geometric-consistent continuous model.

The interface nonlinear links can be distinguished as orthogonal Nlinks and shear-sliding Nlinks. In the following, the main steps needed for the calibration procedure are described with reference to each group of nonlinear links.

2.5.1 Calibration of the nonlinear links orthogonal to the interfaces

In the orthogonal nonlinear links the mechanical properties of the represented masonry macro-portion are incorporated considering the masonry as an orthotropic homogeneous medium. Each orthogonal link inherits the nonlinear behaviour of the corresponding masonry fiber, along a given material direction, Figure 10b. Making reference, for simplicity, to a regular three-dimensional macro-element, each Nlink is calibrated assuming that the masonry strip is a homogeneous inelastic material [61]. Aiming at providing an example, reference is made to a single orthotropic panel under monotonic loadings, Figure 13. In this case the flexural behaviour of the masonry panel is characterized by different mechanical properties along two directions. E_h and E_v are the Young's moduli of the

homogenized orthotropic masonry medium; σ_{ch}, σ_{th} and σ_{cv}, σ_{tv} are the corresponding compressive and tensile maximum stresses, G_{ch}, G_{th} and G_{cv}, G_{tv} are the fracture energies in compression and tension. Coherently with the adopted fiber calibration approach, the flexural stiffness calibration of the panel is simply obtained by assigning to each link the axial stiffness of the corresponding masonry strip. Each masonry strip is identified by its influence area and the half-dimension of the panel in the direction perpendicular to the interface, Figure 10b.

The initial stiffness K, the compressive and tensile yielding strengths, f_c and f_t, and the corresponding ultimate displacements, u_c and u_t (under the simplified hypothesis of rectangular shape of the panel and linear softening) of the links relative to the horizontal and vertical interfaces are reported in Table 1 as a function of the mechanical and geometrical properties of the masonry panel.

DIRECTION	k	f_c	f_t	u_c	u_t
HORIZONTAL	$\frac{2E_h\lambda_h\lambda_s}{B}$	$\sigma_{ch}\lambda_h\lambda_s$	$\sigma_{th}\lambda_h\lambda_s$	$\frac{2G_{ch}}{\sigma_{ch}}$	$\frac{2G_{th}}{\sigma_{th}}$
VERTICAL	$\frac{2E_v\lambda_v\lambda_s}{B}$	$\sigma_{cv}\lambda_v\lambda_s$	$\sigma_{tv}\lambda_v\lambda_s$	$\frac{2G_{cv}}{\sigma_{cv}}$	$\frac{2G_{tv}}{\sigma_{tv}}$

Table 1- Mechanical calibration of the orthogonal Nlinks for a rectangular panel

B and H are the length and the height of the panel, λ_h and λ_v are the in-plane distances between the springs along the interfaces arranged according to the two fundamental directions, and λ_s is the out-of-plane distance between the rows of springs.

2.5.2 Calibration of the non-linear links along the interface

The nonlinear links, lying along the interface and identified as shear-sliding springs, rule the torsional and shear-sliding behaviour along the interfaces. In the discretization here adopted, one single link is considered

for the in-plane model Figure 8 while three nonlinear links have been considered for the spatial models (Figure 10 and Figure 11) [59].

The shear-sliding behaviour is ruled by a single Nlink, governing the in-plane sliding of the element along the interface and is calibrated according to a Mohr–Coulomb law. The out-of-plane shear deformability is ruled by two parallel springs, which take care of the out-of-plane sliding behaviour and the torsional elastic and inelastic response of the connected adjacent panels. The two out-of-plane shear-sliding nonlinear links are required to control the out-of-plane sliding mechanisms as well as the torsion around the axis perpendicular to the plane of the interface.

Aiming at maintaining a simple fiber calibration approach, the out-of-plane shear deformability of each link, connecting two adjacent panels, is calibrated according to their influence volumes. Referring to two identical adjacent macro-elements, with thickness s, width B and height H, shear modulus G, cohesion c, and friction coefficient μ_s, the calibration procedure is summarized providing the main parameters that govern the mechanical behaviour of the sliding links. Table 2

DIRECTION	k_s	d	f_{sy}
HORIZONTAL	∞	–	$(\mathrm{c}+\mu_{\mathrm{s}}\mathrm{N})\mathrm{A}$
VERTICAL	$\frac{1}{2}\frac{\mathbf{GBs}}{\mathbf{H}}$	$2\mathrm{s}\sqrt{\frac{1}{3}-0{,}21\frac{\mathrm{s}}{\mathrm{B}}\left(1-\frac{\mathrm{s}^4}{12\mathrm{B}^4}\right)}$	$\frac{1}{2}(\mathrm{c}+\mu_{\mathrm{s}}\mathrm{N})\mathrm{A}$

Table 2- Mechanical calibration of the shear sliding Nlinks for a rectangular panel

Once the elastic shear out-of-plane stiffness has been assigned, according to the formulas reported in Table 2, the relative distance d between the two out-of-plane sliding links is assigned according to an equivalence with the corresponding elastic continuum in terms of torsional behaviour [59]. The yielding strength of each spring is associated with the

current contact area A of the interface and to the current axial force N associated with the orthogonal links of the interface.

2.5.3 Calibration of the diagonal link

The diagonal shear failure collapse of the panel is related to a single degree of freedom; this allows to associate the nonlinear response to a single diagonal nonlinear link. Several yielding criteria can be adopted to account for the shear capacity, which is strongly dependent on the vertical compression stresses in the wall. In the elastic range, the diagonal shear spring is calibrated by imposing an energy equivalence between the articulated quadrilateral, ruled by the diagonal spring and a continuous reference elastic model. The yielding forces are associated with the limits of tensile or compressive stresses in the reference continuous model, while the post-elastic behaviour is ruled by a suitable constitutive law. A Mohr–Coulomb law or a Turnsek Cacovic law [57] can generally be adopted for the calibration of the diagonal link, although any constitutive law can also be considered.

3 A SOLID CO-ROTATIONAL DISCRETE MACRO-ELEMENT

3.1 Introduction

In this chapter a new solid discrete macro-element able to exhibit large rotations and small deformations is proposed. This element represents a further significant contribution in the context of the DMEM proposed by Caliò et al. [33]. The main novelties of the proposed solid co-rotational element can be summarised as follows:

- The previously introduced discrete macro-elements were formulated under the assumption of linearized kinematics. The solid element here proposed can exhibit large rotations and large displacements assuming a kinematics that allows small shear deformations, within each element, and small relative displacements at the interfaces between adjacent macro-elements. The large displacement capabilities are taken into account by considering an original co-rotational strategy, based on local reference systems accounting for the small deformations at the interfaces between the corresponding adjacent solid macro-elements.

- Although other spatial elements have been already proposed, these are characterised by a shear deformability only in one plane related to a simple kinematics associated to a reference articulated quadrilateral [62]. The solid element here proposed is more general being characterised by a uniform infinitesimal spatial strain tensor corresponding to a pure shear deformation.

- Differently from the previous spatial discrete macro-elements, the zero-thickness two-dimensional cohesive interfaces, inheriting the

masonry properties, are continuously distributed. This allows the use more general constitutive laws and the adoption of different integration strategies along the interfaces.

As discussed the last chapter, the generality of the solid macro-element formulation will allow the investigation of structures both at macro or at meso-scale accounting for complex geometrical layouts and different sources of constitutive nonlinearities. Its application it is not limited to masonry structures, as will be shown the next chapter in which more general benchmarks are considered.

In the following the theoretical formulation of the proposed solid macro-element is reported. The kinematics is described according to DMEM, this allows to consider the minimum required degrees of freedom leading to a computational advantage with respect to macro-modelling strategy based on FEM strategies.

Two different approaches are considered for the co-rotational framework based on different parametrization of rotations previously proposed in the literature by Battini [63] [64] and Izzuddin [65] [66] [67] [68]. For simplicity, the two approaches are identified as "*Approach I* and *II* ". The last section of this chapter is devoted to the mechanical calibration of the solid element that follows a straightforward fiber discretization approach that, its simplicity, provides very accurate results, as demonstrated in the next chapter reporting some numerical applications and validation examples.

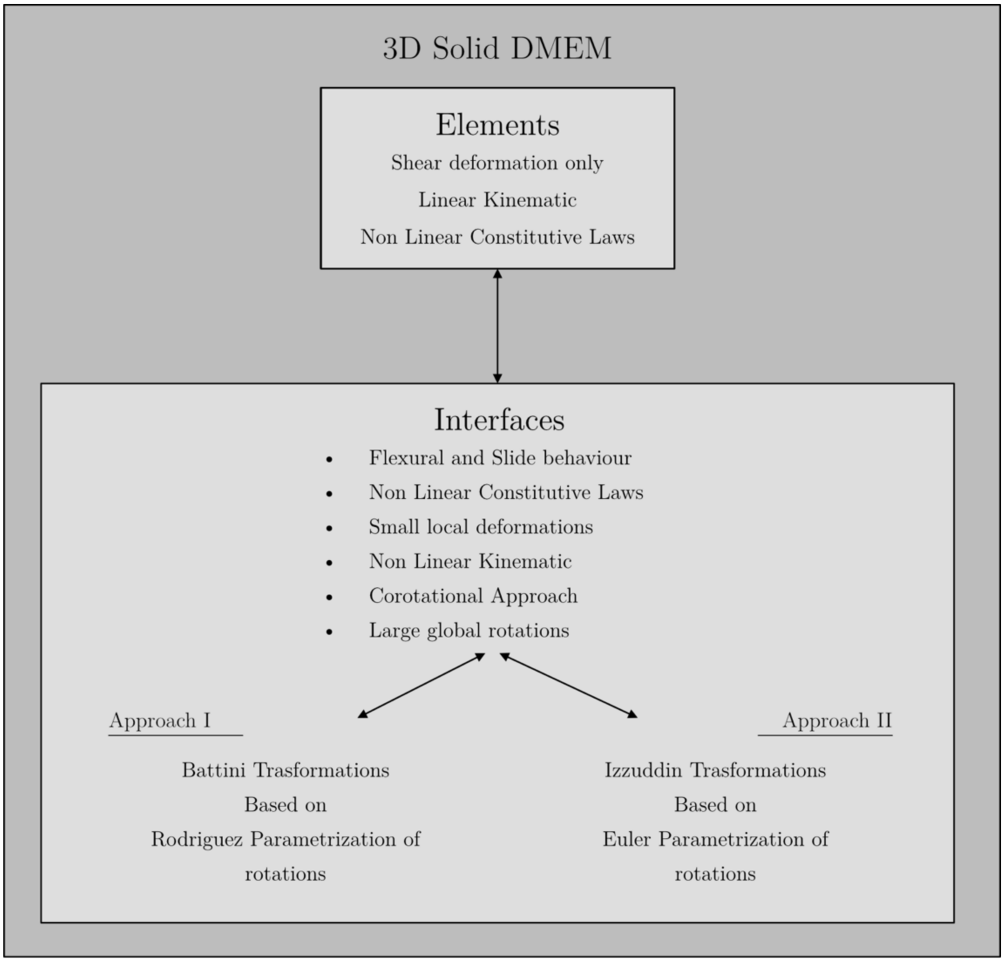

Figure 14 – Scheme of 3D Solid DMEM

Figure 14 reports a concise description of the main features of elements and interface that will be better described in the following.

3.2 The co-rotational framework

The co-rotational approach is currently one of the most adopted method for modelling geometrical nonlinearities in structures for which the deformation gradients can be considered small enough to be described by linearized strain tensors although large rigid motions of the elements can occur. The main assumption is that displacements and rotations are large, but deformations are small. The description of the deformation motion is possible using different Lagrangian parameter and local reference systems in order to describe the small deformation and the rigid body motion separately. The deformation of the body is described in the co-rotational reference system fixed to the body, while the large displacements and rotations are evaluated taking into account the rigid movement of the chosen local co-rotational reference systems.

If the local degrees of freedom, related to the deformation, are properly defined, the main advantage of the co-rotational approach is the possibility to easily extend classical linear elements to large displacement using standard kinematic transformations and its variation (co-rotational framework).

Many co-rotational frameworks were formulated using different approaches to manage large rotations. Crisfield proposed a co-rotational strategy for beams and shells [69]. More recently, Battini [63] formulated a co-rotational approach for three-dimensional beams, using a classical Rodriguez representation of large rotations, for static and dynamic problems. Also Felippa and Haugen [70] proposed a unified co-rotational framework that generalized the problem using the Rodriguez parametrization of rotations. Of particular interest is the approach proposed by Izzuddin [65] based on an incremental formulation of rotation,

considering Euler angles, applied for solving constitutive and geometric non-linear problems for frame structures, shell elements [68] as well as interface models [17]. This framework has been implemented within the large purpose nonlinear FEM software Adaptic [71].

The co-rotational framework is based on the assumption that the virtual work expressions, written in the local co-rotational system and in the global reference system, for different groups of parameters, must be the same. So, it is possible to consider the deformations in a local reference system using a particular group of kinematic parameters $\delta \mathbf{p_c}$ and evaluate the entire motion in the global reference system using other groups of kinematic parameters $\delta \mathbf{p_g}$. This consideration leads to the following simple expression of the Internal Virtual Work:

$$\delta \mathbf{p_g^T q_g} = \delta \mathbf{p_c^T q_c} \tag{3.1}$$

where:

- $\delta \mathbf{p_g}$ is a column vector that contains variational global kinematics Lagrangian parameters in the global reference system;
- $\mathbf{q_g}$ is a column vector that contains the conjugated forces of $\delta \mathbf{p_g}$;
- $\delta \mathbf{p_c}$ is a column vector that contains variational co-rotational kinematics Lagrangian parameters in the local reference system;
- $\mathbf{q_c}$ is a column vector that contains the conjugated forces of $\delta \mathbf{p_c}$;

Considering that a certain relationship between $\mathbf{p_c}$ and $\mathbf{p_g}$, that connects local and global parameters, must exist, this relation can be written in general form as:

$$\mathbf{p_c} = \mathbf{p_c}(\mathbf{p_g}) \tag{3.2}$$

the variation of the (3.2) can be expressed in the following form:

$$\delta\mathbf{p_c} = \mathbf{B}(\mathbf{p_g})\delta\mathbf{p_g} \tag{3.3}$$

where the matrix $\mathbf{B}(\mathbf{p_g})$ is a compatibility kinematic matrix between global and co-rotational degrees of freedom. For a lighter notation in the following $\mathbf{B}(\mathbf{p})$ will be written as $\mathbf{B}$.

In view of (3.1) equation (3.3) becomes:

$$\delta\mathbf{p^T q} = \delta\mathbf{p^T B^T q_c} \qquad \forall\ \delta\mathbf{p^T} \tag{3.4}$$

The equation (3.4) is valid $\forall\ \delta\mathbf{p^T}$ leading to:

$$\mathbf{q} = \mathbf{B^T q_c} \tag{3.5}$$

Considering the variation of the (3.5) the following expression is obtained:

$$\delta\mathbf{q} = \delta\mathbf{B^T q_c} + \mathbf{B^T}\delta\mathbf{q_c} \tag{3.6}$$

In the co-rotational reference system is also possible to obtain the relation between co-rotational Lagrangian parameters and the conjugated forces:

$$\delta\mathbf{q_c} = \mathbf{K_c}\delta\mathbf{p_c} \tag{3.7}$$

In which, the matrix $\mathbf{K_c}$ is the co-rotational stiffness matrix. The dependency between $\mathbf{K_c}$ and $\mathbf{p_c}$ is only related to the nonlinearity of the constitutive law of the material because in the co-rotational reference system deformations are considered small.

Substituting the (3.7) and (3.3) into (3.6) the following expression is obtained:

$$\delta\mathbf{q} = \delta\mathbf{B^T q_c} + \mathbf{B^T K_c B}\delta\mathbf{p} \tag{3.8}$$

The first term of the (3.8) is related to the Geometric Stiffness Matrix, and the second term is related to the Material Stiffness Matrix.

The quantity $\delta\mathbf{B}^{\mathbf{T}}$ is a third order matrix and it contains $\delta\mathbf{p}$.

The same equation can be obtained using the Stationarity of the Total stain energy.

In this study the co-rotational strategy is adopted only for the description of the mechanical behaviour of the interfaces since the shear deformation of the solid elements is governed by internal degrees of freedoms independent on the rigid body motion. A co-rotational two-node interface element is formulated for each interface connecting two solid elements.

3.3 The solid macro-element

The basic geometrical and kinematics assumptions of the proposed 3D macro-element are presented in this section.

In its initial configuration the element is represented by a regular rectangular parallelepiped, Figure 15

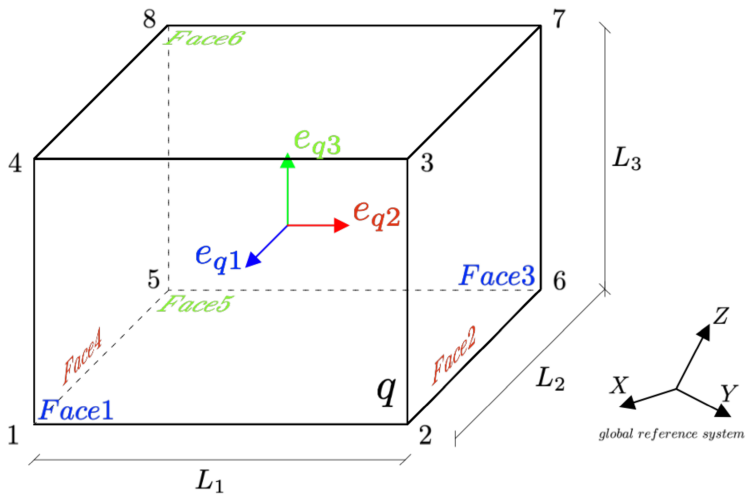

Figure 15 - The generic element q and its local and global reference systems

With reference to the generic element q, an orthonormal Cartesian *local element* system $\mathbf{e}_{q1}, \mathbf{e}_{q2}$ $\mathbf{e}_{q3}$, oriented according to the sides of the parallelepiped L_1, L_2, L_3, is centered on the centroid of the element. The unit vectors $\mathbf{e}_{qi}$(i=1,2,3) refer to the global reference system OXYZ.

A conventional numbering of faces and vertices is assumed as reported in Figure 15. In particular unit vectors $\mathbf{e}_{q1}$ and $-\mathbf{e}_{q1}$ identifies the faces 1 and 3 of the element, unit vectors $\mathbf{e}_{q2}$ and $-\mathbf{e}_{q2}$ identifies the faces 2 and 4, unit vectors $\mathbf{e}_{q3}$ and $-\mathbf{e}_{q3}$ identifies the faces 6 and 5 of the element; Vertices are identified as reported in Figure 15 following an anti-

clockwise numbering of face 1 from 1 to 4 and for face 3 from 5 to 8 being the vertexes 1 and 5 along the direction $\mathbf{e}_{q1}$.

The macro-element is therefore identified by the orthogonal tensor:

$$\mathbf{R_q} = [\mathbf{e}_{q1} \quad \mathbf{e}_{q2} \quad \mathbf{e}_{q3}] \tag{3.9}$$

Following the same strategy adopted for the already proposed macro-elements [33], [59], [4] this solid macro-element will allow to describe the nonlinear behaviour of a structure by considering a mesh of macro-elements characterized by a shear deformability, within the elements, while axial- flexural, torsional and shear sliding behaviour are in the adjacent elements' interfaces.

The solid element here formulated can exhibit large rotations and large displacements assuming a kinematics that allows small shear deformations within each element and small deformations at the interfaces between adjacent elements.

The element is conceived to be adopted either at macro or at meso-scale, as reported in Figure 16.

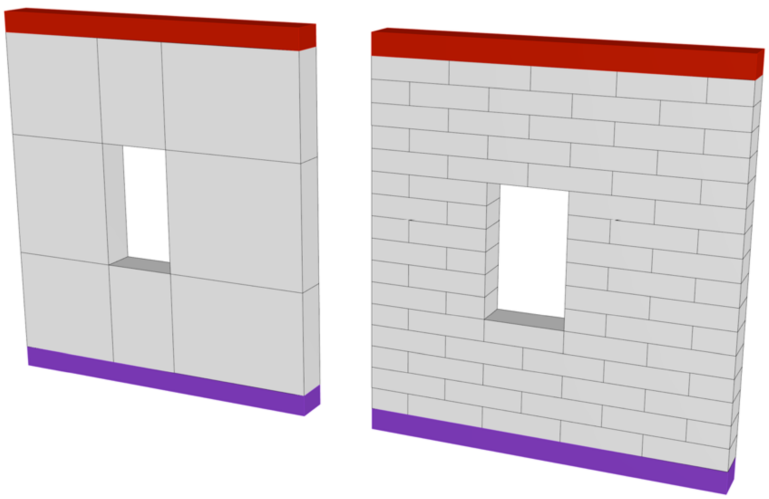

Figure 16 - Macro and mesco scale model

The kinematics of each solid element is governed by nine degrees of freedom, six associated to the rigid body motion and three related to the internal shear deformability.

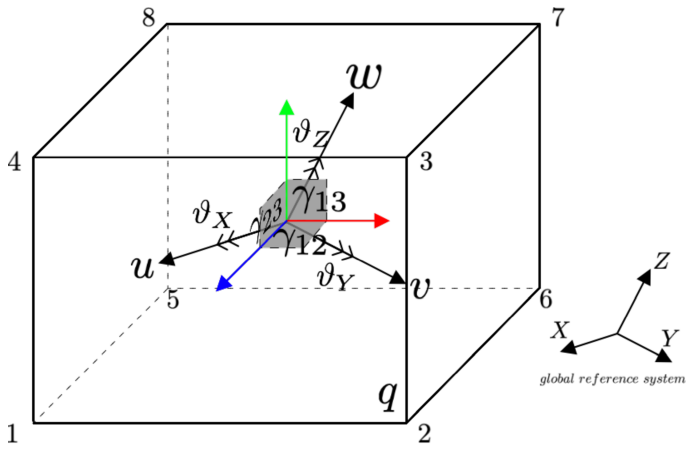

Figure 17 - The q macro-element and the corresponding degrees of freedom

The chosen Lagrangian parameters are indicated in Figure 17, with reference to the generic element q. The degrees of freedom associated to the rigid body motion (measured with respect to the global reference system 0XYZ) are the global translational displacements u_q,v_q,w_q and the global rotations ϑ_{Xq}, ϑ_{Yq} and ϑ_{Zq}.

The three 'internal' degrees of freedom are the shear angles γ_{12q}, γ_{13q}, γ_{23q} (related to the local reference system of the element).

The nine Lagrangian parameters of the q-macro-element are collected in the vector $\mathbf{p}_{\mathrm{gq}}^{T}$ as follows:

$$\mathbf{p}_{\mathrm{gq}}^{T} = [u_q \quad v_q \quad w_q \quad \vartheta_{Xq} \quad \vartheta_{Yq} \quad \vartheta_{Zq} \quad \gamma_{12q} \quad \gamma_{13q} \quad \gamma_{23q}] \tag{3.10}$$

that can be partitioned as:

$$\mathbf{p}_{\mathrm{gq}}^{\mathrm{T}} = [\mathbf{u}_{\mathbf{gq}}^{\mathbf{T}} \quad \boldsymbol{\vartheta}_{\mathbf{gq}}^{\mathbf{T}} \quad \boldsymbol{\Gamma}_{\mathbf{q}}^{\mathbf{T}}] \tag{3.11}$$

with

$$\mathbf{u_{gq}^T} = [u_q \quad v_q \quad w_q] \quad \boldsymbol{\vartheta}_{\mathbf{gq}}^{\mathbf{T}} = [\vartheta_{Xq} \quad \vartheta_{Yq} \quad \vartheta_{Zq}] \quad \boldsymbol{\Gamma}_{\mathbf{q}}^{\mathbf{T}} = [\gamma_{12q} \quad \gamma_{13q} \quad \gamma_{23q}]$$

3.3.1 The element shear deformability

It is assumed that each element, initially shaped according to a regular rectangular parallelepiped, can be subjected to rigid body motions and can deform accordingly to a uniform shear deformation whose principal planes are coincident with the planed of the local reference system of the element, Figure 18.

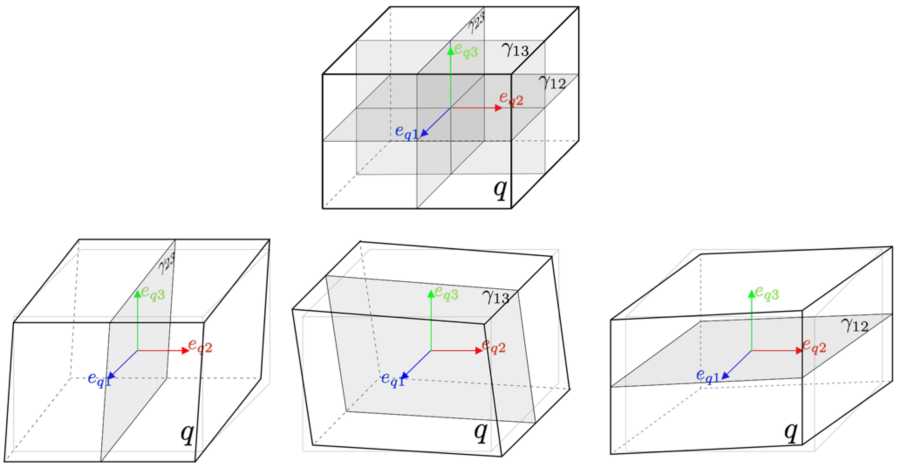

Figure 18 - Shear deformation plane considered for the regular element

As a result, the small shear deformation of the solid macro-element is described by the shear angles $\gamma_{12q} \quad \gamma_{13q} \quad \gamma_{23q}$ identifying a linearized strain tensor in the local reference system of the element as follows:

$$\mathbf{E} = \begin{bmatrix} 0 & \frac{\gamma_{12}}{2} & \frac{\gamma_{13}}{2} \\ \frac{\gamma_{12}}{2} & 0 & \frac{\gamma_{23}}{2} \\ \frac{\gamma_{13}}{2} & \frac{\gamma_{23}}{2} & 0 \end{bmatrix} \tag{3.12}$$

Due to the assumption of homogeneous linearized strain, the only allowed small deformation displacements of the element are related to the shear deformation and are given by:

$$\mathbf{u_q} = \mathbf{E}\ \mathbf{x_q} \tag{3.13}$$

being:

- $\mathbf{x_q} = \mathrm{x}\ \mathbf{e_{q1}} + \mathrm{y}\ \mathbf{e_{q2}} + \mathrm{z}\ \mathbf{e_{q3}}$ the position of the generic point inside the dominium of the element in the local reference system;
- $\mathbf{u_q}$ the displacement of the point $\mathbf{x}$ in the local reference system;

Equation (3.13) can be written in the following form

$$\mathbf{u_q} = \begin{bmatrix} \frac{\mathrm{y}}{2} & \frac{\mathrm{z}}{2} & 0 \\ \frac{\mathrm{x}}{2} & 0 & \frac{\mathrm{z}}{2} \\ 0 & \frac{\mathrm{x}}{2} & \frac{\mathrm{y}}{2} \end{bmatrix} \begin{bmatrix} \gamma_{12} \\ \gamma_{13} \\ \gamma_{23} \end{bmatrix} = \mathbf{B_\ell \Gamma_q^T} \tag{3.14}$$

It is worth noticing that the element shear deformability is not affected by the rigid body motion of the solid elements. However, the relative displacements of the generic interface are related to the shear deformations and the rigid body motions of the adjacent elements sharing the interface. The mechanical behaviour of each interface is described according to an original co-rotational strategy based on a Eulerian reference system connecting the two nodes of the adjacent elements. The adopted strategy is detailed described in the following sub-section

3.4 The two-node corotational interface element

The two-node co-rotational interface element is formulated using two different co-rotational frameworks, proposed in the literature with reference to three-dimensional beam-columns. Namely the approaches proposed by Battini [63] and by Izzuddin [65] are considered. The main differences between these two approaches are related to the parametrization of rotation.

Elements interact by means of nonlinear interfaces that, in the initial configuration, possess zero-thickness. Following the same strategy adopted in the DMEM, described in the previous Chapter 2, the interfaces rule the interaction between the macro-elements and embed the axial-flexural, shear-sliding and torsional elements' deformability as well as the shear sliding behaviour.

In this formulation both the shear and interface deformabilities are assumed small while each solid element can be subjected to large rigid motions.

The approach here adopted has been implemented in a Matlab code MEX (Macro_EXtreme), that has been entirely developed as part of the thesis work. The code can import the three-dimensional geometry of the structure from a cad drawing, furthermore an automatic procedure for the identification of nonconforming interfaces is implemented. This procedure allows to contain the computational burden associated to the numerical simulations by avoiding further subdivision of the elements sharing nonconforming interfaces.

The formulation of the corotational two-node interface element requires the definition of several configurations and reference systems, Figure 19, as specified in what follows:

- the "initial configuration" identifying the initial ($t = 0$) geometry of the model.

- the "*current configuration*" that identifies the state of the model at the pseudo-time $t > 0$.

- The global reference system defined by the triad of unit orthogonal vectors $\mathbf{E}_i$ (i = 1, 2, 3).

- Two local reference systems, for the adjacent elements p and q, that in the initial configurations are identified by triads $\mathbf{e}_{0pi}$ and (i = 1,2,3) $\mathbf{e}_{0qi}$ (i = 1, 2, 3) while in the current configuration are given by the unit vectors $\mathbf{e}_{pi}$ and (i = 1,2,3) $\mathbf{e}_{qi}$ (i = 1, 2, 3).

- a corotational local reference system, which continuously rotates and translates following the interface shared by the element p and q. In the initial and current configurations are identified by $\mathbf{c}_{0pqi}$ (i = 1,2,3) and $\mathbf{c}_{pqi}$ (i = 1,2,3) respectively.

- Two further unit triads, $\boldsymbol{t}_{pi}$ and $\boldsymbol{t}_{qi}$ (i = 1, 2, 3), rigidly attached to the centroids of the elements p and q. These two triads embed the rigid part and the deformational part of the motion.

- A plane local reference system that identifies the interface coordinates in the initial, $\boldsymbol{i}_{0pq1i}$ (i=1,2,3), and current, $\boldsymbol{i}_{pq1i}$ (i=1,2,3), configurations.

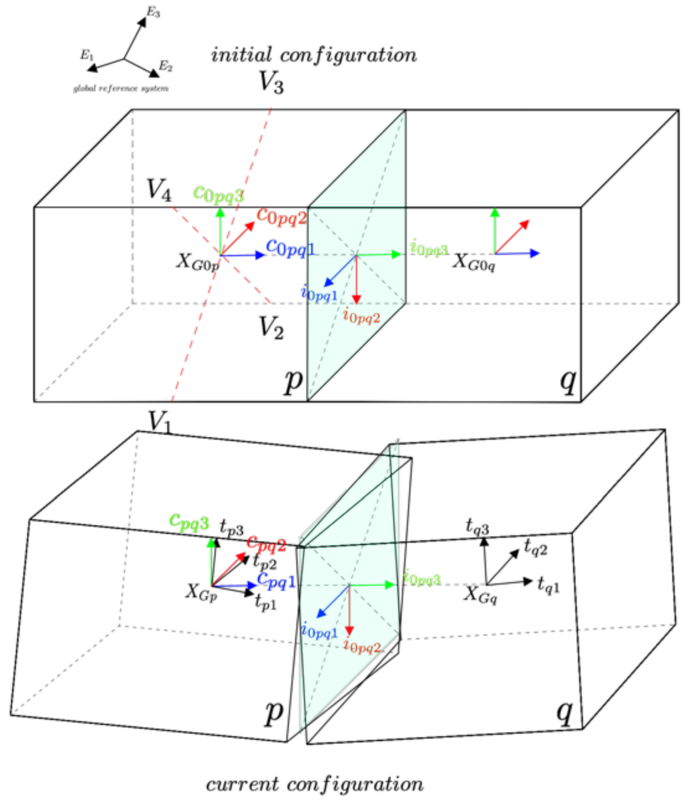

Figure 19 - Unit triads

According to the main idea of the co-rotational approach, the motion of the element is divided into a rigid body motion and a small deformational part. The rigid body motion consists of a rigid translation and rotation of the local corotational system. The definition of the unit triads, $\boldsymbol{t}_{pi}$ and $\boldsymbol{t}_{qi}$ (i = 1, 2, 3), is related to the adopted corotational framework.

The corotational reference system is initially identified by connecting the two centroids of the macro-elements, $\mathbf{X}_{0\mathrm{G}p}$ and $\mathbf{X}_{0\mathrm{G}q}$. The origin of the reference system is located in the centroid of the element p, accordingly the unit vectors of the corresponding reference system will be identified as $\mathbf{c}_{0pqi}$, (i=1,2,3), being the direction $\mathbf{c}_{0pq1}$ connecting the

centroids from p to q. The other two units vector are chosen with the intersection of the plane, identified by the normal to $\mathbf{c}_{0pq1}$, and the direction of edge of the solid parallelepiped p orthogonal to the interface. The plane quadrilateral with the vertices $\mathbf{V}_i$ $(i = 1 \dots 4)$ is identified and the triad $\mathbf{c}_{0pqi}$ (i = 1,2,3) can therefore be evaluated by considering the following expressions:

$$\mathbf{c}_{0\mathrm{pq1}} = \frac{\mathbf{X}_{\mathrm{G0q}} - \mathbf{X}_{\mathrm{G0p}}}{\left|\mathbf{X}_{\mathrm{G0q}} - \mathbf{X}_{\mathrm{G0p}}\right|} \quad \mathbf{c}_{0\mathrm{pq2}} = \frac{\mathbf{c}_{013} + \mathbf{c}_{024}}{\left|\mathbf{c}_{013} + \mathbf{c}_{024}\right|} \quad \mathbf{c}_{0\mathrm{pq3}} = \mathbf{c}_{0\mathrm{pq1}} \times \mathbf{c}_{0\mathrm{pq2}} \tag{3.15}$$

With:

$$\mathbf{c}_{0ij} = \frac{\mathbf{V}_i - \mathbf{V}_j}{\left|\mathbf{V}_i - \mathbf{V}_j\right|} \tag{3.16}$$

alternatively, the co-rotational system can be identified by the rotational tensor:

$$\mathbf{R}_{0\mathrm{C}} = [\mathbf{c}_{0\mathrm{qp1}} \quad \mathbf{c}_{0\mathrm{qp2}} \quad \mathbf{c}_{0\mathrm{qp3}}] \tag{3.17}$$

Figure 20, reports an example of a nonconforming interface. It is assumed that in the initial configuration the two adjacent faces of the elements share the same plane and the corresponding solid elements maintain the same orientation. Under these assumptions the initial geometry of the interface is given by the regular rectangular quadrilateral obtained by intersection of the two elements' sides.

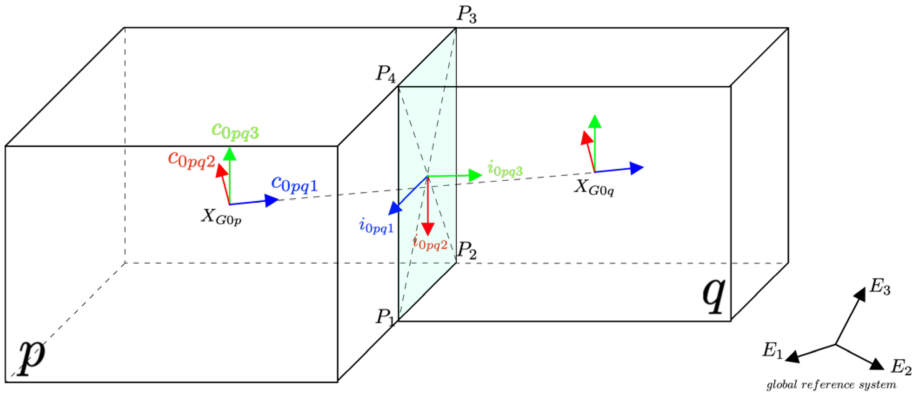

Figure 20 - Automatic procedure due to the generation of the middle plane interface

Once the positions $\mathrm{P}_1, \mathrm{P}_2, \mathrm{P}_3, \mathrm{P}_4$ of the four vertices are evaluated, the local reference system is obtained by considering the following expressions

$$\mathrm{P}_{31} = \frac{P_3 - P_1}{\|P_3 - P_1\|} \quad \mathrm{P}_{42} = \frac{P_4 - P_2}{\|P_4 - P_2\|} \tag{3.18}$$

$$\mathbf{i_{0pq1}} = \frac{\mathrm{P}_{31} - \mathrm{P}_{42}}{\|\mathrm{P}_{31} - \mathrm{P}_{42}\|} \quad \mathbf{i_{0pq2}} = \frac{\mathrm{P}_{31} + \mathrm{P}_{42}}{\|\mathrm{P}_{31} + \mathrm{P}_{42}\|} \quad \mathbf{i_{0pq3}} = \mathbf{i_{0pq1}} \times \mathbf{i_{0pq2}} \tag{3.19}$$

The correspondent rotational matrix, identifying the initial position of the interface in the global reference system, is therefore given by:

$$\mathbf{R}_{0pqint} = [\mathbf{i_{0pq1}} \quad \mathbf{i_{0pq2}} \quad \mathbf{i_{0pq2}}] \tag{3.20}$$

Although each element can exhibit large displacement and large rotations, the relative displacements at the interfaces are assumed to be small, therefore can be described according to a linearized kinematics as reported in the following.

The kinematics of the interface connecting two adjacent elements p and q is described by the degrees of freedom of the corresponding adjacent elements $\mathbf{p}_{\mathrm{gp}}^T$ and $\mathbf{p}_{\mathrm{gq}}^T$ without the need to introduce further degrees of freedom.

In order to describe the interface kinematics, it is convenient to collect the 18 the degrees of freedom of the adjacent elements as follows:

$$\mathbf{p}_{\mathrm{gpq}}^{\mathbf{T}} = [\mathbf{u}_{\mathbf{pG}}^{\mathbf{T}} \quad \boldsymbol{\vartheta}_{\mathbf{qG}}^{\mathbf{T}} \quad \mathbf{u}_{\mathbf{pG}}^{\mathbf{T}} \quad \boldsymbol{\vartheta}_{\mathbf{qG}}^{\mathbf{T}} \quad \boldsymbol{\Gamma}_{\mathbf{p}}^{\mathbf{T}} \quad \boldsymbol{\Gamma}_{\mathbf{q}}^{\mathbf{T}}] \tag{3.21}$$

Considering that, each solid element, in its initial configuration, is represented by a regular parallelepiped and the internal deformation is described by a linearized homogenous shear deformation, the interface deformation displacements are associated to the motion of the two planes corresponding to each element face that will remain plane during the analysis. Each interface point is identified by its initial coordinates in the local reference system of the interface $\mathbf{i}_{\mathbf{0}pqi}$ (i=1,2,3).

Since the interface relative displacements are assumed to be small it can also be assumed that the points belonging to each element faces will not change their relative positions, within their own plane.

The following two subsections report the theoretical formulation of the co-rotational two-node interface element according to the two adopted co-rotational frameworks based on the strategies adopted by Battini [63] and Izzuddin [65] with reference to three-dimensional beam-columns.

3.4.1 The co-rotational framework based on rotational vector and Rodriguez formula. Approach I

A central issue in the development of a co-rotational approach is the treatment of finite [72] independent parameters. One alternative in this context, is based on the so-called "rotational vector" [72], [73], [74] [75], defined by:

$$\mathbf{\Psi} = \psi \bullet \mathbf{u} \tag{3.22}$$

Expression (3.22) states that any finite rotation can be represented by a unique rotation with an angle ψ about an axis defined by the unit vector $\mathbf{u}$.

The magnitude ψ is given by:

$$\psi = \sqrt{\Psi_1^2 + \Psi_2^2 + \Psi_3^2} \tag{3.23}$$

where Ψ_{i}, $(i = 1, 2, 3)$ are the components of $\mathbf{\Psi}$. In terms of Ψ, the orthogonal matrix $\mathbf{R}$ admits the following representation

$$\mathbf{R} = \mathbf{I} + \frac{\sin\psi}{\psi}\widetilde{\mathbf{\Psi}} + \frac{1}{2}\left[\frac{\sin\left(\frac{\psi}{2}\right)}{\frac{\psi}{2}}\right]^2 \widetilde{\mathbf{\Psi}}^2 \tag{3.24}$$

For the sake of simplicity further details on the treatment of large rotations are reported in Appendix A. In the subsection A.2 the parametrization of the rotation based on the spatial rotational vector and Rodriguez formula is illustrated.

In this subsection the co-rotational framework adopted by Battini [63] [64], based on the Rodriguez formula and the spatial rotational vector, is applied to the two-node interface element. Using this parametrization, the rotation is descripted by a vector $\boldsymbol{\vartheta}$ of three components that indicate the rotation axis. Its modulus indicates the magnitude of the rotation.

Equation (A.7), here reported again

$$\mathbf{R} = \exp[\tilde{\boldsymbol{\omega}}] = \mathbf{I} + \frac{\sin\|\boldsymbol{\omega}\|}{\|\boldsymbol{\omega}\|}\tilde{\boldsymbol{\omega}} + \frac{1}{2}\frac{\sin^2(\frac{1}{2}\|\boldsymbol{\omega}\|)}{(\frac{1}{2}\|\boldsymbol{\omega}\|)^2}\tilde{\boldsymbol{\omega}}^2 \tag{3.25}$$

is the Rodriguez formula that allow to obtain the rotational matrix from the rotational pseudo-vector $\boldsymbol{\vartheta}$.

It is important to underling that different parametrization of rotations does not produce any difference in terms of final result, however it produces a different meaning in the vector 3x1 that contains rotation. So, for example the rotational pseudo-vector here defined is not additive because it indicates the rotation axis. It is possible to switch from a non-additive to an additive formulation using the (A.22). This choice has impact to the way in which the analysis is conduct and how the result has to be interpreted. In this document the additive formulation is omitted, and results are obtained using an incremental formulation.

According to the main idea of the co-rotational formulation, the motion of the element from the initial to the final deformed configuration is split into a rigid body component and a deformational part. The rigid body component consists of a rigid translation and rotation of the local element frame.

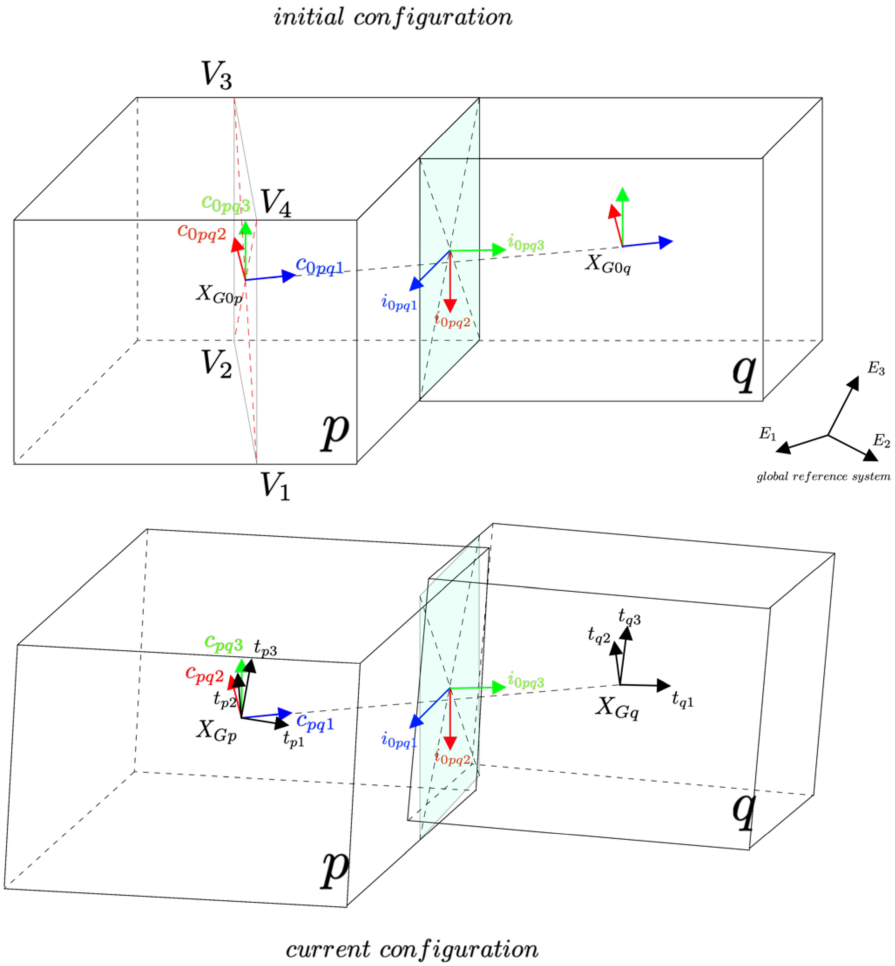

Figure 21 - Non conforming interface

Figure 21 reports the co-rotational reference system in the *current configuration*, this is evaluated according to:

$$\mathbf{R}_{\mathrm{C}} = [\mathbf{c}_{pq1} \quad \mathbf{c}_{pq2} \quad \mathbf{c}_{pq3}] \tag{3.26}$$

The first unit vector $\mathbf{c}_{pq1}$ has the same direction of the line that connects centroids of the elements p and q.

$$\mathbf{c}_{pq1} = \frac{\mathbf{X_{G0q}} + \mathbf{u_{Gq}}) - (\mathbf{X_{G0p}} + \mathbf{u_{Gp}})}{\ell_{pq}} \tag{3.27}$$

where:

$$\ell_{pq} = \left\|(\mathbf{X_{G0p}} + \mathbf{u_{Gp}}) - (\mathbf{X_{G0q}} + \mathbf{u_{Gq}})\right\| \tag{3.28}$$

With $\mathbf{u_{Gp}} = [^{u}\mathbf{_{Gp}} \quad ^{v}\mathbf{_{Gp}} \quad ^{w}\mathbf{_{Gp}}]$ and $\mathbf{u_{Gq}} = [^{u}\mathbf{_{Gq}} \quad ^{v}\mathbf{_{Gq}} \quad ^{w}\mathbf{_{Gq}}]$.

The remaining two axes are evaluated by considering an auxiliary vector $\mathbf{q}$. In the initial configuration $\mathbf{q}$ is directed along the $\mathbf{c}_{0pq2}$ direction while in the current configuration its orientation is obtained from the condition:

$$\mathbf{q} = \frac{1}{2}(\mathbf{q}_1 + \mathbf{q}_2) \quad \mathbf{q}_i = \mathbf{R}_{iG}\mathbf{R}_{0C}[0 \quad 1 \quad 0]^{T} \quad with\ i = 1,2 \tag{3.29}$$

Where $\mathbf{R}_{iG}$ are the two orthogonal matrices that are used to describe the rotation of the nodal triads $\boldsymbol{t}_{pi}$ and $\boldsymbol{t}_{qi}$ (i = 1, 2, 3), $\mathbf{R}_{0C}$ describes the orientation of the local co-rotational system in the initial configuration. The auxiliary vector $\mathbf{q}$ is an "average" vector evaluated between the direction $\boldsymbol{t}_{p2}$ and $\boldsymbol{t}_{q2}$ in the global reference system.

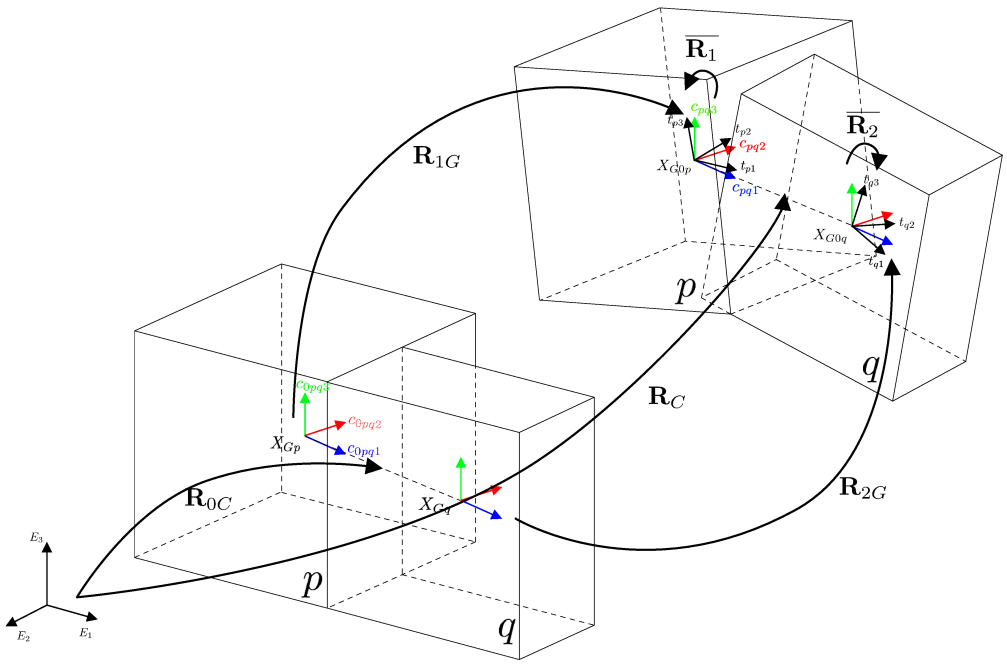

Figure 22 - Coordinate systems of the interface.

In order to obtain the current triad $\boldsymbol{t}_{pi}$ and $\boldsymbol{t}_{qi}$ in the global reference system it is possible to consider the column of the matrix $\mathbf{R}_{\mathrm{iG}}\mathbf{R}_{0\mathrm{C}}$. At the beginning of the analysis, $\boldsymbol{t}_{pi}$ and $\boldsymbol{t}_{qi}$ are coincident to $\mathbf{c}_{0pqi}$ and matrices $\mathbf{R}_{\mathrm{iG}} = identity$.

The unit vector $\mathbf{c}_{pq2}$ and $\mathbf{c}_{pq3}$ are obtained using the following formula:

$$\mathbf{c}_{pq3} = \frac{\mathbf{c}_{pq1} \times \mathbf{q}}{\left\|\mathbf{c}_{pq1} \times \mathbf{q}\right\|} \quad \mathbf{c}_{pq2} = \mathbf{c}_{pq3} \times \mathbf{c}_{pq1} \tag{3.30}$$

The rigid motion is accompanied by local deformational displacements in the interfaces with respect to the local co-rotational reference system $\mathbf{c}_{pq\mathrm{i}}$. In this context, due to the particular choice of the local system, the local translations at the centroid of the element p will be zero. Moreover, at the centroid of the element q, the only non-zero component is the translation along $\mathbf{c}_{pq1}$. This can be evaluated according to:

$$\bar{u} = \ell_{pq} - \ell_{0pq} \tag{3.31}$$

Being $\ell_{0pq} = \|\mathbf{X}_{\mathbf{G0q}} - \mathbf{X}_{\mathbf{G0p}}\|$ the distance between the nodes in the initial configuration.

According to the Figure 22 it is also possible to evaluate the two rotational matrices that contain the deformational part of the motion, identified with an overbar and expressed in the current co-rotational reference system.

These matrices are calculated from:

$$\bar{\mathbf{R}}_i = \mathbf{R}_{\mathrm{C}}^T \mathbf{R}_{\mathrm{iG}} \mathbf{R}_{0\mathrm{C}} \tag{3.32}$$

In this approach the parametrization of rotation follows the Rodriguez Formula as reported in (3.24) where $\boldsymbol{\vartheta}$ is the spatial pseudo vector that indicate the rotational axis.

The rotations in the co-rotational reference system are evaluated using:

$$\bar{\boldsymbol{\vartheta}}_i = \log \bar{\mathbf{R}}_i \tag{3.33}$$

Degrees of freedom, in the local reference system of the elements, related to the shear deformation of the elements are equal to:

$$\begin{aligned} \boldsymbol{\Gamma}_{\mathbf{p}}^{\mathbf{T}} &= [\gamma_{12\mathrm{p}} \quad \gamma_{13\mathrm{p}} \quad \gamma_{23\mathrm{p}}]^{\mathbf{T}} \\ \boldsymbol{\Gamma}_{\mathbf{q}}^{\mathbf{T}} &= [\gamma_{12\mathrm{q}} \quad \gamma_{13\mathrm{q}} \quad \gamma_{23\mathrm{q}}]^{\mathbf{T}} \end{aligned} \tag{3.34}$$

Shear parameters are considered always as local degree of freedom. This simplification is allowed because of the small shear deformation of the elements.

The degree of freedom considered in the co-rotational reference system are collected in the vector $\mathbf{p}_{\mathrm{C}}$:

$$\mathbf{p}_{\mathrm{C}}^{\mathbf{T}} = [\bar{\mathrm{u}} \quad \bar{\boldsymbol{\vartheta}}_{\mathrm{p}}^{\mathrm{T}} \quad \bar{\boldsymbol{\vartheta}}_{\mathrm{q}}^{\mathrm{T}} \quad \boldsymbol{\Gamma}_{\mathrm{p}}^{\mathbf{T}} \quad \boldsymbol{\Gamma}_{\mathrm{q}}^{\mathbf{T}}]^T \tag{3.35}$$

in which the 13 components are:

- $\bar{u}$ is the displacement along unit vector $\mathbf{c}_{pq1}$;
- $\bar{\boldsymbol{\vartheta}}_{\mathrm{p}}^T = [\bar{\vartheta}_{\mathrm{p1}} \quad \bar{\vartheta}_{\mathrm{p2}} \quad \bar{\vartheta}_{\mathrm{p3}}]$ are the spatial rotational pseudo-vector of the element p in the co-rotational reference system that are related only to the deformation of the interface;
- $\bar{\boldsymbol{\vartheta}}_{\mathrm{q}}^T = [\bar{\vartheta}_{\mathrm{q1}} \quad \bar{\vartheta}_{\mathrm{q2}} \quad \bar{\vartheta}_{\mathrm{q3}}]$ are the spatial rotational pseudo-vector of the element q in the co-rotational reference system that are related only to the deformation of the interface;
- $\boldsymbol{\Gamma}_{\mathrm{p}}^{\mathbf{T}} = [\gamma_{12\mathrm{p}} \quad \gamma_{13\mathrm{p}} \quad \gamma_{23\mathrm{p}}]^{\mathbf{T}}$are the shear deformations of the element p;
- $\boldsymbol{\Gamma}_{\mathrm{q}}^{\mathbf{T}} = [\gamma_{12\mathrm{q}} \quad \gamma_{13\mathrm{q}} \quad \gamma_{23\mathrm{q}}]^{\mathbf{T}}$are the shear deformations of the element q;

The angles $\bar{\boldsymbol{\vartheta}}_{\mathrm{p}}^T$ and $\bar{\boldsymbol{\vartheta}}_{\mathrm{q}}^T$ are referred to the centroid of the element p and q and their components are referred respectively to the co-rotational

$1-2-3$ axes using the right-hand rule. So, they are positive if counterclockwise.

The corresponding nodal forces are:

$$\mathbf{f}_{\mathrm{C}}^{\mathbf{T}} = [\mathrm{f}_{\mathrm{c1}} \quad \boldsymbol{m}^{\mathbf{T}}]^{\mathbf{T}} \quad \boldsymbol{m} = [\mathrm{f}_{\mathrm{c2}} \quad \mathrm{f}_{\mathrm{c3}} \quad \mathrm{f}_{\mathrm{c4}} \quad \mathrm{f}_{\mathrm{c5}} \quad \mathrm{f}_{\mathrm{c6}} \quad \mathrm{f}_{\mathrm{c7}} \quad \mathbf{f}_{\boldsymbol{\Gamma \mathbf{q}}} \quad \mathbf{f}_{\boldsymbol{\Gamma \mathbf{p}}}]^{\mathbf{T}} \tag{3.36}$$

where f_{c1} denotes the axial force whereas $\mathrm{f}_{\mathrm{c2}}, \mathrm{f}_{\mathrm{c3}}, \mathrm{f}_{\mathrm{c4}}, \mathrm{f}_{\mathrm{c5}}, \mathrm{f}_{\mathrm{c6}}, \mathrm{f}_{\mathrm{c7}}$ denote the moments at nodes p and q, respectively. The two vector (3x1) $\mathbf{f}_{\boldsymbol{\Gamma \mathbf{q}}}$, $\mathbf{f}_{\boldsymbol{\Gamma \mathbf{p}}}$ are forces related to the shear deformation.

3.4.2 The co-rotational framework based on incremental application of rotation. Approach II

In this section an alternative approach based on an incremental application of rotations in 3D space, as proposed by Izzuddin [65] [66] [67] [68], is considered. The procedure has been originally proposed for modelling the effects of large displacements on the response of space frames subjected to conservative loading. In this case the displacements, referred to the co-rotational reference system, are obtained by means of element-based local vectors. These vectors follow the current configuration of the solid elements sharing the interface and are continuously updated to a position normal to the element chord (main axis of the co-rotational system).

Following the same approach adopted by Izzuddin, the nonlinear solution procedure is formalized in terms of transformations between the co-rotational and the global systems and expressions for geometric stiffness and transformation matrices are explicitly expressed.

The procedure is based on the hypothesis that the loading consists only of forces applied at the nodal positions, since the effect of finite

rotations is sequence-dependent and therefore sensitive to the type of applied moments and the particular definition of rotations employed.

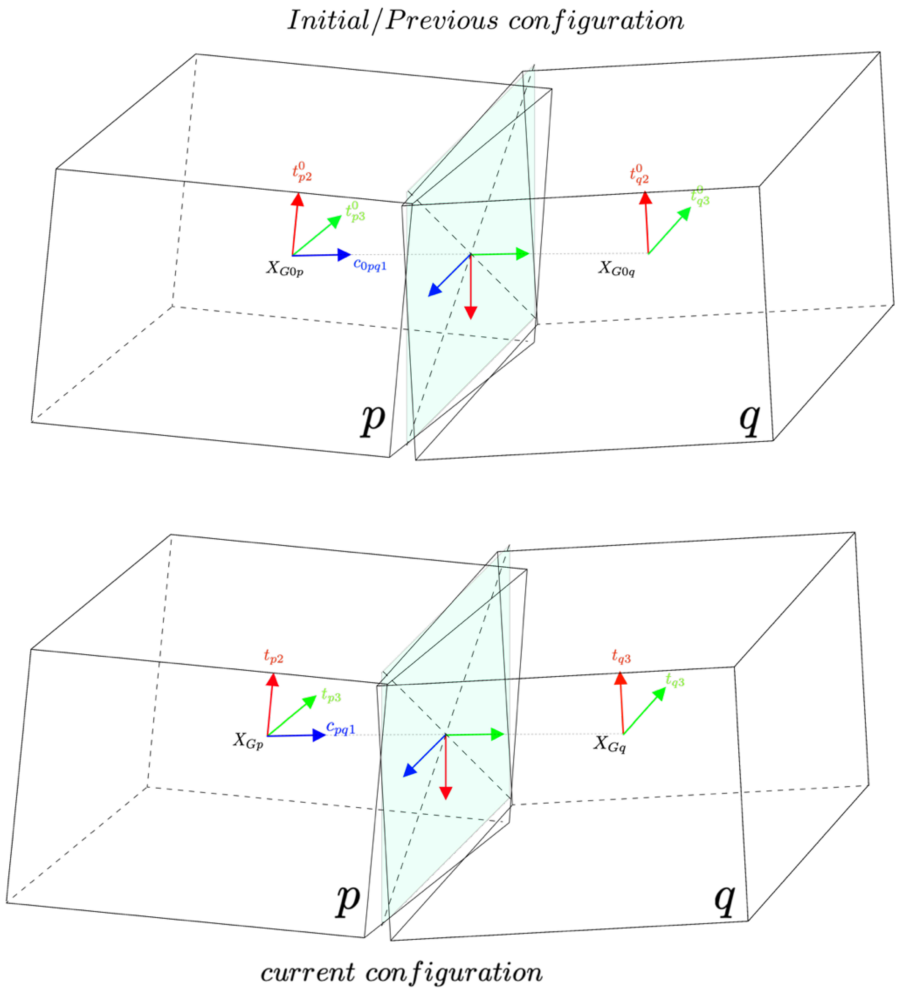

Figure 23 - Co-rotational reference system Approach 2

The co-rotational system is shown in Figure 23. Two triads are considered for describing the deformation of the interface in the co-rotational system, one has origin in the centroid of the element p and the other in the centroid of the element q.

At the beginning of the analysis these two triad assume the same orientation of the co-rotational system:

$$\begin{aligned} \mathbf{t^0_{p3}} &= \mathbf{t^0_{q3}} = \mathbf{c}_{0\mathrm{pq}2} \\ \mathbf{t^0_{p2}} &= \mathbf{t^0_{q2}} = \mathbf{c}_{0\mathrm{pq}3} \end{aligned} \tag{3.37}$$

$\mathbf{t_{p2}}$, $\mathbf{t_{p3}}$, $\mathbf{t_{q2}}$, $\mathbf{t_{q3}}$ represent the elements orientation vectors in the *current configuration* and $\mathbf{t_{pq}}$ identifies the twist rotation between the two solid elements.

The incremental global elements' displacements of the solids elements sharing the interface are expressed by 18 degrees of freedom collected in the vector

$$\mathbf{p^T_{gpq}} = [\mathbf{u^T_{pG}} \quad \boldsymbol{\vartheta}^{\mathbf{T}}_{\mathbf{pG}} \quad \mathbf{u^T_{qG}} \quad \boldsymbol{\vartheta}^{\mathbf{T}}_{\mathbf{qG}} \quad \boldsymbol{\Gamma}^{\mathbf{T}}_{\mathbf{p}} \quad \boldsymbol{\Gamma}^{\mathbf{T}}_{\mathbf{q}}] \tag{3.38}$$

The global nodal displacements $\mathbf{u^T_{pG}}$ and $\mathbf{u^T_{qG}}$ identify the positions of the elements nodes defining the orientation of the co-rotational system in the current iterative configuration:

$$\mathbf{c}_{\mathrm{pq}1} = \frac{\mathbf{X}_{\mathrm{Gq}} - \mathbf{X}_{\mathrm{Gp}}}{\left\|\mathbf{X}_{\mathrm{Gq}} - \mathbf{X}_{\mathrm{Gp}}\right\|} \tag{3.39}$$

with

$$\mathbf{X}_{\mathrm{Gp}} = \mathbf{X}_{\mathrm{G0p}} + \mathbf{u_{pG}} \tag{3.40}$$

$$\mathbf{X}_{\mathrm{Gq}} = \mathbf{X}_{\mathrm{G0q}} + \mathbf{u_{qG}} \tag{3.41}$$

In order to obtain the rotated unit vectors $\mathbf{t_{p2}}$, $\mathbf{t_{p3}}$, $\mathbf{t_{q2}}$, $\mathbf{t_{q3}}$, $\mathbf{t_{pq}}$ it is possible to use different rotation matrix.

Oran in [76] was the first that used a first order rotation matrix to describe the transformation of vector due to an increment of global rotations about the three global axes $(\mathrm{X}, \mathrm{Y}, \mathrm{Z})$ as follows:

$$\mathbf{T} = \begin{bmatrix} 1 & -\vartheta_z & \vartheta_y \\ \vartheta_z & 1 & -\vartheta_x \\ -\vartheta_y & \vartheta_x & 1 \end{bmatrix} \tag{3.42}$$

Where ϑ_x, ϑ_y, ϑ_z are incremental rotations about global axes;
The rotated vector $\mathbf{u}'$ is equal to:

$$\mathbf{t}' = \mathbf{T}\ \mathbf{t} \tag{3.43}$$

However, this relationship can be applied to very small increments since the orthogonality property of transformed unit vectors is satisfied only to the first order in rotations. Izzuddin proposed an higher order transformation applied to the rotational increment.

The incremental description is relative to the last known equilibrium configuration, the adopted definition for rotation is based on a resultant rotational vector, the effect of which is approximated by the following second order transformation matrix $\mathbf{T_r}$, whose derivation is reported in appendix A, expression(A.25).

$$\mathbf{T_r} = \begin{bmatrix} 1 - \dfrac{(\vartheta_y{}^2 + \vartheta_z{}^2)}{2} & -\vartheta_z + \dfrac{\vartheta_y \vartheta_x}{2} & \vartheta_y + \dfrac{\vartheta_x \vartheta_z}{2} \\ \vartheta_z + \dfrac{\vartheta_x \vartheta_y}{2} & 1 - \dfrac{(\vartheta_x{}^2 + \vartheta_z{}^2)}{2} & -\vartheta_x + \dfrac{\vartheta_y \vartheta_z}{2} \\ -\vartheta_y + \dfrac{\vartheta_x \vartheta_z}{2} & \vartheta_x + \dfrac{\vartheta_y \vartheta_z}{2} & 1 - \dfrac{(\vartheta_x{}^2 + \vartheta_y{}^2)}{2} \end{bmatrix} \tag{3.44}$$

that provide the rotated vector $\mathbf{t}'$ as a function of the vector $\mathbf{t}$, relative to the last known equilibrium configuration.

$$\mathbf{t}' = \mathbf{T_r}\mathbf{t} \tag{3.45}$$

As highlighted by Izzuddin [66], the use of such second order transformation reduces the amount of spurious lengthening of vectors upon incremental rotation and preserves to a greater extent the orthogonality property of unit vectors.

As reported in the Appendix A it is also possible to remove any approximation from the evaluation of the rotated vector using a complete transformation $\mathbf{T_r}$ based on Euler/Tait Brian parametrization (A.24).

The global nodal rotations $\boldsymbol{\vartheta}^{\mathbf{T}}_{\mathbf{pG}}$ and $\boldsymbol{\vartheta}^{\mathbf{T}}_{\mathbf{qG}}$ allow to identify two vector transformation matrices at the two elements nodes, $\mathbf{T_p}(\boldsymbol{\vartheta}^{\mathbf{T}}_{\mathbf{pG}})$ and $\mathbf{T_q}(\boldsymbol{\vartheta}^{\mathbf{T}}_{\mathbf{qG}})$, leading to the current orientation vectors for the two solid elements sharing the interface.

$$\mathbf{t_{ij}} = \mathbf{T_i}\ \mathbf{t^0_{ij}} \text{ with i} = \text{p, q and j} = 2,3 \tag{3.46}$$

Where the apex zero identifies the vectors at the last equilibrium configuration.

As specified in Figure 23, the two vector set ($\mathbf{t^0_{p2}}$, $\mathbf{t^0_{p3}}$) and ($\mathbf{t^0_{q2}}$, $\mathbf{t^0_{q3}}$) are not normal to $\mathbf{c}_{0\text{pq1}}$ and not identical because the solid elements can be subjected to a cumulative twisting rotation during the response.

In the current configuration, the global nodal DOF, expressed by vector $\mathbf{p}^{\mathbf{T}}_{\text{gpq}}$, combined with $\mathbf{t}_{\text{p2}}$, $\mathbf{t}_{\text{p3}}$, $\mathbf{t}_{\text{q2}}$, $\mathbf{t}_{\text{q3}}$ and $\mathbf{t}_{\text{pq}}$ provide the local deformation in terms of $\mathbf{p}_{\text{cpq}}$ leading to an implicit nonlinear relationship between local and global degrees of freedom as specified in the following sub-section. In this way, the deformation of the interface can be measures using the following parameters reported in Figure 24, Figure 25, Figure 26:

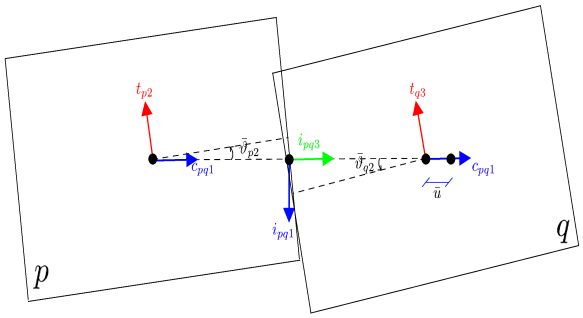

Figure 24 – Plane 1 - 2

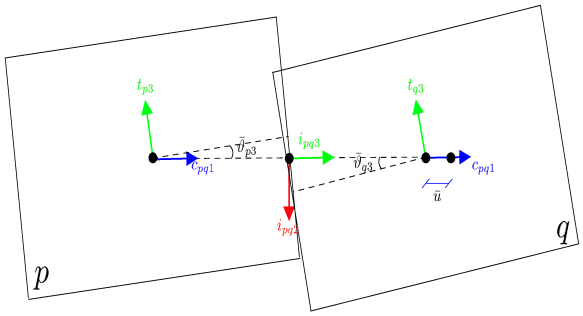

Figure 25 – Plane 1 - 3

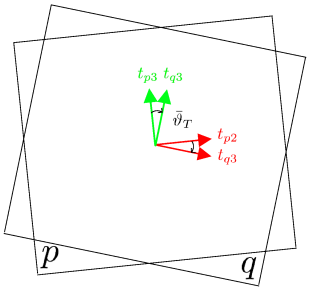

Figure 26 – Plane 2 – 3

For small increment values of the global displacements $\delta\,\mathbf{p}_{\mathrm{gpq}}$ the increment of co-rotational degrees of freedom $\delta\mathbf{p}_{\mathrm{cpq}}$ can be expressed as:

$$\delta\bar{\vartheta}_{\mathrm{p2}} = -\mathbf{c}^{\mathbf{T}}_{\mathrm{pq1}}\mathbf{t}_{\mathbf{p2}} \tag{3.47}$$

$$\delta\bar{\vartheta}_{\mathrm{p3}} = -\mathbf{c}^{\mathbf{T}}_{\mathrm{pq1}}\mathbf{t}_{\mathbf{p3}} \tag{3.48}$$

$$\delta\bar{\vartheta}_{\mathrm{q2}} = -\mathbf{c}^{\mathbf{T}}_{\mathrm{pq1}}\mathbf{t}_{\mathbf{q2}} \tag{3.49}$$

$$\delta\bar{\vartheta}_{\mathrm{q3}} = -\mathbf{c}^{\mathbf{T}}_{\mathrm{pq1}}\mathbf{t}_{\mathbf{q3}} \tag{3.50}$$

$$\delta\bar{\mathrm{u}} = \ell_{pq} - \ell_{0pq} \tag{3.51}$$

$$\delta\bar{\vartheta}_{\mathrm{T}} = \mathbf{t}^{\mathbf{T}}_{\mathbf{p3}}\mathbf{t}_{\mathbf{pq}} \tag{3.52}$$

with

$$\ell_{pq} = \left\|\mathbf{X}_{\mathrm{Gq}} - \mathbf{X}_{\mathrm{Gp}}\right\| \tag{3.53}$$

$$\ell_{0pq} = \left\|\mathbf{X}_{\mathrm{G0q}} - \mathbf{X}_{\mathrm{G0p}}\right\| \tag{3.54}$$

Figure 24, Figure 25 and Figure 26, qualitative report the increment in terms of rotations. Namely, the quantity $\delta\bar{\vartheta}_{\mathrm{p2}}$ is referred to the centroid of the element p and it is the increment of rotation in the plane 1-2; $\delta\bar{\vartheta}_{\mathrm{q2}}$ is referred to the centroid of the element q and it is the increment of rotation in the same plane 1-2; $\delta\bar{\vartheta}_{\mathrm{p3}}$ and $\delta\bar{\vartheta}_{\mathrm{q3}}$ are referred to elements p and q and are the increment of rotation in the plane 1-3. $\delta\bar{\vartheta}_{\mathrm{T}}$ is relative to the twisting increment of element q with respect to element p.

These deformative parameters are collected in the vector:

$$\delta\mathbf{p}_{\boldsymbol{cpq}} = \begin{bmatrix}\delta\bar{\vartheta}_{\mathrm{p2}} & \delta\bar{\vartheta}_{\mathrm{p3}} & \delta\bar{\vartheta}_{\mathrm{q2}} & \delta\bar{\vartheta}_{\mathrm{q3}} & \delta\bar{\mathrm{u}} & \delta\bar{\vartheta}_{\mathrm{T}} & \delta\boldsymbol{\Gamma}^{\mathbf{T}}_{\mathbf{p}} & \delta\boldsymbol{\Gamma}^{\mathbf{T}}_{\mathbf{q}}\end{bmatrix}^{\mathrm{T}} \tag{3.55}$$

It is worth noticing that the six internal degrees of freedom collected in the vectors $\delta\boldsymbol{\Gamma}^{\mathbf{T}}_{\mathbf{p}}$ and $\delta\boldsymbol{\Gamma}^{\mathbf{T}}_{\mathbf{q}}$ are not affected by the rigid motion, however they contribute to the relative displacements of the interface shared by the elements p and q.

The corresponding nodal forces are collected in the following vector:

$$\mathbf{f_C^T} = [\mathrm{f_{c1}} \quad \mathrm{f_{c2}} \quad \mathrm{f_{c3}} \quad \mathrm{f_{c4}} \quad \mathrm{f_{c5}} \quad \mathrm{f_{c6}} \quad \mathbf{f_{\Gamma p}} \quad \mathbf{f_{\Gamma q}}]^{\mathbf{T}} \tag{3.56}$$

where $\mathrm{f_{c5}}$ denotes the axial force whereas $\mathrm{f_{c1}}, \mathrm{f_{c2}}, \mathrm{f_{c3}}, \mathrm{f_{c4}}, \mathrm{f_{c6}}$ denote the moments at nodes p and q, respectively. The two vector (3x1) $\mathbf{f_{\Gamma p}}$, $\mathbf{f_{\Gamma q}}$ collect the forces related to the shear deformability of the elements.

In this and the previous paragraph two different approaches for the co-rotational framework with reference to the parametrization of rotations have been considered. In the adopted approaches, the co-rotational reference systems, the related degrees of freedom and the strategy adopted for the parametrization of large rotations have been defined. As better specified in the following, the two approaches provide different tangent matrices and are based on different incremental iterative procedures.

The transformations reported in the following, lead to evaluation of tangent stiffness matrices for both the considered strategies.

3.4.3 Interface kinematics and virtual work

In the formulation of the two-node interface it is needed to define the interface kinematics as a function of the degrees of freedom of the corresponding solid elements.

Let us consider two adjacent elements p and q sharing the i-th interface, where the p-th element is located on the bottom whereas the q-th element is located on the top, Figure 27.

It is assumed that at time t=0 the elements share a zero-thickness plane interface corresponding to the rectangular common plane. The mechanical behaviour of the interface is related to the relative displacements of the interface points of the corresponding solid elements.

The interface displacements are expressed in the local reference systems of the interface $\boldsymbol{i}_{pq1i}$ (i=1,2,3) as a function of their position identified by the coordinates x and y as follows:

$$\Delta\hat{\mathbf{u}}^{\mathbf{T}}(x,y) = [\Delta\hat{\mathrm{u}}(x,y) \quad \Delta\hat{\mathrm{v}}(x,y) \quad \Delta\widehat{\mathrm{w}}(x,y)] \tag{3.57}$$

being:

- x, y are the coordinates of the 2D planar interface in the local reference system $\mathbf{i}_{\boldsymbol{pq1}}, \mathbf{i}_{\boldsymbol{pq2}}, \mathbf{i}_{\boldsymbol{pq3}}$;
- $\Delta\hat{\mathrm{u}}(x,y)$ is the relative displacement in the in-plane $\mathbf{i}_{\boldsymbol{pq1}}$ direction between initially adjacent points of the element p and element q;
- $\Delta\hat{\mathrm{v}}(x,y)$ is the relative displacement in the in-plane $\mathbf{i}_{\boldsymbol{pq2}}$ direction between initially adjacent points of the element p and element q;
- $\Delta\widehat{\mathrm{w}}(x,y)$is the relative displacement in the out-of-plane $\mathbf{i}_{\boldsymbol{pq3}}$ direction between initially adjacent points of element p and element q;

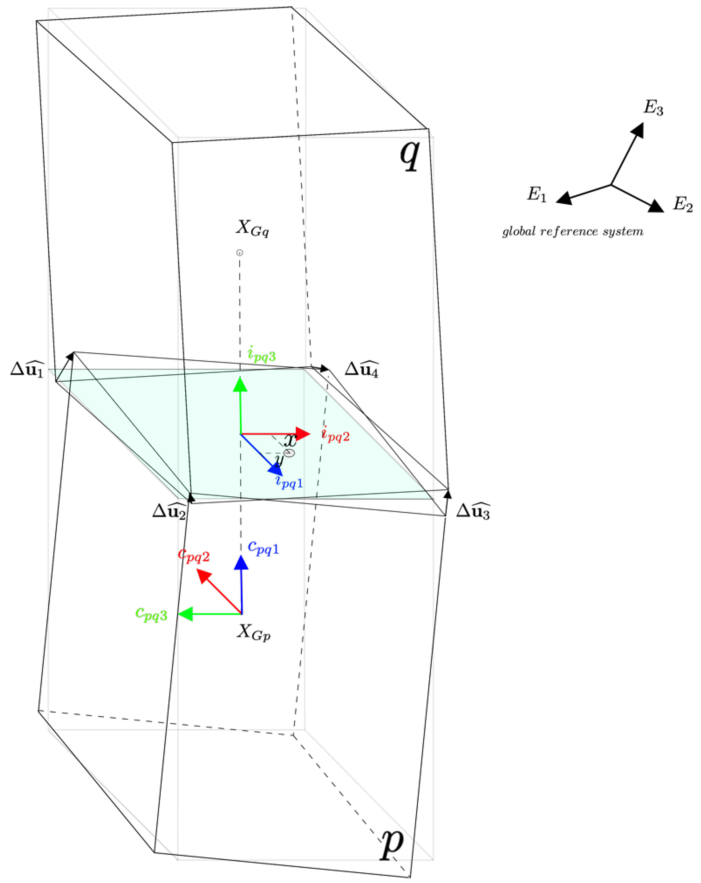

Figure 27 - Interface reference system referred to the initial configuration

In order to relate the interface displacements to the degrees of freedom of the corresponding solid elements, it is convenient to express the interface relative displacements (3.7) as a function of the displacements of the four vertices of the interface

$$\Delta\hat{\mathbf{u}}_{\mathrm{n}}^{\mathbf{T}} = [\Delta\hat{\mathrm{u}}_n \quad \Delta\hat{\mathrm{v}}_n \quad \Delta\widehat{\mathrm{w}}_n] \quad n = 1\ldots4 \tag{3.58}$$

The interface displacements can be expressed with reference to an intrinsic coordinate system as follows

$$\Delta\hat{\mathbf{u}} = \boldsymbol{\psi}\Delta\hat{\mathbf{p}}_{\ell} \tag{3.59}$$

$\Delta\hat{\mathbf{p}}_\ell^{\mathbf{T}} = [\Delta\hat{\mathbf{u}}_1^{\mathbf{T}} \quad \Delta\hat{\mathbf{u}}_2^{\mathbf{T}} \quad \Delta\hat{\mathbf{u}}_3^{\mathbf{T}} \quad \Delta\hat{\mathbf{u}}_4^{\mathbf{T}}]$ a 12x1 vector containing the relative displacement of the interface vertices and $\boldsymbol{\psi}$ a matrix containing the linear shape functions expressed as follows

$$\boldsymbol{\psi}^{\mathrm{T}} = \begin{bmatrix} \psi_1 & 0 & 0 \\ 0 & \psi_1 & 0 \\ 0 & 0 & \psi_1 \\ \psi_2 & 0 & 0 \\ 0 & \psi_2 & 0 \\ 0 & 0 & \psi_2 \\ \psi_3 & 0 & 0 \\ 0 & \psi_3 & 0 \\ 0 & 0 & \psi_3 \\ \psi_4 & 0 & 0 \\ 0 & \psi_4 & 0 \\ 0 & 0 & \psi_4 \end{bmatrix} \tag{3.60}$$

$$\begin{aligned} \psi_n = \frac{1}{4}(1+\xi\xi_n)(1+\eta\eta_n) \qquad & n = 1 \dots 4 \\ \xi_1 = -1; \quad \eta_1 = -1; & \\ \xi_2 = +1; \quad \eta_2 = -1; & \\ \xi_3 = +1; \quad \eta_3 = +1; & \\ \xi_4 = -1; \quad \eta_4 = +1; & \end{aligned} \tag{3.61}$$

As better specified in the following, the interfaces are assumed to be continuously distributed and their mechanical behaviour can be associated to general constitutive laws. In the present formulation a simplified constitutive model is considered according to the following stiffness matrix:

$$\mathbf{k}_{\mathrm{int}}(x,y) = \begin{bmatrix} \mathrm{k}_{//1}(x,y) & 0 & 0 \\ 0 & \mathrm{k}_{//2}(x,y) & 0 \\ 0 & 0 & \mathrm{k}_{\_|\_}(x,y) \end{bmatrix} \tag{3.62}$$

- $\mathrm{k}_{//1}(x,y)$ is the stiffness of the generic point of the interface along the x direction;

- $\mathrm{k}_{//2}(x, y)$ is the stiffness of the generic point of the interface along the y direction;
- $\mathrm{k}_{\_|\_}(x, y)$ is the stiffness of the generic point of the interface along the z direction;

These quantities will be evaluated in the next sub-section entitled 'mechanical characterization of the interfaces'.

The Internal Virtual Work of the interface in the local reference system can be written in the following form:

$$L_i = \iint_A \delta\Delta\hat{\mathbf{u}}^{\mathbf{T}}\mathbf{k}_{\mathrm{int}}\Delta\hat{\mathbf{u}}\, dA \tag{3.63}$$

Using the definition of total derivative, the following formula is obtained:

$$\begin{aligned} \mathrm{dx} &= \frac{\partial \mathrm{x}}{\partial \xi}\mathrm{d}\xi + \frac{\partial \mathrm{x}}{\partial \eta}\mathrm{d}\eta \\ \mathrm{dy} &= \frac{\partial \mathrm{y}}{\partial \xi}\mathrm{d}\xi + \frac{\partial \mathrm{y}}{\partial \eta}\mathrm{d}\eta \end{aligned} \tag{3.64}$$

In matrix form:

$$\begin{bmatrix} \mathrm{dx} \\ \mathrm{dy} \end{bmatrix} = \begin{bmatrix} \dfrac{\partial \mathrm{x}}{\partial \xi} & \dfrac{\partial \mathrm{x}}{\partial \eta} \\ \dfrac{\partial \mathrm{y}}{\partial \xi} & \dfrac{\partial \mathrm{y}}{\partial \eta} \end{bmatrix} \begin{bmatrix} \mathrm{d}\xi \\ \mathrm{d}\eta \end{bmatrix} \tag{3.65}$$
$$\begin{bmatrix} \mathrm{dx} \\ \mathrm{dy} \end{bmatrix} = \mathrm{J} \begin{bmatrix} \mathrm{d}\xi \\ \mathrm{d}\eta \end{bmatrix}$$

With J, Jacobian matrix of the transformation;

Using the (3.65) $\mathrm{dA} = \mathrm{dxdy}$ is equal to:

$$\mathrm{dxdy} = \det(\mathrm{J})\mathrm{d}\xi\mathrm{d}\eta \tag{3.66}$$

With (3.59)(3.66) the (3.63) is equal to:

$$L_i = \iint_{-1}^{1} \delta\Delta\hat{\boldsymbol{p}}_\ell^{\mathbf{T}} \boldsymbol{\psi}^{\mathbf{T}} \mathbf{k}_{\mathrm{int}} \boldsymbol{\psi} \Delta\hat{\boldsymbol{p}}_\ell \det(\mathrm{J}) \mathrm{d}\xi \mathrm{d}\eta \tag{3.67}$$

Using the Gauss – Legendre integration it is possible to transform the (3.67) as follow:

$$L_i \cong \delta\Delta\hat{\boldsymbol{p}}_\ell^{\mathbf{T}} \sum_{\mathrm{i}=1}^{\mathrm{N}} \sum_{\mathrm{j}=1}^{\mathrm{M}} \varpi_{\mathrm{i}} \varpi_{\mathrm{j}} \boldsymbol{\psi}^{\mathbf{T}}(\xi_{\mathrm{i}}, \eta_{\mathrm{i}}) \mathbf{k}_{\mathrm{int}} \boldsymbol{\psi}(\xi_{\mathrm{i}}, \eta_{\mathrm{i}}) \det(\mathrm{J}) \Delta\hat{\boldsymbol{p}}_\ell \tag{3.68}$$

With:

- N number of Gauss point in the ξ direction;
- M number of Gauss point in the η direction;
- ξ_{i} and η_{i} Gaussian Point;
- ϖ_{i} and ϖ_{j} Gaussian Weight;

It's important to note that the equation (3.68) can be rewritten in the following form:

$$\begin{gathered} \Delta\hat{\boldsymbol{q}}_\ell = \sum_{\mathrm{i}=1}^{\mathrm{N}} \sum_{\mathrm{j}=1}^{\mathrm{M}} \varpi_{\mathrm{i}} \varpi_{\mathrm{j}} \boldsymbol{\psi}^{\mathbf{T}}(\xi_{\mathrm{i}}, \eta_{\mathrm{i}}) \mathbf{k}_{\mathrm{int}} \boldsymbol{\psi}(\xi_{\mathrm{i}}, \eta_{\mathrm{i}}) \det(\mathrm{J}) \Delta\hat{\boldsymbol{p}}_\ell \\ L_i \cong \delta\Delta\hat{\boldsymbol{p}}_\ell^{\mathbf{T}} \Delta\hat{\boldsymbol{q}}_\ell \end{gathered} \tag{3.69}$$

The local stiffness matrix is equal to:

$$\begin{gathered} \delta\Delta\hat{\boldsymbol{q}}_\ell = \sum_{\mathrm{i}=1}^{\mathrm{N}} \sum_{\mathrm{j}=1}^{\mathrm{M}} \varpi_{\mathrm{i}} \varpi_{\mathrm{j}} \boldsymbol{\psi}^{\mathbf{T}}(\xi_{\mathrm{i}}, \eta_{\mathrm{i}}) \mathbf{k}_{\mathrm{int}} \boldsymbol{\psi}(\xi_{\mathrm{i}}, \eta_{\mathrm{i}}) \det(\mathrm{J}) \delta\Delta\hat{\boldsymbol{p}}_\ell \\ \delta\Delta\hat{\boldsymbol{q}}_\ell = \mathbf{K}_{int} \delta\Delta\hat{\boldsymbol{p}}_\ell \end{gathered} \tag{3.70}$$

With:

$$\mathbf{K}_{int} = \sum_{\mathrm{i}=1}^{\mathrm{N}} \sum_{\mathrm{j}=1}^{\mathrm{M}} \varpi_{\mathrm{i}} \varpi_{\mathrm{j}} \boldsymbol{\psi}^{\mathbf{T}}(\xi_{\mathrm{i}}, \eta_{\mathrm{i}}) \mathbf{k}_{\mathrm{int}} \boldsymbol{\psi}(\xi_{\mathrm{i}}, \eta_{\mathrm{i}}) \det(\mathrm{J}) \tag{3.71}$$

3.4.4 From local to global forces and tangent stiffness matrix

As reported in the paragraph 3.2, the matrices $\mathbf{K_c}$, $\mathbf{B}$ and $\delta\mathbf{B}^{\mathbf{T}}\mathbf{q_c}$ are needed in order to obtain stiffness matrices of the two-node interface. These matrices are different for the two considered approaches.

- $\mathbf{K_c}$ represents the co-rotational stiffness matrix and is obtained considering the relative displacement of the interface (3.7) in terms of the co-rotational degrees of freedom $\mathbf{p_c}$. A changing of variables from $\delta\Delta\hat{\mathbf{p}}_\ell \rightarrow \delta\mathbf{p_c}$ is needed, this implies a series of transformations, descripted in the following for the two considered approaches.
- $\mathbf{B}$ and $\delta\mathbf{B^T q_c}$ relate the co-rotational parameters $\mathbf{p_c}$ to the global parameters $\mathbf{p}_{\mathrm{gpq}}$.

3.4.4.1 Expression of $\Delta\boldsymbol{p}_\ell$ in the co-rotational system. Transformation $\delta\Delta\hat{\boldsymbol{p}}_\ell \rightarrow \delta\Delta\boldsymbol{p}_\ell$

The vector expressing the relative displacement of the interface vertices in the local reference system of the interface $\Delta\hat{\mathbf{p}}_\ell$ has to be expressed in the co-rotational reference system

$$\Delta\boldsymbol{p}_\ell = [\Delta\mathbf{u}_1^{\mathbf{T}} \quad \Delta\mathbf{u}_2^{\mathbf{T}} \quad \Delta\mathbf{u}_3^{\mathbf{T}} \quad \Delta\mathbf{u}_4^{\mathbf{T}}] \tag{3.72}$$

system. This transformation can be written in the form

$$\Delta\hat{\boldsymbol{p}}_\ell = \mathbf{A_1}\Delta\boldsymbol{p}_\ell \tag{3.73}$$

Being

$$\mathbf{A_1} = \begin{bmatrix} \mathbf{R}^{\mathrm{Cor}\rightarrow\mathrm{Loc}} & 0 & 0 & 0 \\ 0 & \mathbf{R}^{\mathrm{Cor}\rightarrow\mathrm{Loc}} & 0 & 0 \\ 0 & 0 & \mathbf{R}^{\mathrm{Cor}\rightarrow\mathrm{Loc}} & 0 \\ 0 & 0 & 0 & \mathbf{R}^{\mathrm{Cor}\rightarrow\mathrm{Loc}} \end{bmatrix} \tag{3.74}$$

With:

$$\mathbf{R}^{\mathrm{Cor}\rightarrow\mathrm{Loc}} = \mathbf{R}_{\mathrm{0pqint}}\mathbf{R}_{\mathbf{C0}}^{\mathbf{T}} \tag{3.75}$$

It is worth to notice that, since the interface deformations are small, it can be assumed that the local reference system of the interface is

subjected to the same rigid motion of the co-rotational system at every step of the analysis

$$\mathbf{R_{0pqint}}\mathbf{R_{C0}^T} = \mathbf{R_{pqint}}\mathbf{R_C^T} \tag{3.76}$$

Where $\mathbf{R_{pqint}}$ and $\mathbf{R_C}$ are respectively matrices of the reference system of the interface and co-rotational reference system in current configurations.

As a consequence, the variation of relationship (3.73) is simply expressed by

$$\delta\Delta\hat{\boldsymbol{p}}_\ell = \mathbf{A_1}\delta\Delta\boldsymbol{p}_\ell \tag{3.77}$$

3.4.4.2 Expression of $\delta\Delta\boldsymbol{p}_\ell$ as a function of the node displacement of the adjacent solid elements. Transformation $\delta\Delta\boldsymbol{p}_\ell \rightarrow \delta\boldsymbol{p}_{pq}$

The components of vector $\Delta\boldsymbol{p}_\ell$ are the relative displacement of vertices of the *pq* interface. This vector can be expressed as a function of the corresponding displacements of the solid elements. By collecting in a vector $\boldsymbol{p}_{\mathrm{pq}}$ the vertices' displacement of each element:

$$\boldsymbol{p}_{\mathrm{pq}}^{\mathbf{T}} = [\mathbf{u}_{\mathrm{q1}}^{\mathbf{T}} \quad \mathbf{u}_{\mathrm{q2}}^{\mathbf{T}} \quad \mathbf{u}_{\mathrm{q3}}^{\mathbf{T}} \quad \mathbf{u}_{\mathrm{q4}}^{\mathbf{T}} \quad \mathbf{u}_{\mathrm{p1}}^{\mathbf{T}} \quad \mathbf{u}_{\mathrm{p2}}^{\mathbf{T}} \quad \mathbf{u}_{\mathrm{p3}}^{\mathbf{T}} \quad \mathbf{u}_{\mathrm{p4}}^{\mathbf{T}}] \tag{3.78}$$

expressed in the co-rotational reference system. The kinematic relationship between $\Delta\boldsymbol{p}_\ell$ and $\boldsymbol{p}_{\mathrm{pq}}$ is given by:

$$\Delta\boldsymbol{p}_\ell = [-\mathbf{I}_{12\mathrm{x}12} \quad \mathbf{I}_{12\mathrm{x}12}]\boldsymbol{p}_{\mathrm{pq}} = \mathbf{A_2}\boldsymbol{p}_{\mathrm{pq}} \tag{3.79}$$

With $\mathbf{I}_{12\mathrm{x}12}$ identity matrix 12x12 and $\mathbf{A_2} = [-\mathbf{I}_{12\mathrm{x}12} \quad \mathbf{I}_{12\mathrm{x}12}]$. Therefore the following transformation holds:

$$\delta\Delta\boldsymbol{p}_\ell = \mathbf{A_2}\delta\boldsymbol{p}_{\mathrm{pq}} \tag{3.80}$$

3.4.4.3 Expression of $\delta \boldsymbol{p}_{pq}$ as a function of the co-rotational degrees of freedom for the Approach I. Transformation $\delta \boldsymbol{p}_{pq} \rightarrow \delta \boldsymbol{p}_{\boldsymbol{c}}$

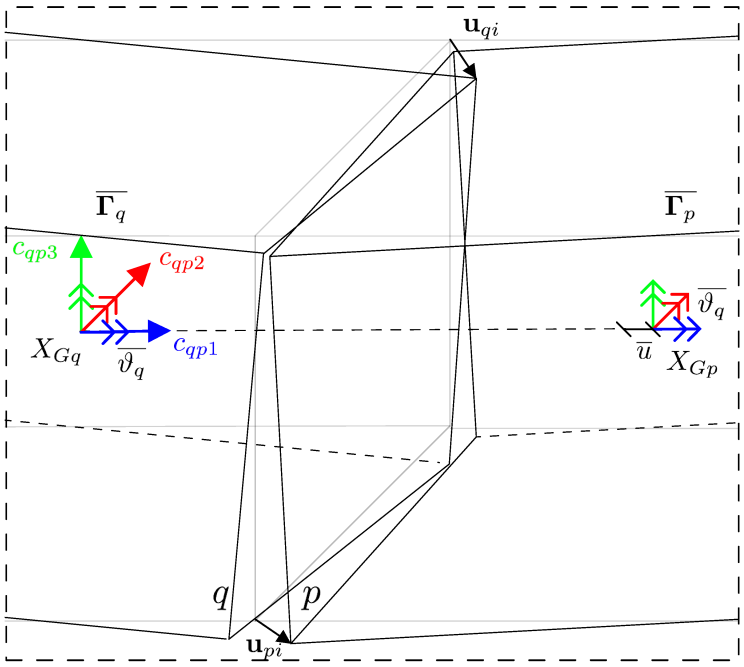

Figure 28 – Kinematic transformation between nodal displacement and co-rotational parameters;

In the following, the nodal displacement of the vertices of the interface for each solid element are expressed as a function of the co-rotational reference system.

In this reference system only deformational quantities are evaluated so the rotational components can be considered small and additive.

- vertices interface displacements of the element $\boldsymbol{p}$

The vertices displacements of the interface belonging to the element p can be expressed as:

$$\mathbf{u_{pi}} = \tilde{\bar{\boldsymbol{\vartheta}}}_{\mathbf{p}} \mathbf{x_{pi0}} + \overline{\mathbf{E}}_{\mathbf{cp}} \mathbf{x_{pi0}} \tag{3.81}$$

being:

- $\tilde{\bar{\boldsymbol{\vartheta}}}_{\mathbf{p}} = \begin{bmatrix} 0 & -\bar{\vartheta}_{p3} & \bar{\vartheta}_{p2} \\ \bar{\vartheta}_{p3} & 0 & -\bar{\vartheta}_{p1} \\ -\bar{\vartheta}_{p2} & \bar{\vartheta}_{p1} & 0 \end{bmatrix}$ the skew-matrix related to the small incremental rotation of the element p;
- $\mathbf{E_{cp}}$ the strain tensor that descript the pure shear deformation in local reference system of the element p whose counterpart in the co-rotational reference system is given by:

$$\overline{\mathbf{E}}_{\mathbf{cp}} = \mathbf{R}^{\mathbf{T}}_{\mathbf{C0}} \mathbf{R}_{\mathbf{p0}} \overline{\mathbf{E}} \mathbf{R}^{\mathbf{T}}_{\mathbf{p0}} \mathbf{R}_{\mathbf{C0}} \tag{3.82}$$

- $\mathbf{x_{pi}}$ (i=1..4) identify the position vectors of the element vertices in the co-rotational reference system:

$$\mathbf{x_{pi0}} = \mathbf{R}^{\mathbf{T}}_{\mathbf{C0}} (\mathbf{X_{pi0}} - \mathbf{X_{Gp0}}) \tag{3.83}$$

In view of the expressions (3.82) and (3.83) the (3.81) becomes:

$$\mathbf{u_{pi}} = \tilde{\bar{\boldsymbol{\vartheta}}}_{\mathbf{p}} \mathbf{R}^{\mathbf{T}}_{\mathbf{C0}} (\mathbf{X_{pi0}} - \mathbf{X_{Gp0}}) + \mathbf{R}^{\mathbf{T}}_{\mathbf{C0}} \mathbf{R}_{\mathbf{p0}} \overline{\mathbf{E}} \mathbf{R}^{\mathbf{T}}_{\mathbf{p0}} (\mathbf{X_{pi0}} - \mathbf{X_{Gp0}}) \tag{3.84}$$

whose variation is given by:

$$\delta\mathbf{u_{pi}} = \delta\tilde{\bar{\boldsymbol{\vartheta}}}_{\mathbf{p}} \mathbf{R}^{\mathbf{T}}_{\mathbf{C0}} (\mathbf{X_{pi0}} - \mathbf{X_{Gp0}}) + \mathbf{R}^{\mathbf{T}}_{\mathbf{C0}} \mathbf{R}_{\mathbf{p0}} \delta\overline{\mathbf{E}} \mathbf{R}^{\mathbf{T}}_{\mathbf{p0}} (\mathbf{X_{pi0}} - \mathbf{X_{Gp0}}) \tag{3.85}$$

Using the following property of skew matrix:

$$\tilde{\boldsymbol{a}}\boldsymbol{b} = -\tilde{\boldsymbol{b}}\boldsymbol{a} \tag{3.86}$$

the equation (3.85) can be written in the following form:

$$\delta\mathbf{u_{pi}} = -\left(\mathbf{R}^{\mathbf{T}}_{\mathbf{C0}} (\widetilde{\mathbf{X_{pi0}} - \mathbf{X_{Gp0}}})\right) \delta\bar{\boldsymbol{\vartheta}}_{\mathbf{p}} - \mathbf{R}^{\mathbf{T}}_{\mathbf{C0}} \mathbf{R}_{\mathbf{p0}} \delta\overline{\mathbf{E}} \mathbf{R}^{\mathbf{T}}_{\mathbf{p0}} (\mathbf{X_{pi0}} - \mathbf{X_{Gp0}}) \tag{3.87}$$

After some manipulation the following equation is obtained

$$\delta \mathbf{u_{pi}} = \mathbf{C_{pi}} \delta \mathbf{p_c} \tag{3.88}$$

- *vertices interface displacements of the element* $\boldsymbol{q}$

The vertices displacements of the interface belonging to the element q can be expressed as:

$$\mathbf{u_{qi}} = \boldsymbol{\Delta} + \tilde{\bar{\boldsymbol{\vartheta}}}_{\mathbf{q}} \mathbf{x_{qi0}} + \bar{\mathbf{E}}_{\mathbf{cq}} \mathbf{x_{qi0}} \tag{3.89}$$

being:

- $\boldsymbol{\Delta}^{\mathbf{T}} = [\bar{\mathrm{u}} \quad 0 \quad 0]^{\boldsymbol{T}}$ the deformation in the direction $\mathbf{c}_{pq1}$,with $\bar{\mathrm{u}}$ the variation of distance between the centroids of the two elements;
- $\tilde{\bar{\boldsymbol{\vartheta}}}_{\mathbf{q}} = \begin{bmatrix} 0 & -\vartheta_{q3} & \vartheta_{q2} \\ \vartheta_{q3} & 0 & -\vartheta_{q1} \\ -\vartheta_{q2} & \vartheta_{q1} & 0 \end{bmatrix}$ the skew-matrix related to the small incremental rotation of the element q;
- $\mathbf{E_{cq}}$ the strain tensor that descript the pure shear deformation in local reference system of the element q whose counterpart in the co-rotational reference system is given by:

$$\mathbf{E_{cq}} = \mathbf{R_{C0}^T R_{q0}} \bar{\mathbf{E}} \mathbf{R_{q0}^T R_{C0}} \tag{3.90}$$

- $\mathbf{x_{qi}}$ (i=1..4) identify the position vectors of the element vertices in the co-rotational reference system:

$$\mathbf{x_{qi0}} = \mathbf{R_{C0}^T} (\mathbf{X_{qi0}} - \mathbf{X_{Gq0}}) \tag{3.91}$$

Using the (3.90) and (3.91), the (3.89) becomes:

$$\mathbf{u_{qi}} = \boldsymbol{\Delta} + \tilde{\bar{\boldsymbol{\vartheta}}}_{\mathbf{q}} \mathbf{R_{C0}^T} (\mathbf{X_{qi0}} - \mathbf{X_{Gq0}}) + \mathbf{R_{C0}^T R_{q0}} \bar{\mathbf{E}} \mathbf{R_{q0}^T} (\mathbf{X_{qi0}} - \mathbf{X_{Gq0}}) \tag{3.92}$$

whose variation is equal to:

$$\delta\mathbf{u_{qi}} = \delta\boldsymbol{\Delta} + \delta\tilde{\bar{\boldsymbol{\vartheta}}}_{\mathbf{q}}\mathbf{R}^{\mathbf{T}}_{\mathbf{C0}}(\mathbf{X_{qi0}} - \mathbf{X_{Gq0}}) + \mathbf{R}^{\mathbf{T}}_{\mathbf{C0}}\mathbf{R_{q0}}\delta\bar{\mathbf{E}}\mathbf{R}^{\mathbf{T}}_{\mathbf{q0}}(\mathbf{X_{qi0}} - \mathbf{X_{Gq0}}) \tag{3.93}$$

In view of the (3.86) the (3.93) becomes:

$$\delta\mathbf{u_{qi}} = \delta\boldsymbol{\Delta} - \left(\mathbf{R}^{\mathbf{T}}_{\mathbf{C0}}(\widetilde{\mathbf{X_{qi0}} - \mathbf{X_{Gq0}}})\right)\delta\bar{\boldsymbol{\vartheta}}_{\mathbf{q}} - \mathbf{R}^{\mathbf{T}}_{\mathbf{C0}}\mathbf{R_{q0}}\delta\bar{\mathbf{E}}\mathbf{R}^{\mathbf{T}}_{\mathbf{q0}}(\mathbf{X_{qi0}} - \mathbf{X_{Gq0}}) \tag{3.94}$$

After some algebraic manipulations, the previous equation can be written in the following form:

$$\delta\mathbf{u_{qi}} = \mathbf{C_{qi}}\delta\mathbf{p_c} \tag{3.95}$$

Combining the equation (3.88) and (3.95) the following expression is obtained:

$$\delta\mathbf{p_{pq}} = \mathbf{A_3}\delta\mathbf{p_c} \tag{3.96}$$

Being the interfaces subjected to small relative displacements, the matrix $\mathbf{A_3} = [\mathbf{C_{pi}}\ \mathbf{C_{qi}}]$, that relates the interface vertices displacements of the elements p and q to the co-rotational degrees of freedom, is calculated at the beginning of the analysis and maintained constant.

3.4.4.1 Expression of $\delta\boldsymbol{p}_{pq}$ as a function of the co-rotational degrees of freedom for the Approach II. Transformation $\delta\boldsymbol{p}_{pq} \rightarrow \delta\boldsymbol{p}_{\boldsymbol{c}}$

Following the same algebraic manipulation considered in the previous paragraph the following expressions relative to the approach II are given

- vertices interface displacements of the element $\boldsymbol{p}$

The vertices displacements of the interface belonging to the element p can be expressed as:

$$\mathbf{u_{pi}} = \tilde{\bar{\boldsymbol{\vartheta}}}_{\mathbf{p}} \mathbf{x_{pi0}} + \mathbf{E_{cp}} \mathbf{x_{pi0}} \tag{3.97}$$

being:

- $\tilde{\bar{\boldsymbol{\vartheta}}}_{\mathbf{p}} = \begin{bmatrix} 0 & -\bar{\vartheta}_{p2} & -\bar{\vartheta}_{p3} \\ \bar{\vartheta}_{p2} & 0 & 0 \\ \bar{\vartheta}_{p3} & 0 & 0 \end{bmatrix}$ the rotational matrix of element p;
- $\mathbf{E_{cp}}$ the shear deformation strain tensor of the element p whose counterpart in the co-rotational reference system is given by:

$$\overline{\mathbf{E}}_{\mathbf{cp}} = \mathbf{R}_{\mathbf{C0}}^{\mathbf{T}} \mathbf{R}_{\mathbf{p0}} \overline{\mathbf{E}} \mathbf{R}_{\mathbf{p0}}^{\mathbf{T}} \mathbf{R}_{\mathbf{C0}} \tag{3.98}$$

- $\mathbf{x_{qi}}$ (i=1..4) identify the position vectors of the element p vertices in the co-rotational reference system:

$$\mathbf{x_{pi0}} = \mathbf{R}_{\mathbf{C0}}^{\mathbf{T}} (\mathbf{X_{pi0}} - \mathbf{X_{Gp0}}) \tag{3.99}$$

Using the (3.98) and (3.99) the (3.97) becomes:

$$\mathbf{u_{pi}} = \tilde{\bar{\boldsymbol{\vartheta}}}_{\mathbf{p}} \mathbf{R}_{\mathbf{C0}}^{\mathbf{T}} (\mathbf{X_{pi0}} - \mathbf{X_{Gp0}}) + \mathbf{R}_{\mathbf{C0}}^{\mathbf{T}} \mathbf{R}_{\mathbf{p0}} \overline{\mathbf{E}} \mathbf{R}_{\mathbf{p0}}^{\mathbf{T}} (\mathbf{X_{pi0}} - \mathbf{X_{Gp0}}) \tag{3.100}$$

The variation of the (3.100) is given by:

$$\delta \mathbf{u_{pi}} = \delta \tilde{\bar{\boldsymbol{\vartheta}}}_{\mathbf{p}} \mathbf{R}_{\mathbf{C0}}^{\mathbf{T}} (\mathbf{X_{pi0}} - \mathbf{X_{Gp0}}) + \mathbf{R}_{\mathbf{C0}}^{\mathbf{T}} \mathbf{R}_{\mathbf{p0}} \delta \overline{\mathbf{E}} \mathbf{R}_{\mathbf{p0}}^{\mathbf{T}} (\mathbf{X_{pi0}} - \mathbf{X_{Gp0}}) \tag{3.101}$$

After some algebraic manipulations, equation (3.101) can be written in the following form:

$$\delta \mathbf{u_{pi}} = \mathbf{C_{pi}} \delta \mathbf{p_c} \tag{3.102}$$

- vertices interface displacements of the element ***q***

The vertices displacements of the interface belonging to the element q can be expressed as:

$$\mathbf{u_{qi}} = \mathbf{\Delta} + \tilde{\bar{\vartheta}}_{\mathbf{q}}\mathbf{x_{qi0}} + \bar{\mathbf{E}}_{\mathbf{cq}}\mathbf{x_{qi0}} \tag{3.103}$$

With:

- $\mathbf{\Delta^T} = [\bar{\mathrm{u}} \quad 0 \quad 0]^{\boldsymbol{T}}$ deformation in the direction $\mathbf{c}_{pq1}$, $\bar{\mathrm{u}}$ represents the distance between the centroids of the two elements;
- $\tilde{\bar{\vartheta}}_{\mathbf{q}} = \begin{bmatrix} 0 & -\bar{\vartheta}_{\mathrm{q2}} & -\bar{\vartheta}_{\mathrm{q3}} \\ \bar{\vartheta}_{\mathrm{q2}} & 0 & -\bar{\vartheta}_{\mathrm{T}} \\ \bar{\vartheta}_{\mathrm{q3}} & \bar{\vartheta}_{\mathrm{T}} & 0 \end{bmatrix}$ the rotational matrix of element p;
- $\mathbf{E_{cq}}$ the shear deformation strain tensor of the element q whose counterpart in the co-rotational reference system is given by:

$$\mathbf{E_{cq}} = \mathbf{R^T_{C0}R_{q0}}\bar{\mathbf{E}}\mathbf{R^T_{q0}R_{C0}} \tag{3.104}$$

- $\mathbf{x_{qi}}$ (i=1..4) identify the position vectors of the element p vertices in the co-rotational reference system:

$$\mathbf{x_{qi0}} = \mathbf{R^T_{C0}}(\mathbf{X_{qi0}} - \mathbf{X_{Gq0}}) \tag{3.105}$$

Using the (3.104) and (3.105), the (3.103) becomes:

$$\mathbf{u_{qi}} = \mathbf{\Delta} + \tilde{\bar{\vartheta}}_{\mathbf{q}}\mathbf{R^T_{C0}}(\mathbf{X_{qi0}} - \mathbf{X_{Gq0}}) + \mathbf{R^T_{C0}R_{q0}}\bar{\mathbf{E}}\mathbf{R^T_{q0}}(\mathbf{X_{qi0}} - \mathbf{X_{Gq0}}) \tag{3.106}$$

The variation of the is provided by:

$$\delta\mathbf{u_{qi}} = \delta\tilde{\bar{\vartheta}}_{\mathbf{p}}\mathbf{R^T_{C0}}(\mathbf{X_{qi0}} - \mathbf{X_{Gq0}}) + \mathbf{R^T_{C0}R_{q0}}\delta\bar{\mathbf{E}}\mathbf{R^T_{q0}}(\mathbf{X_{qi0}} - \mathbf{X_{Gq0}}) \tag{3.107}$$

After some algebraic manipulations, the equation (3.107) can be written in the following form:

$$\delta \mathbf{u_{qi}} = \mathbf{C_{qi}} \delta \mathbf{p_c} \tag{3.108}$$

Combining the equation (3.102) and (3.106) the following expression is obtained:

$$\delta \mathbf{p_{pq}} = \mathbf{A_3} \delta \mathbf{p_c} \tag{3.109}$$

The matrix $\mathbf{A_3} = [\mathbf{C_{pi}}\ \mathbf{C_{qi}}]$, having 24x12 elements, is considered constant during the entire analysis because being the interface subjected to small deformations.

3.4.4.2 The co-rotational stiffness matrix $\boldsymbol{K_c}$

The transformations reported in the previous paragraphs allow to express the correspondence between the interface relative displacements expressed in the local reference system of the interface and the co-rotational degrees of freedom, $\delta \Delta \hat{\boldsymbol{p}}_\ell \rightarrow \delta \boldsymbol{p}_\mathrm{c}$, as follows:

$$\begin{gathered} \delta \Delta \hat{\boldsymbol{p}}_\ell \rightarrow \delta \Delta \boldsymbol{p}_\ell \rightarrow \delta \boldsymbol{p}_{pq} \rightarrow \delta \boldsymbol{p}_\mathrm{c} \\ \delta \Delta \hat{\boldsymbol{p}}_\ell = \mathbf{A_1 A_2 A_3} \delta \boldsymbol{p}_\mathrm{c} \end{gathered} \tag{3.110}$$

The interface contribution to the internal virtual work in the co-rotational reference system can be written as:

$$\delta \boldsymbol{p}_\mathrm{c}^\mathbf{T} \boldsymbol{q}_\mathrm{c} = \delta \Delta \hat{\boldsymbol{p}}_\ell^\mathbf{T} \Delta \hat{\boldsymbol{q}}_\ell \tag{3.111}$$

substituting the (3.110) into (3.111):

$$\begin{aligned} \delta \boldsymbol{p}_\mathrm{c}^\mathbf{T} \boldsymbol{q}_\mathrm{c} &= \delta \boldsymbol{p}_\mathrm{c}^\mathbf{T} \mathbf{A_3^T A_2^T A_1^T} \Delta \hat{\boldsymbol{q}}_\ell \qquad \forall \delta \boldsymbol{p}_\mathrm{c}^\mathbf{T} \\ \boldsymbol{q}_\mathrm{c} &= \mathbf{A_3^T A_2^T A_1^T} \Delta \hat{\boldsymbol{q}}_\ell \\ \delta \boldsymbol{q}_\mathrm{c} &= \mathbf{A_3^T A_2^T A_1^T} \delta \Delta \hat{\boldsymbol{q}}_\ell \end{aligned} \tag{3.112}$$

The stiffness matrix $\mathbf{K_c}$ rule the correspondence between the displacements $\delta \mathbf{p_c}$ and the corresponding conjugate forces $\delta \mathbf{q_c}$, according to the equation (3.7). In view of equations (3.110) and (3.112) the expression of $\mathbf{K_c}$ is obtained:

$$\mathbf{K_c} = \mathbf{A_3^T A_2^T A_1^T K_{int} A_1 A_2 A_3} \tag{3.113}$$

In the following paragraph the matrix $\mathbf{B}$ and $\boldsymbol{\delta}\mathbf{B}$ are evaluated.

3.4.4.3 Transformation $\delta \boldsymbol{p}_{\mathbf{c}} \rightarrow \delta \boldsymbol{p}_{gpq}$ and evaluation of $\boldsymbol{B}$ matrix for the Approach I

As reported in section 3.2, the $\mathbf{B}$ matrix is a compatibility kinematic matrix between global and co-rotational displacements, $\delta\mathbf{p_c} = \mathbf{B}(\mathbf{p_g})\delta\mathbf{p_{gpq}}$.This transformation involves the large rotations that are attributed to the co-rotational reference system.

In the following the transformations for the co-rotational degrees of freedom adopted in the approach I are evaluated.

- variation of the displacement $\bar{\mathrm{u}}$

The variation of the co-rotational axial displacement $\bar{\mathrm{u}}$, eq. (3.51), is given by:

$$\delta\bar{\mathrm{u}} = \delta\ell_{pq} = \mathbf{c}\boldsymbol{\delta}\mathbf{p_{gpq}} \tag{3.114}$$

With:

$$\mathbf{c} = [-\mathbf{c_{pq1}^T} \quad \mathbf{0_{1x3}} \quad \mathbf{c_{pq1}^T} \quad \mathbf{0_{1x3}} \quad \mathbf{0_{1x3}} \quad \mathbf{0_{1x3}}] \tag{3.115}$$

- variation of the rotational degrees of freedom $\bar{\boldsymbol{\vartheta}}_{\mathrm{p}}^{\mathrm{T}}$ *and* $\bar{\boldsymbol{\vartheta}}_{\mathrm{q}}^{\mathrm{T}}$

The variation of the rotational degrees of freedom is evaluated starting from the expression (3.32) that reports the rotational matrices containing the deformational part of the motion for the generic solid element *i*.

$$\delta\bar{\mathbf{R}}_i = \delta\mathbf{R}_{\mathrm{C}}^T\mathbf{R}_{\mathrm{iG}}\mathbf{R}_{0\mathrm{C}} + \mathbf{R}_{\mathrm{C}}^T\delta\mathbf{R}_{\mathrm{iG}}\mathbf{R}_{0\mathrm{C}} \tag{3.116}$$

The $\delta\mathbf{R}_{\mathrm{C}}^T$ and $\delta\mathbf{R}_{\mathrm{iG}}$ are computed using the spatial form of the equation (A.16)

$$\delta\mathbf{R}_{\mathrm{iG}} = \delta\tilde{\boldsymbol{\vartheta}}_{\mathbf{iG}}\mathbf{R}_{\mathrm{iG}} \qquad with \quad \mathrm{i} = \mathrm{p}, \mathrm{q} \tag{3.117}$$

And:

$$\delta\mathbf{R}_{\mathbf{C}} = \delta\tilde{\boldsymbol{\vartheta}}_{\mathbf{C}}\mathbf{R}_{\mathbf{C}} \tag{3.118}$$

$$\delta\bar{\mathbf{R}}_i = \delta\bar{\tilde{\boldsymbol{\vartheta}}}_{\mathbf{i}}\bar{\mathbf{R}}_i \tag{3.119}$$

$\delta\mathbf{R}_{\mathbf{C}}$ is calculated using the orthogonality condition $\mathbf{R}_{\mathbf{C}}\mathbf{R}_{\mathbf{C}}^{\mathbf{T}} = \mathbf{I}$:

$$\delta\mathbf{R}_{\mathbf{C}}\mathbf{R}_{\mathbf{C}}^{\mathbf{T}} + \mathbf{R}_{\mathbf{C}}\delta\mathbf{R}_{\mathbf{C}}^{\mathbf{T}} = \mathbf{0} \tag{3.120}$$

Substituting the (3.118) into (3.120):

$$\delta\tilde{\boldsymbol{\vartheta}}_{\mathbf{C}}\mathbf{R}_{\mathbf{C}}\mathbf{R}_{\mathbf{C}}^{\mathbf{T}} + \mathbf{R}_{\mathbf{C}}\delta\mathbf{R}_{\mathbf{C}}^{\mathbf{T}} = \mathbf{0} \tag{3.121}$$

$$\delta\mathbf{R}_{\mathbf{C}}^{\mathbf{T}} = -\mathbf{R}_{\mathbf{C}}^{\mathbf{T}}\delta\tilde{\boldsymbol{\vartheta}}_{\mathbf{C}} \tag{3.122}$$

Using the (3.117), (3.119), (3.122) equation (3.116) becomes:

$$\delta\bar{\tilde{\boldsymbol{\vartheta}}}_{\mathbf{i}}\bar{\mathbf{R}}_i = -\mathbf{R}_{\mathbf{C}}^{\mathbf{T}}\delta\tilde{\boldsymbol{\vartheta}}_{\mathbf{C}}\mathbf{R}_{\mathrm{iG}}\mathbf{R}_{0\mathrm{C}} + \mathbf{R}_{\mathrm{C}}^{T}\delta\tilde{\boldsymbol{\vartheta}}_{\mathbf{iG}}\mathbf{R}_{\mathrm{iG}}\mathbf{R}_{0\mathrm{C}} \tag{3.123}$$

$$\delta\bar{\tilde{\boldsymbol{\vartheta}}}_{\mathbf{i}}\bar{\mathbf{R}}_i = -\mathbf{R}_{\mathbf{C}}^{\mathbf{T}}\delta\tilde{\boldsymbol{\vartheta}}_{\mathbf{C}}\mathbf{R}_{\mathbf{C}}\mathbf{R}_{\mathbf{C}}^{\mathbf{T}}\mathbf{R}_{\mathrm{iG}}\mathbf{R}_{0\mathrm{C}} + \mathbf{R}_{\mathrm{C}}^{T}\delta\tilde{\boldsymbol{\vartheta}}_{\mathbf{iG}}\mathbf{R}_{\mathbf{C}}\mathbf{R}_{\mathbf{C}}^{\mathbf{T}}\mathbf{R}_{\mathrm{iG}}\mathbf{R}_{0\mathrm{C}} \tag{3.124}$$

It is possible to define the following quantities:

$$\delta\tilde{\boldsymbol{\vartheta}}_{\mathbf{C}}^{\boldsymbol{e}} = \mathbf{R}_{\mathbf{C}}^{\mathbf{T}}\delta\tilde{\boldsymbol{\vartheta}}_{\mathbf{C}}\mathbf{R}_{\mathbf{C}} \tag{3.125}$$

$$\delta\tilde{\boldsymbol{\vartheta}}_{\mathbf{iG}}^{\boldsymbol{e}} = \mathbf{R}_{\mathbf{C}}^{\mathbf{T}}\delta\tilde{\boldsymbol{\vartheta}}_{\mathbf{iG}}\mathbf{R}_{\mathbf{C}} \tag{3.126}$$

$\delta\tilde{\boldsymbol{\vartheta}}_{\mathbf{C}}^{\boldsymbol{e}}$ and $\delta\tilde{\boldsymbol{\vartheta}}_{\mathbf{iG}}^{\boldsymbol{e}}$ are skew - matrices rotated in the co-rotational reference system.

Substituting equations (3.125), (3.126) into (3.124), the following equation is obtained:

$$\delta\bar{\tilde{\boldsymbol{\vartheta}}}_{\mathbf{i}} = \left(\delta\tilde{\boldsymbol{\vartheta}}_{\mathbf{iG}}^{\mathbf{e}} - \delta\tilde{\boldsymbol{\vartheta}}_{\mathbf{C}}^{\mathbf{e}}\right) \tag{3.127}$$

The equation (3.127) involve skew-matrices. It is possible to change from this matrix notation to a vector notation without introducing error. Therefore equation (3.127) can be rewritten as:

$$\delta\bar{\boldsymbol{\vartheta}}_{\mathbf{i}} = \delta\boldsymbol{\vartheta}^{\mathbf{e}}_{\mathbf{iG}} - \delta\boldsymbol{\vartheta}^{\mathbf{e}}_{\mathbf{C}} \qquad \text{with} \quad \mathrm{i} = \mathrm{p}, \mathrm{q} \tag{3.128}$$

It's important to note that a vector $\mathbf{x}_{\boldsymbol{G}}$ and the skew-matrix $\hat{\mathbf{x}}_{\boldsymbol{G}}$ in the global reference system can be obtained in the local reference system using the following equations:

$$\mathbf{x}^{\mathbf{e}}_{\boldsymbol{G}} = \mathbf{R}^{\mathbf{T}}_{\mathrm{C}}\mathbf{x}_{\boldsymbol{G}} \quad \tilde{\mathbf{x}}^{\mathbf{e}}_{\boldsymbol{G}} = \mathbf{R}^{\mathbf{T}}_{\mathrm{C}}\tilde{\mathbf{x}}_{\boldsymbol{G}}\mathbf{R}_{\mathbf{C}} \tag{3.129}$$

So, the following vectors are defined:

$$\mathbf{p}^{\mathbf{e}}_{\mathrm{gpq}}{}^{\mathrm{T}} = [\mathbf{u}^{\mathbf{e}}_{\mathbf{pG}}{}^{\mathbf{T}} \quad \boldsymbol{\vartheta}^{\mathbf{e}}_{\mathbf{pG}}{}^{\mathbf{T}} \quad \mathbf{u}^{\mathbf{e}}_{\mathbf{qG}}{}^{\mathbf{T}} \quad \boldsymbol{\vartheta}^{\mathbf{e}}_{\mathbf{qG}}{}^{\mathbf{T}} \quad \boldsymbol{\Gamma}^{\mathbf{T}}_{\mathbf{p}} \quad \boldsymbol{\Gamma}^{\mathbf{T}}_{\mathbf{q}}] \tag{3.130}$$

- $\mathbf{p}^{\mathbf{e}}_{\mathbf{g}}$ is the global degrees of freedom vector evaluated in the co-rotational reference system.

$$\delta\mathbf{p}^{\mathbf{e}}_{\mathbf{gpq}} = \mathbf{L}^{\mathbf{T}}\delta\mathbf{p}_{\mathbf{gpq}} \tag{3.131}$$

With:

$$\mathbf{L} = \begin{bmatrix} \mathbf{R_C} & \mathbf{0} & \mathbf{0} & \mathbf{0} & \mathbf{0} & \mathbf{0} \\ \mathbf{0} & \mathbf{R_C} & \mathbf{0} & \mathbf{0} & \mathbf{0} & \mathbf{0} \\ \mathbf{0} & \mathbf{0} & \mathbf{R_C} & \mathbf{0} & \mathbf{0} & \mathbf{0} \\ \mathbf{0} & \mathbf{0} & \mathbf{0} & \mathbf{R_C} & \mathbf{0} & \mathbf{0} \\ \mathbf{0} & \mathbf{0} & \mathbf{0} & \mathbf{0} & \mathbf{I} & \mathbf{0} \\ \mathbf{0} & \mathbf{0} & \mathbf{0} & \mathbf{0} & \mathbf{0} & \mathbf{I} \end{bmatrix} \tag{3.132}$$

Quantities $\boldsymbol{\Gamma}^{\mathbf{T}}_{\mathbf{q}}$ and $\boldsymbol{\Gamma}^{\mathbf{T}}_{\mathbf{p}}$ are not transformed because are always considered as local parameters.

Using the chain rule $\delta\bar{\boldsymbol{\vartheta}}_{\mathbf{i}}$ is given by:

$$\delta\bar{\boldsymbol{\vartheta}}_{\mathbf{i}} = \frac{\partial\bar{\boldsymbol{\vartheta}}_{\mathbf{i}}}{\partial\mathbf{p}^{\mathbf{e}}_{\mathbf{gpq}}}\frac{\partial\mathbf{p}^{\mathbf{e}}_{\mathbf{gpq}}}{\partial\mathbf{p}_{\mathbf{gpq}}}\delta\mathbf{p}_{\mathbf{gpq}} = \frac{\partial\bar{\boldsymbol{\vartheta}}_{\mathbf{i}}}{\partial\mathbf{p}^{\mathbf{e}}_{\mathbf{gpq}}}\mathbf{L}^{\mathbf{T}}\delta\mathbf{p}_{\mathbf{gpq}} \qquad \text{with } \mathrm{i} = \mathrm{p}, \mathrm{q} \tag{3.133}$$

Being:

$$\mathbf{L^T} = \frac{\partial \mathbf{p^e_{gpq}}}{\partial \mathbf{p_{gpq}}} \tag{3.134}$$

In view of (3.128) the following expression can be rewritten as:

$$\begin{bmatrix} \delta\bar{\boldsymbol{\vartheta}}_\mathbf{q} \\ \delta\bar{\boldsymbol{\vartheta}}_\mathbf{p} \\ \delta\boldsymbol{\Gamma}_\mathbf{q} \\ \delta\boldsymbol{\Gamma}_\mathbf{p} \end{bmatrix} = \left(\begin{bmatrix} \mathbf{0} & \mathbf{I} & \mathbf{0} & \mathbf{0} & \mathbf{0} & \mathbf{0} \\ \mathbf{0} & \mathbf{0} & \mathbf{0} & \mathbf{I} & \mathbf{0} & \mathbf{0} \\ \mathbf{0} & \mathbf{0} & \mathbf{0} & \mathbf{0} & \mathbf{I} & \mathbf{0} \\ \mathbf{0} & \mathbf{0} & \mathbf{0} & \mathbf{0} & \mathbf{0} & \mathbf{I} \end{bmatrix} - \begin{bmatrix} \mathbf{G^T} \\ \mathbf{G^T} \\ \mathbf{0} \\ \mathbf{0} \end{bmatrix} \right) \mathbf{L^T} \delta\mathbf{p_g} \tag{3.135}$$
$$= \mathbf{P}\mathbf{L^T}\delta\mathbf{p_g}$$

Being:

$$\mathbf{P} = \begin{bmatrix} \mathbf{0} & \mathbf{I} & \mathbf{0} & \mathbf{0} & \mathbf{0} & \mathbf{0} \\ \mathbf{0} & \mathbf{0} & \mathbf{0} & \mathbf{I} & \mathbf{0} & \mathbf{0} \\ \mathbf{0} & \mathbf{0} & \mathbf{0} & \mathbf{0} & \mathbf{I} & \mathbf{0} \\ \mathbf{0} & \mathbf{0} & \mathbf{0} & \mathbf{0} & \mathbf{0} & \mathbf{I} \end{bmatrix} - \begin{bmatrix} \mathbf{G^T} \\ \mathbf{G^T} \\ \mathbf{0} \\ \mathbf{0} \end{bmatrix} \tag{3.136}$$

with:

$$\mathbf{G} = \frac{\partial \boldsymbol{\vartheta}^\mathbf{e}_\mathbf{C}}{\partial \mathbf{p}^\mathrm{e}_\mathbf{gpq}} \tag{3.137}$$

has to be evaluated.

From the (3.118), the equation (3.126) can be written as:

$$\delta\hat{\boldsymbol{\vartheta}}^{\boldsymbol{e}}_\mathbf{C} = \mathbf{R^T_C}\delta\mathbf{R_C} \tag{3.138}$$

Using the definition of $\mathbf{R_C}$ the above equation becomes:

$$\begin{bmatrix} 0 & -\delta\vartheta^\mathrm{e}_{\mathrm{C}3} & \delta\vartheta^\mathrm{e}_{\mathrm{C}2} \\ \delta\vartheta^\mathrm{e}_{\mathrm{C}3} & 0 & -\delta\vartheta^\mathrm{e}_{\mathrm{C}1} \\ -\delta\vartheta^\mathrm{e}_{\mathrm{C}2} & \delta\vartheta^\mathrm{e}_{\mathrm{C}1} & 0 \end{bmatrix} = \begin{bmatrix} \mathbf{c^T_{pq1}} \\ \mathbf{c^T_{pq2}} \\ \mathbf{c^T_{pq3}} \end{bmatrix} \begin{bmatrix} \delta\mathbf{c}_{\mathrm{pq}\mathbf{1}} & \delta\mathbf{c}_{\mathrm{pq}\mathbf{2}} & \delta\mathbf{c}_{\mathrm{pq}\mathbf{3}} \end{bmatrix} =$$
$$= \begin{bmatrix} \mathbf{c^T_{pq1}}\delta\mathbf{c}_{\mathrm{qp}\mathbf{1}} & \mathbf{c^T_{pq1}}\delta\mathbf{c}_{\mathrm{pq}\mathbf{2}} & \mathbf{c^T_{pq1}}\delta\mathbf{c}_{\mathrm{pq}\mathbf{3}} \\ \mathbf{c^T_{pq2}}\delta\mathbf{c}_{\mathrm{qp}\mathbf{1}} & \mathbf{c^T_{pq2}}\delta\mathbf{c}_{\mathrm{pq}\mathbf{2}} & \mathbf{c^T_{pq2}}\delta\mathbf{c}_{\mathrm{pq}\mathbf{3}} \\ \mathbf{c^T_{pq3}}\delta\mathbf{c}_{\mathrm{qp}\mathbf{1}} & \mathbf{c^T_{pq3}}\delta\mathbf{c}_{\mathrm{pq}\mathbf{2}} & \mathbf{c^T_{pq3}}\delta\mathbf{c}_{\mathrm{pq}\mathbf{3}} \end{bmatrix} \tag{3.139}$$

hence the equation (3.139) can be rewritten as:

$$\delta\boldsymbol{\vartheta}^{\mathbf{e}}_{\mathbf{C}} = \begin{bmatrix}\delta\vartheta^{\mathrm{e}}_{\mathrm{C1}}\\ \delta\vartheta^{\mathrm{e}}_{\mathrm{C2}}\\ \delta\vartheta^{\mathrm{e}}_{\mathrm{C3}}\end{bmatrix} = \begin{bmatrix}-\mathbf{c}^{\mathbf{T}}_{\mathrm{pq}\mathbf{2}}\delta\mathbf{c}_{\mathrm{pq}\mathbf{3}}\\ -\mathbf{c}^{\mathbf{T}}_{\mathrm{pq}\mathbf{3}}\delta\mathbf{c}_{\mathrm{pq}\mathbf{1}}\\ \mathbf{c}^{\mathbf{T}}_{\mathrm{pq}\mathbf{2}}\delta\mathbf{c}_{\mathrm{pq}\mathbf{1}}\end{bmatrix} \tag{3.140}$$

Differentiation of (3.27)gives:

$$\delta\mathbf{c}_{\mathrm{pq}\mathbf{1}} = \frac{1}{\ell_{pq}}\left[\mathbf{I} - \mathbf{c}_{\mathrm{pq}\mathbf{1}}\mathbf{c}^{\mathbf{T}}_{\mathrm{pq}\mathbf{1}}\right]\begin{bmatrix}\delta\mathrm{u}_{\mathrm{qG}} - \delta\mathrm{u}_{\mathrm{pG}}\\ \delta\mathrm{v}_{\mathrm{qG}} - \delta\mathrm{v}_{\mathrm{pG}}\\ \delta\mathrm{w}_{\mathrm{qG}} - \delta\mathrm{w}_{\mathrm{pG}}\end{bmatrix} \tag{3.141}$$

The equation (3.141) using the (3.129) becomes:

$$\delta\mathbf{c}^{\mathbf{e}}_{\mathrm{pq}\mathbf{1}} = \frac{1}{\ell_{pq}}\begin{bmatrix}\delta\mathrm{u}^{\mathrm{e}}_{\mathrm{qG}} - \delta\mathrm{u}^{\mathrm{e}}_{\mathrm{pG}}\\ \delta\mathrm{v}^{\mathrm{e}}_{\mathrm{qG}} - \delta\mathrm{v}^{\mathrm{e}}_{\mathrm{pG}}\\ \delta\mathrm{w}^{\mathrm{e}}_{\mathrm{qG}} - \delta\mathrm{w}^{\mathrm{e}}_{\mathrm{pG}}\end{bmatrix} \tag{3.142}$$

The local expression of $\mathbf{c}^{\mathbf{e}}_{\mathrm{pq}\mathbf{2}}$ and $\mathbf{c}^{\mathbf{e}}_{\mathrm{pq}\mathbf{3}}$ are given by:

$$\begin{aligned}\mathbf{c}^{\mathbf{e}}_{\mathrm{pq}\mathbf{2}} &= [0 \quad 1 \quad 0]^{\mathrm{T}}\\ \mathbf{c}^{\mathbf{e}}_{\mathrm{pq}\mathbf{3}} &= [0 \quad 0 \quad 1]^{\mathrm{T}}\end{aligned} \tag{3.143}$$

Therefore, from (3.142), (3.143) the equation (3.140) gives:

$$\begin{bmatrix}\delta\vartheta^{\mathrm{e}}_{\mathrm{C2}}\\ \delta\vartheta^{\mathrm{e}}_{\mathrm{C3}}\end{bmatrix} = \frac{1}{\ell_{pq}}\begin{bmatrix}-\left(\delta\mathrm{w}^{\mathrm{e}}_{\mathrm{pG}} - \delta\mathrm{w}^{\mathrm{e}}_{\mathrm{qG}}\right)\\ \left(\delta\mathrm{v}^{\mathrm{e}}_{\mathrm{pG}} - \delta\mathrm{v}^{\mathrm{e}}_{\mathrm{qG}}\right)\end{bmatrix} \tag{3.144}$$

Evaluation of $\delta\vartheta^{e}_{C1}$

Differentiation (3.29) of gives:

$$\delta\mathbf{q} = \frac{1}{2}(\delta\mathbf{R}_{\mathrm{qG}}\mathbf{R}_{0\mathrm{C}} + \delta\mathbf{R}_{\mathrm{pG}}\mathbf{R}_{0\mathrm{C}})[0 \quad 1 \quad 0]^{T} \tag{3.145}$$

Substituting the (3.117) into (3.145), the following equation is obtained:

$$\begin{aligned}\delta\mathbf{q} &= \frac{1}{2}\left(\delta\hat{\boldsymbol{\vartheta}}_{\mathbf{qG}}\mathbf{R}_{\mathrm{qG}}\mathbf{R}_{0\mathrm{C}} + \delta\hat{\boldsymbol{\vartheta}}_{\mathbf{pG}}\mathbf{R}_{\mathrm{pG}}\mathbf{R}_{0\mathrm{C}}\right)[0 \quad 1 \quad 0]^{T}\\ &= \frac{1}{2}\left(\delta\hat{\boldsymbol{\vartheta}}_{\mathbf{qG}}\mathbf{q}_{\mathbf{q}} + \delta\hat{\boldsymbol{\vartheta}}_{\mathbf{pG}}\mathbf{q}_{\mathbf{p}}\right)\end{aligned} \tag{3.146}$$

The local expressions of $\mathbf{q}_{\mathbf{q}}$ and $\mathbf{q}_{\mathbf{p}}$ are:

$$\mathbf{q}^{\mathbf{e}} = \mathbf{R}^{\mathbf{T}}_{\mathrm{C}}\mathbf{q} = \begin{bmatrix}\mathrm{q}_1\\ \mathrm{q}_2\\ 0\end{bmatrix} \quad \mathbf{q}^{\mathbf{e}}_{\mathbf{q}} = \mathbf{R}^{\mathbf{T}}_{\mathrm{C}}\mathbf{q}_{\mathbf{q}} = \begin{bmatrix}\mathrm{q}_{\mathrm{q}1}\\ \mathrm{q}_{\mathrm{q}2}\\ \mathrm{q}_{\mathrm{q}3}\end{bmatrix} \quad \mathbf{q}^{\mathbf{e}}_{\mathbf{p}} = \mathbf{R}^{\mathbf{T}}_{\mathrm{C}}\mathbf{q}_{\mathbf{p}} = \begin{bmatrix}\mathrm{q}_{\mathrm{p}1}\\ \mathrm{q}_{\mathrm{p}2}\\ \mathrm{q}_{\mathrm{p}3}\end{bmatrix} \tag{3.147}$$

Substituting the equation (3.129) and (3.147) into (3.146) the following equations is obtained:

$$\delta\mathbf{q^e} = \frac{1}{2}\left(\delta\hat{\boldsymbol{\vartheta}}^{\boldsymbol{e}}_{\mathbf{qG}}\begin{bmatrix}\mathrm{q_{q1}}\\ \mathrm{q_{q2}}\\ \mathrm{q_{q3}}\end{bmatrix} + \delta\hat{\boldsymbol{\vartheta}}^{\boldsymbol{e}}_{\mathbf{pG}}\begin{bmatrix}\mathrm{q_{p1}}\\ \mathrm{q_{p2}}\\ \mathrm{q_{p3}}\end{bmatrix}\right) \tag{3.148}$$

After some calculation the (3.148) is equal to:

$$\delta\mathbf{q^e} = \frac{1}{2}\begin{bmatrix}-\mathrm{q_{q2}}\delta\vartheta^{\mathrm{e}}_{\mathrm{qG3}} + \mathrm{q_{q3}}\delta\vartheta^{\mathrm{e}}_{\mathrm{qG2}} - \mathrm{q_{p2}}\delta\vartheta^{\mathrm{e}}_{\mathrm{pG3}} + \mathrm{q_{p3}}\delta\vartheta^{\mathrm{e}}_{\mathrm{pG2}}\\ +\mathrm{q_{q1}}\delta\vartheta^{\mathrm{e}}_{\mathrm{qG3}} - \mathrm{q_{q3}}\delta\vartheta^{\mathrm{e}}_{\mathrm{qG1}} + \mathrm{q_{p1}}\delta\vartheta^{\mathrm{e}}_{\mathrm{pG3}} - \mathrm{q_{p3}}\delta\vartheta^{\mathrm{e}}_{\mathrm{pG1}}\\ -\mathrm{q_{q1}}\delta\vartheta^{\mathrm{e}}_{\mathrm{qG2}} + \mathrm{q_{q2}}\delta\vartheta^{\mathrm{e}}_{\mathrm{qG1}} - \mathrm{q_{p1}}\delta\vartheta^{\mathrm{e}}_{\mathrm{pG2}} + \mathrm{q_{p2}}\delta\vartheta^{\mathrm{e}}_{\mathrm{pG1}}\end{bmatrix} \tag{3.149}$$

Combining equation (3.30) with (3.140) and nothing that $\mathrm{q_2} = \left\|\mathbf{c}_{pq1} \times \mathbf{q}\right\|$ the following equation is obtained:

$$\begin{aligned}\delta\vartheta^{\mathrm{e}}_{\mathrm{C1}} = &-\frac{\mathbf{c^T_{qp2}}}{q_2}\delta\mathbf{c}_{pq1} \times \mathbf{q} - \frac{\mathbf{c^T_{qp2}}}{q_2}\mathbf{c}_{pq1} \times \delta\mathbf{q^e}\\ &-\delta\left(\frac{1}{\mathrm{q_2}}\right)\mathbf{c^T_{qp2}}(\mathbf{c}_{pq1} \times \mathbf{q})\end{aligned} \tag{3.150}$$

The last term of the equation (3.156)is zero.

The following notations are introduced:

$$\bar{\eta} = \frac{\mathrm{q_1}}{\mathrm{q_2}} \quad \bar{\eta}_{\mathrm{q1}} = \frac{\mathrm{q_{q1}}}{\mathrm{q_2}} \quad \bar{\eta}_{\mathrm{q2}} = \frac{\mathrm{q_{q2}}}{\mathrm{q_2}} \quad \bar{\eta}_{\mathrm{p1}} = \frac{\mathrm{q_{p1}}}{\mathrm{q_2}} \quad \bar{\eta}_{\mathrm{p2}} = \frac{\mathrm{q_{p2}}}{\mathrm{q_2}} \tag{3.151}$$

Substituting the (3.141), (3.149) and (3.151) into equation (3.150) the following equation is obtained:

$$\begin{aligned}\delta\vartheta^{\mathrm{e}}_{\mathrm{C1}} = &\frac{\bar{\eta}}{\ell_{pq}}\left(\delta\mathrm{w^e_q} - \delta\mathrm{w^e_p}\right) + \frac{\bar{\eta}_{\mathrm{q2}}}{2}\delta\vartheta^{\mathrm{e}}_{\mathrm{qG1}} - \frac{\bar{\eta}_{\mathrm{q1}}}{2}\delta\vartheta^{\mathrm{e}}_{\mathrm{qG2}} + \frac{\bar{\eta}_{\mathrm{p2}}}{2}\delta\vartheta^{\mathrm{e}}_{\mathrm{pG1}}\\ &-\frac{\bar{\eta}_{\mathrm{p1}}}{2}\delta\vartheta^{\mathrm{e}}_{\mathrm{pG2}}\end{aligned} \tag{3.152}$$

Once, $\delta\vartheta^{\mathrm{e}}_{\mathrm{C1}}$, $\delta\vartheta^{\mathrm{e}}_{\mathrm{C2}}$, $\delta\vartheta^{\mathrm{e}}_{\mathrm{C3}}$ expressions are obtained, the **G** matrix is determinates and it is equal to:

$$\mathbf{G^T} = \begin{bmatrix}0 & 0 & \frac{\bar{\eta}}{\ell_{pq}} & \frac{\bar{\eta}_{\mathrm{q2}}}{2} & -\frac{\bar{\eta}_{\mathrm{q1}}}{2} & 0 & 0 & 0 & -\frac{\bar{\eta}}{\ell_{pq}} & \frac{\bar{\eta}_{\mathrm{p2}}}{2} & -\frac{\bar{\eta}_{\mathrm{p1}}}{2} & 0 & 0 & 0 & 0 & 0 & 0 & 0\\ 0 & 0 & \frac{1}{\ell_{pq}} & 0 & 0 & 0 & 0 & 0 & -\frac{1}{\ell_{pq}} & 0 & 0 & 0 & 0 & 0 & 0 & 0 & 0 & 0\\ 0 & -\frac{1}{\ell_{pq}} & 0 & 0 & 0 & 0 & 0 & \frac{1}{\ell_{pq}} & 0 & 0 & 0 & 0 & 0 & 0 & 0 & 0 & 0 & 0\end{bmatrix} \tag{3.153}$$

Finally, the transformation between $\mathbf{\delta p_c}$ and $\mathbf{\delta p_{gpq}}$ is equal to:

$$\mathbf{\delta p_c} = \mathbf{B}\mathbf{\delta p_{gpq}}; \quad \text{with} \quad \mathbf{B} = \begin{bmatrix} \mathbf{c} \\ \mathbf{P}\mathbf{L}^{\mathbf{T}} \end{bmatrix} \tag{3.154}$$

3.4.4.4 Evaluation of $\boldsymbol{\delta B}$ matrix - Approach I

In order to obtain the geometric stiffness matrix, it is necessary to calculate the quantity $\mathbf{\delta B^T}$. By considering equation (3.154), the following equation can be written:

$$\delta \mathbf{B}^{\mathbf{T}}\mathbf{q_c} = [\mathbf{\delta c}^{\mathbf{T}} \quad \mathbf{\delta L P}^{\mathbf{T}} + \mathbf{L}\mathbf{\delta P}^{\mathbf{T}}]\mathbf{q_c} \tag{3.155}$$

From the (3.120),(3.141) $\mathbf{\delta c^T}$ is equal to:

$$\mathbf{\delta c}^{\mathbf{T}} = \mathbf{D}\mathbf{\delta p_{gpq}}; \quad \mathbf{D} = \begin{bmatrix} \mathbf{D_3} & \mathbf{0} & -\mathbf{D_3} & \mathbf{0} & \mathbf{0} & \mathbf{0} \\ \mathbf{0} & \mathbf{0} & \mathbf{0} & \mathbf{0} & \mathbf{0} & \mathbf{0} \\ -\mathbf{D_3} & \mathbf{0} & \mathbf{D_3} & \mathbf{0} & \mathbf{0} & \mathbf{0} \\ \mathbf{0} & \mathbf{0} & \mathbf{0} & \mathbf{0} & \mathbf{0} & \mathbf{0} \\ \mathbf{0} & \mathbf{0} & \mathbf{0} & \mathbf{0} & \mathbf{0} & \mathbf{0} \\ \mathbf{0} & \mathbf{0} & \mathbf{0} & \mathbf{0} & \mathbf{0} & \mathbf{0} \end{bmatrix}; \quad \mathbf{D_3} = \frac{1}{\ell_{pq}} \tag{3.156}$$

$- \mathbf{c_{pq1}}\mathbf{c_{pq1}^T}$);

By considering the expressions of internal forces:

$$\mathbf{q}_{\mathrm{c}} = \mathbf{A_3^T}\mathbf{A_2^T}\mathbf{A_1^T}\Delta\hat{\mathbf{q}}_{\ell} = [\mathrm{f_{c1}} \quad \boldsymbol{m}^{\mathbf{T}}]^{\mathbf{T}} \quad \boldsymbol{m} = [\mathrm{f_{c2}} \quad \mathrm{f_{c3}} \quad \mathrm{f_{c4}} \quad \mathrm{f_{c5}} \quad \mathrm{f_{c6}} \quad \mathrm{f} \tag{3.157}$$

The quantity $\mathbf{\delta}(\mathbf{LP}^{\mathbf{T}})\boldsymbol{m}$ can be written as:

$$\mathbf{\delta}(\mathbf{LP}^{\mathbf{T}})\boldsymbol{m} = \mathbf{\delta L P}^{\mathbf{T}}\boldsymbol{m} + \mathbf{L}\mathbf{\delta P}^{\mathbf{T}}\boldsymbol{m} \tag{3.158}$$

In order to evaluate the quantity $\mathbf{\delta L P}^{\mathbf{T}}\boldsymbol{m}$ it is convenient to define the following 18x1vector

$$\mathbf{P}^{\mathbf{T}}\boldsymbol{m} = \begin{bmatrix} \boldsymbol{n_1} \\ \boldsymbol{m_1} \\ \boldsymbol{n_2} \\ \boldsymbol{m_2} \\ \mathbf{0_{6x1}} \end{bmatrix} \tag{3.159}$$

From the (3.132)(3.138), the first term of the (3.158) becomes:

$$\begin{aligned}
&\boldsymbol{\delta \mathbf{L}\mathbf{P}^{\mathbf{T}}\boldsymbol{m}} \\
&= \begin{bmatrix} \mathbf{R_c}\delta\tilde{\boldsymbol{\vartheta}}^{\boldsymbol{e}}_{\mathbf{C}} & \mathbf{0} & \mathbf{0} & \mathbf{0} & \mathbf{0} & \mathbf{0} \\ \mathbf{0} & \mathbf{R_c}\delta\tilde{\boldsymbol{\vartheta}}^{\boldsymbol{e}}_{\mathbf{C}} & \mathbf{0} & \mathbf{0} & \mathbf{0} & \mathbf{0} \\ \mathbf{0} & \mathbf{0} & \mathbf{R_c}\delta\tilde{\boldsymbol{\vartheta}}^{\boldsymbol{e}}_{\mathbf{C}} & \mathbf{0} & \mathbf{0} & \mathbf{0} \\ \mathbf{0} & \mathbf{0} & \mathbf{0} & \mathbf{R_c}\delta\tilde{\boldsymbol{\vartheta}}^{\boldsymbol{e}}_{\mathbf{C}} & \mathbf{0} & \mathbf{0} \\ \mathbf{0} & \mathbf{0} & \mathbf{0} & \mathbf{0} & \mathbf{0} & \mathbf{0} \\ \mathbf{0} & \mathbf{0} & \mathbf{0} & \mathbf{0} & \mathbf{0} & \mathbf{0} \end{bmatrix} \begin{bmatrix} \boldsymbol{n_1} \\ \boldsymbol{m_1} \\ \boldsymbol{n_2} \\ \boldsymbol{m_2} \\ \mathbf{0_{6x1}} \end{bmatrix} \\
&= \mathbf{L} \begin{bmatrix} \delta\tilde{\boldsymbol{\vartheta}}^{\boldsymbol{e}}_{\mathbf{C}}\boldsymbol{n_1} \\ \delta\tilde{\boldsymbol{\vartheta}}^{\boldsymbol{e}}_{\mathbf{C}}\boldsymbol{m_1} \\ \delta\tilde{\boldsymbol{\vartheta}}^{\boldsymbol{e}}_{\mathbf{C}}\boldsymbol{n_2} \\ \delta\tilde{\boldsymbol{\vartheta}}^{\boldsymbol{e}}_{\mathbf{C}}\boldsymbol{m_2} \\ \mathbf{0_{6x1}} \end{bmatrix}
\end{aligned} \tag{3.160}$$

Using the relation $\tilde{\mathbf{a}}\mathbf{b} = -\tilde{\mathbf{b}}\mathbf{a}$ the previous equation becomes:

$$\boldsymbol{\delta \mathbf{L}\mathbf{P}^{\mathbf{T}}\boldsymbol{m}} = -\mathbf{L}\mathbf{Q}\delta\boldsymbol{\vartheta}^{\boldsymbol{e}}_{\mathbf{C}} \quad \mathbf{Q} = \begin{bmatrix} \tilde{\boldsymbol{n}}_{\mathbf{1}} \\ \widetilde{\boldsymbol{m}}_{\mathbf{1}} \\ \tilde{\boldsymbol{n}}_{\mathbf{2}} \\ \widetilde{\boldsymbol{m}}_{\mathbf{2}} \\ \tilde{\mathbf{0}}_{\mathbf{6x1}} \end{bmatrix} \tag{3.161}$$

Finally, using the (3.131) and (3.137) it becomes:

$$\boldsymbol{\delta \mathbf{L}\mathbf{P}^{\mathbf{T}}\boldsymbol{m}} = -\mathbf{L}\mathbf{Q}\mathbf{G}^{\mathbf{T}}\mathbf{L}^{\mathbf{T}}\boldsymbol{\delta \mathbf{p}_{\mathbf{gpq}}} \tag{3.162}$$

In order to evaluate the quantity $\boldsymbol{\delta \mathbf{P}^{\mathbf{T}}}$, the following matrix in defined:

$$\begin{aligned}
&\mathbf{A}^{\mathbf{T}}_{\mathbf{G}} \\
&= \begin{bmatrix} 0 & 0 & 0 & 0 & 0 & 0 & 0 & 0 & 0 & 0 & 0 & 0 & 0 & 0 & 0 & 0 & (\\ 0 & 0 & 0 & 0 & 0 & 0 & 0 & 0 & -\ell_{pq} & 0 & 0 & 0 & 0 & 0 & 0 & 0 & (\\ 0 & 0 & 0 & 0 & 0 & 0 & 0 & \ell_{pq} & 0 & 0 & 0 & 0 & 0 & 0 & 0 & 0 & (\end{bmatrix}
\end{aligned} \tag{3.163}$$

It is possible to note that:

$$\mathbf{A}^{\mathbf{T}}_{\mathbf{G}}\mathbf{G} = \mathbf{I} \tag{3.164}$$

Differentiation of the above equation gives:

$$\boldsymbol{\delta \mathbf{A}^{\mathbf{T}}_{\mathbf{G}}\mathbf{G}} + \mathbf{A}^{\mathbf{T}}_{\mathbf{G}}\boldsymbol{\delta \mathbf{G}} = \mathbf{0} \rightarrow \ \boldsymbol{\delta \mathbf{G}} = \ -\mathbf{A}^{-\mathbf{T}}_{\mathbf{G}}\boldsymbol{\delta \mathbf{A}^{\mathbf{T}}_{\mathbf{G}}\mathbf{G}} = -\mathbf{G}\boldsymbol{\delta \mathbf{A}^{\mathbf{T}}_{\mathbf{G}}\mathbf{G}} \tag{3.165}$$

From the definition of $\mathbf{P}$ in(3.135), it is possible to obtain:

$$\boldsymbol{\delta P} = -\mathbf{C_G}\ \boldsymbol{\delta G^T} \quad \mathbf{C_G} = \begin{bmatrix} \mathbf{I} \\ \mathbf{I} \\ \mathbf{0} \\ \mathbf{0} \end{bmatrix} \tag{3.166}$$

The transpose matrix of $\boldsymbol{\delta P}$ is equal to:

$$\boldsymbol{\delta P^T} = -\boldsymbol{\delta G}\ \mathbf{C_G^T} = \ \mathbf{G}\ \boldsymbol{\delta A_G^T}\ \mathbf{G}\ \mathbf{C_G^T} \tag{3.167}$$

therefore, the quantity $\mathbf{L\delta P^T}\boldsymbol{m}$: becomes:

$$\mathbf{L\delta P^T}\boldsymbol{m} = \mathbf{L}\ \mathbf{G}\ \boldsymbol{\delta A_G^T}\ \mathbf{G}\ \mathbf{C_G^T}\ \boldsymbol{m} \tag{3.168}$$

After some manipulation the equation (3.168) can be written as:

$$\mathbf{L\delta P^T}\boldsymbol{m} = \mathbf{L}\ \mathbf{G}\ \mathbf{a_G}\boldsymbol{\delta \ell_{pq}} = \mathbf{L}\ \mathbf{G}\ \mathbf{a_G}\ \mathbf{c}\ \boldsymbol{\delta p_{gpq}} \tag{3.169}$$

With:

$$\mathbf{a_G} = \begin{bmatrix} 0 \\ \dfrac{\bar{\eta}}{\ell_{pq}}(\mathrm{f_{c2}} + \mathrm{f_{c5}}) - \dfrac{1}{\ell_{pq}}(\mathrm{f_{c3}} + \mathrm{f_{c6}}) \\ \dfrac{1}{\ell_{pq}}(\mathrm{f_{c4}} + \mathrm{f_{c7}}) \end{bmatrix} \tag{3.170}$$

Combining the (3.155),(3.156),(3.162),(3.172) it is possible to obtain the geometrical stiffness matrix expression $\mathbf{K_{gpq}}$:

$$\delta\mathbf{B^T q_c} = (\mathbf{D} - \mathbf{LQG^TL^T} + \mathbf{L}\ \mathbf{G}\ \mathbf{a_G}\ \mathbf{c})\ \boldsymbol{\delta p_{gpq}} = \mathbf{K_{gpq}}\ \boldsymbol{\delta p_{gpq}} \tag{3.171}$$

3.4.4.5 Transformation $\delta \boldsymbol{p}_{\boldsymbol{c}} \rightarrow \delta \boldsymbol{p}_{gpq}$ and evaluation of $\boldsymbol{B}$ matrix for the Approach II

The transformation between $\mathbf{\delta p_c}$ and $\mathbf{\delta p_{gpq}}$ is given by:

$$\mathbf{\delta p_c} = \mathbf{B} \mathbf{\delta p_{gpg}} \rightarrow \mathbf{B} = \frac{\mathbf{\delta p_c}}{\mathbf{\delta p_{gpq}}} \tag{3.172}$$

Where:

$$\frac{\partial \delta \bar{\vartheta}_{\mathrm{p2}}}{\partial \mathbf{p_{gpq}}} = -\mathbf{t_{p2}^T} \frac{\partial \mathbf{c_{pq1}}}{\partial \mathbf{p_{gpq}}} - \mathbf{c}_{\mathrm{pq1}}^{\mathbf{T}} \frac{\partial \mathbf{t_{p2}}}{\partial \mathbf{p_{gpq}}} \tag{3.173}$$

$$\frac{\partial \delta \bar{\vartheta}_{\mathrm{p3}}}{\partial \mathbf{p_{gpq}}} = -\mathbf{t_{p3}^T} \frac{\partial \mathbf{c_{pq1}}}{\partial \mathbf{p_{gpq}}} - \mathbf{c}_{\mathrm{pq1}}^{\mathbf{T}} \frac{\partial \mathbf{t_{p3}}}{\partial \mathbf{p_{gpq}}} \tag{3.174}$$

$$\frac{\partial \delta \bar{\vartheta}_{\mathrm{q2}}}{\partial \mathbf{p_{gpq}}} = -\mathbf{t_{q2}^T} \frac{\partial \mathbf{c_{pq1}}}{\partial \mathbf{p_{gpq}}} - \mathbf{c}_{\mathrm{pq1}}^{\mathbf{T}} \frac{\partial \mathbf{t_{q2}}}{\partial \mathbf{p_{gpq}}} \tag{3.175}$$

$$\frac{\partial \delta \bar{\vartheta}_{\mathrm{q3}}}{\partial \mathbf{p_{gpq}}} = -\mathbf{t_{q3}^T} \frac{\partial \mathbf{c_{pq1}}}{\partial \mathbf{p_{gpq}}} - \mathbf{c}_{\mathrm{pq1}}^{\mathbf{T}} \frac{\partial \mathbf{t_{q3}}}{\partial \mathbf{p_{gpq}}} \tag{3.176}$$

$$\frac{\partial \delta \bar{\mathrm{u}}}{\partial \mathbf{p_{gpq}}} = \frac{\partial \ell_{pq}}{\partial \mathbf{p_{gpq}}} \tag{3.177}$$

$$\frac{\partial \delta \bar{\vartheta}_{\mathrm{T}}}{\partial \mathbf{p_{gpq}}} = \mathbf{t_{pq}^T} \frac{\partial \mathbf{t_{p3}}}{\partial \mathbf{p_{gpq}}} + \mathbf{t_{p3}^T} \frac{\partial \mathbf{t_{pq}}}{\partial \mathbf{p_{gpq}}} \tag{3.178}$$

with:

$$\frac{\partial \mathbf{c_{pq1}}}{\partial \mathbf{p_{gpq}}} = \left[\frac{\mathbf{c_{pq1}} \mathbf{c_{pq1}^T} - \mathbf{I}}{\ell_{pq}} \quad \mathbf{0_{3x3}} \quad -\frac{\mathbf{c_{pq1}} \mathbf{c_{pq1}^T} - \mathbf{I}}{\ell_{pq}} \quad \mathbf{0_{3x3}} \quad \mathbf{0_{3x6}} \right]^{\mathbf{T}} \tag{3.179}$$

$$\frac{\partial \mathbf{t_{p2}}}{\partial \mathbf{p_{gpq}}} = \left[\mathbf{0_{3x3}} \quad \frac{\partial \mathbf{T_p}}{\partial \vartheta_{\mathrm{xp}}} \mathbf{t_{p2}^0} \quad \frac{\partial \mathbf{T_p}}{\partial \vartheta_{\mathrm{yp}}} \mathbf{t_{p2}^0} \quad \frac{\partial \mathbf{T_q}}{\partial \vartheta_{\mathrm{zp}}} \mathbf{t_{p2}^0} \quad \mathbf{0_{3x3}} \quad \mathbf{0_{3x3}} \quad \mathbf{0_{3x6}} \right] \tag{3.180}$$

$$\frac{\partial \mathbf{t_{p3}}}{\partial \mathbf{p_{gpq}}} = \left[\mathbf{0_{3x3}} \quad \frac{\partial \mathbf{T_p}}{\partial \vartheta_{\mathrm{xp}}} \mathbf{t_{p3}^0} \quad \frac{\partial \mathbf{T_p}}{\partial \vartheta_{\mathrm{yp}}} \mathbf{t_{p3}^0} \quad \frac{\partial \mathbf{T_p}}{\partial \vartheta_{\mathrm{zp}}} \mathbf{t_{p3}^0} \quad \mathbf{0_{3x3}} \quad \mathbf{0_{3x3}} \quad \mathbf{0_{3x6}} \right] \tag{3.181}$$

$$\frac{\partial \mathbf{t_{q2}}}{\partial \mathbf{p_{gpq}}} = \left[\mathbf{0_{3x3}} \quad \mathbf{0_{3x3}} \quad \mathbf{0_{3x3}} \quad \frac{\partial \mathbf{T_q}}{\partial \vartheta_{\mathrm{xq}}} \mathbf{t_{q2}^0} \quad \frac{\partial \mathbf{T_q}}{\partial \vartheta_{\mathrm{yq}}} \mathbf{t_{q2}^0} \quad \frac{\partial \mathbf{T_q}}{\partial \vartheta_{\mathrm{zq}}} \mathbf{t_{q2}^0} \quad \mathbf{0_{3x6}} \right] \tag{3.182}$$

$$\frac{\partial \mathbf{t_{q3}}}{\partial \mathbf{p_{gpq}}} = \left[\mathbf{0_{3x3}} \quad \mathbf{0_{3x3}} \quad \mathbf{0_{3x3}} \quad \frac{\partial \mathbf{T_q}}{\partial \vartheta_{\mathrm{xq}}} \mathbf{t_{q3}^0} \quad \frac{\partial \mathbf{T_p}}{\partial \vartheta_{\mathrm{yq}}} \mathbf{t_{q3}^0} \quad \frac{\partial \mathbf{T_q}}{\partial \vartheta_{\mathrm{zq}}} \mathbf{t_{q3}^0} \quad \mathbf{0_{3x6}} \right] \tag{3.183}$$

$$\frac{\partial \mathbf{t_{pq}}}{\partial \mathbf{p_{gpq}}} = \begin{bmatrix} \mathbf{0_{3x3}} & \mathbf{0_{3x3}} & \mathbf{0_{3x3}} & \frac{\partial \mathbf{T_q}}{\partial \vartheta_{xq}}\mathbf{t^0_{p2}} & \frac{\partial \mathbf{T_q}}{\partial \vartheta_{yq}}\mathbf{t^0_{p2}} & \frac{\partial \mathbf{T_q}}{\partial \vartheta_{zq}}\mathbf{t^0_{p2}} & \mathbf{0_{3x6}} \end{bmatrix} \tag{3.184}$$

$$\frac{\partial \ell_{pq}}{\partial \mathbf{p_{gpq}}} = [-\mathbf{c^T_{pq1}} \quad \mathbf{0_{1x3}} \quad -\mathbf{c^T_{pq1}} \quad \mathbf{0_{1x3}} \quad \mathbf{0_{1x6}}] \tag{3.185}$$

Differentiating the equation (A.25) the following equations are obtained.

$$\frac{\partial \mathbf{T_n}}{\partial \vartheta_{xn}} = \begin{bmatrix} 0 & \frac{1}{2}\vartheta_{yn} & \frac{1}{2}\vartheta_{zn} \\ \frac{1}{2}\vartheta_{yn} & -\vartheta_{xn} & -1 \\ \frac{1}{2}\vartheta_{zn} & 1 & \vartheta_{xn} \end{bmatrix} \quad (\mathrm{n} = \mathrm{p}, \mathrm{q}) \tag{3.186}$$

$$\frac{\partial \mathbf{T_n}}{\partial \vartheta_{yn}} = \begin{bmatrix} -\vartheta_{yn} & \frac{1}{2}\vartheta_{xn} & 1 \\ \frac{1}{2}\vartheta_{xn} & 0 & \frac{1}{2}\vartheta_{zn} \\ -1 & \frac{1}{2}\vartheta_{zn} & -\vartheta_{yn} \end{bmatrix} \quad (\mathrm{n} = \mathrm{p}, \mathrm{q}) \tag{3.187}$$

$$\frac{\partial \mathbf{T_n}}{\partial \vartheta_{zn}} = \begin{bmatrix} -\vartheta_{zn} & -1 & \frac{1}{2}\vartheta_{xn} \\ 1 & -\vartheta_{zn} & \frac{1}{2}\vartheta_{yn} \\ \frac{1}{2}\vartheta_{xn} & \frac{1}{2}\vartheta_{yn} & 0 \end{bmatrix} \quad (\mathrm{n} = \mathrm{p}, \mathrm{q}) \tag{3.188}$$

In the same way it is possible to differentiate the equation (A.24) in order to obtain a more accurate transformation.

After some manipulations the matrix $\mathbf{B}$ is obtained

$$\mathbf{B} = \begin{bmatrix} -\mathbf{t^T_{p2}}\left\{\frac{\partial \mathbf{c_{pq1}}}{\partial \mathbf{p_g}}\right\}_{1:3,1:3} & -\mathbf{c^T_{pq1}}\left\{\frac{\partial \mathbf{t_{p2}}}{\partial \mathbf{p_g}}\right\}_{1:3,4:6} & -\mathbf{t^T_{q2}}\left\{\frac{\partial \mathbf{c_{pq1}}}{\partial \mathbf{p_g}}\right\}_{1:3,7:9} & \mathbf{0_{1x3}} & & \\ -\mathbf{t^T_{p3}}\left\{\frac{\partial \mathbf{c_{pq1}}}{\partial \mathbf{p_g}}\right\}_{1:3,1:3} & -\mathbf{c^T_{pq1}}\left\{\frac{\partial \mathbf{t_{p3}}}{\partial \mathbf{p_g}}\right\}_{1:3,4:6} & -\mathbf{t^T_{p3}}\left\{\frac{\partial \mathbf{c_{pq1}}}{\partial \mathbf{p_g}}\right\}_{1:3,7:9} & \mathbf{0_{1x3}} & & \\ -\mathbf{t^T_{q2}}\left\{\frac{\partial \mathbf{c_{pq1}}}{\partial \mathbf{p_g}}\right\}_{1:3,1:3} & \mathbf{0_{1x3}} & -\mathbf{t^T_{q2}}\left\{\frac{\partial \mathbf{c_{pq1}}}{\partial \mathbf{p_g}}\right\}_{1:3,7:9} & -\mathbf{c^T_{pq1}}\left\{\frac{\partial \mathbf{t_{q2}}}{\partial \mathbf{p_g}}\right\}_{1:3,10:12} & \mathbf{0_{6x6}} & \\ -\mathbf{t^T_{q3}}\left\{\frac{\partial \mathbf{c_{pq1}}}{\partial \mathbf{p_g}}\right\}_{1:3,1:3} & \mathbf{0_{1x3}} & -\mathbf{t^T_{q3}}\left\{\frac{\partial \mathbf{c_{pq1}}}{\partial \mathbf{p_g}}\right\}_{1:3,7:9} & -\mathbf{c^T_{pq1}}\left\{\frac{\partial \mathbf{t_{q3}}}{\partial \mathbf{p_g}}\right\}_{1:3,10:12} & & \\ -\mathbf{c^T_{pq1}} & \mathbf{0_{1x3}} & \mathbf{c^T_{pq1}} & \mathbf{0_{1x3}} & & \\ \mathbf{0_{1x3}} & \mathbf{t^T_{pq}}\left\{\frac{\partial \mathbf{t_{q3}}}{\partial \mathbf{p_g}}\right\}_{1:3,4:6} & \mathbf{0_{1x3}} & \mathbf{t^T_{p3}}\left\{\frac{\partial \mathbf{t_{pq}}}{\partial \mathbf{p_g}}\right\}_{1:3,4:6} & & \\ & \mathbf{0_{6x6}} & & & \mathbf{I_{6x6}} & \end{bmatrix} \tag{3.189}$$

The symbol $\{\mathbf{X}\}_{\mathrm{j_0{:}j_1,i_0{:}i_1}}$ indicate a partition of the matrix $\mathbf{X}$ and $\mathrm{j_0, j_1, i_0, i_1}$are respectively minimum and maximum index of the row and column of the matrix.

3.4.4.6 Evaluation of $\boldsymbol{\delta B}$ matrix - Approach II

The evaluation of $\mathbf{\delta B}$ follows the same derivation already provided by Izzuddin in [65]. For completeness, this derivation is reported again in the following.

Differentiating twice the equation (A.25) the following equations are obtained.

$$\frac{\partial^2 \mathbf{T_n}}{\partial \vartheta_{\mathrm{xn}}^2} = \begin{bmatrix} 0 & 0 & 0 \\ 0 & -1 & 0 \\ 0 & 0 & -1 \end{bmatrix} \quad (n = \mathrm{p, q}) \tag{3.190}$$

$$\frac{\partial^2 \mathbf{T_n}}{\partial \vartheta_{\mathrm{yn}}^2} = \begin{bmatrix} -1 & 0 & 0 \\ 0 & 0 & 0 \\ 0 & 0 & -1 \end{bmatrix} \quad (n = \mathrm{p, q}) \tag{3.191}$$

$$\frac{\partial^2 \mathbf{T_n}}{\partial \vartheta_{\mathrm{zn}}^2} = \begin{bmatrix} -1 & 0 & 0 \\ 0 & -1 & 0 \\ 0 & 0 & 0 \end{bmatrix} \quad (n = \mathrm{p, q}) \tag{3.192}$$

$$\frac{\partial^2 \mathbf{T_n}}{\partial \vartheta_{\mathrm{xn}} \partial \vartheta_{\mathrm{yn}}} = \frac{\partial^2 \mathbf{T_n}}{\partial \vartheta_{\mathrm{yn}} \partial \vartheta_{\mathrm{xn}}} = \begin{bmatrix} 0 & 1/2 & 0 \\ 1/2 & 0 & 0 \\ 0 & 0 & 0 \end{bmatrix} \quad (n = \mathrm{p, q}) \tag{3.193}$$

$$\frac{\partial^2 \mathbf{T_n}}{\partial \vartheta_{\mathrm{xn}} \partial \vartheta_{\mathrm{zn}}} = \frac{\partial^2 \mathbf{T_n}}{\partial \vartheta_{\mathrm{zn}} \partial \vartheta_{\mathrm{xn}}} = \begin{bmatrix} 0 & 0 & 1/2 \\ 0 & 0 & 0 \\ 1/2 & 0 & 0 \end{bmatrix} \quad (n = \mathrm{p, q}) \tag{3.194}$$

$$\frac{\partial^2 \mathbf{T_n}}{\partial \vartheta_{\mathrm{yn}} \partial \vartheta_{\mathrm{zn}}} = \frac{\partial^2 \mathbf{T_n}}{\partial \vartheta_{\mathrm{zn}} \partial \vartheta_{\mathrm{yn}}} = \begin{bmatrix} 0 & 0 & 0 \\ 0 & 0 & 1/2 \\ 0 & 1/2 & 0 \end{bmatrix} \quad (n = \mathrm{p, q}) \tag{3.195}$$

In the same way it is possible to differentiate twice the equation (A.24) in order to obtain a more accurate transformation.

$$\mathbf{\Lambda_1} = \frac{3(\mathbf{c_{pq1}} \mathbf{c_{pq1}^T}) \mathrm{c}_{pq11} - \mathbf{c_{pq1}} \{\mathbf{I}\}_{\mathbf{1,1:3}} - (\mathbf{c_{pq1}} \{\mathbf{I}\}_{\mathbf{1,1:3}})^{\mathbf{T}} - \mathrm{c}_{pq11} \mathbf{I}}{\ell_{pq}^2} \tag{3.196}$$

$$\mathbf{\Lambda_2} = \frac{3(\mathbf{c_{pq1}}\mathbf{c_{pq1}^T})\mathrm{c}_{pq12} - \mathbf{c_{pq1}}\{\mathbf{I}\}_{\mathbf{2,1:3}} - (\mathbf{c_{pq1}}\{\mathbf{I}\}_{\mathbf{2,1:3}})^{\mathbf{T}} - \mathrm{c}_{pq12}\mathbf{I}}{\ell_{pq}^2} \tag{3.197}$$

$$\mathbf{\Lambda_3} = \frac{3(\mathbf{c_{pq1}}\mathbf{c_{pq1}^T})\mathrm{c}_{pq13} - \mathbf{c_{pq1}}\{\mathbf{I}\}_{\mathbf{3,1:3}} - (\mathbf{c_{pq1}}\{\mathbf{I}\}_{\mathbf{3,1:3}})^{\mathbf{T}} - \mathrm{c}_{pq13}\mathbf{I}}{\ell_{pq}^2} \tag{3.198}$$

$$\frac{\partial^2 \mathrm{c}_{pq1k}}{\partial^2 \mathbf{p_{gpq}}} = \begin{bmatrix} \mathbf{\Lambda}_k & \mathbf{0_{3x3}} & -\mathbf{\Lambda}_k & \mathbf{0_{3x3}} & \\ \mathbf{0_{3x3}} & \mathbf{0_{3x3}} & \mathbf{0_{3x3}} & \mathbf{0_{3x3}} & \\ \mathbf{\Lambda}_k & \mathbf{0_{3x3}} & -\mathbf{\Lambda}_k & \mathbf{0_{3x3}} & \mathbf{0_{6x6}} \\ \mathbf{0_{3x3}} & \mathbf{0_{3x3}} & \mathbf{0_{3x3}} & \mathbf{0_{3x3}} & \\ & & \mathbf{0_{6x6}} & & \mathbf{I_{6x6}} \end{bmatrix} \tag{3.199}$$

$$\frac{\partial^2 \mathrm{t_{pmk}}}{\partial^2 \mathbf{p_{gpq}}} = \begin{bmatrix} \mathbf{0_{3x3}} & \mathbf{0_{3x1}} & \mathbf{0_{3x1}} & \mathbf{0_{3x1}} & \mathbf{0_{3x3}} & \mathbf{0_{3x3}} & \\ \mathbf{0_{1x3}} & \left\{\frac{\partial^2\mathbf{T_p}}{\partial\vartheta_{\mathrm{xp}}^2}\right\}_{\mathbf{k,1:3}}\mathbf{t_{pm}^0} & \left\{\frac{\partial^2\mathbf{T_p}}{\partial\vartheta_{\mathrm{xp}}\,\partial\vartheta_{\mathrm{yp}}}\right\}_{\mathbf{k,1:3}}\mathbf{t_{pm}^0} & \left\{\frac{\partial^2\mathbf{T_p}}{\partial\vartheta_{\mathrm{xp}}\,\partial\vartheta_{\mathrm{zp}}}\right\}_{\mathbf{k,1:3}}\mathbf{t_{pm}^0} & \mathbf{0_{3x3}} & \mathbf{0_{3x3}} & \\ \mathbf{0_{1x3}} & \left\{\frac{\partial^2\mathbf{T_p}}{\partial\vartheta_{\mathrm{yp}}\,\partial\vartheta_{\mathrm{xp}}}\right\}_{\mathbf{k,1:3}}\mathbf{t_{pm}^0} & \left\{\frac{\partial^2\mathbf{T_p}}{\partial\vartheta_{\mathrm{yp}}^2}\right\}_{\mathbf{k,1:3}}\mathbf{t_{pm}^0} & \left\{\frac{\partial^2\mathbf{T_p}}{\partial\vartheta_{\mathrm{yp}}\,\partial\vartheta_{\mathrm{zp}}}\right\}_{\mathbf{k,1:3}}\mathbf{t_{pm}^0} & \mathbf{0_{3x3}} & \mathbf{0_{3x3}} & \mathbf{0_{6x6}} \\ \mathbf{0_{1x3}} & \left\{\frac{\partial^2\mathbf{T_p}}{\partial\vartheta_{\mathrm{zp}}\,\partial\vartheta_{\mathrm{xp}}}\right\}_{\mathbf{k,1:3}}\mathbf{t_{pm}^0} & \left\{\frac{\partial^2\mathbf{T_p}}{\partial\vartheta_{\mathrm{zp}}\,\partial\vartheta_{\mathrm{yp}}}\right\}_{\mathbf{k,1:3}}\mathbf{t_{pm}^0} & \left\{\frac{\partial^2\mathbf{T_p}}{\partial\vartheta_{\mathrm{zp}}^2}\right\}_{\mathbf{k,1:3}}\mathbf{t_{pm}^0} & \mathbf{0_{3x3}} & \mathbf{0_{3x3}} & \\ \mathbf{0_{3x3}} & \mathbf{0_{3x1}} & \mathbf{0_{3x1}} & \mathbf{0_{3x1}} & \mathbf{0_{3x3}} & \mathbf{0_{3x3}} & \\ \mathbf{0_{3x3}} & \mathbf{0_{3x1}} & \mathbf{0_{3x1}} & \mathbf{0_{3x1}} & \mathbf{0_{3x3}} & \mathbf{0_{3x3}} & \\ \mathbf{0_{3x3}} & \mathbf{0_{3x1}} & \mathbf{0_{3x1}} & \mathbf{0_{3x1}} & \mathbf{0_{3x3}} & \mathbf{0_{3x3}} & \\ & & \mathbf{0_{6x6}} & & & & \mathbf{I_{6x6}} \end{bmatrix} \tag{3.200}$$

$$\frac{\partial^2 \mathrm{t_{qmk}}}{\partial^2 \mathbf{p_{gpq}}} = \begin{bmatrix} \mathbf{0_{3x3}} & \mathbf{0_{3x3}} & \mathbf{0_{3x3}} & \mathbf{0_{3x1}} & \mathbf{0_{3x1}} & \mathbf{0_{3x1}} & \\ \mathbf{0_{3x3}} & \mathbf{0_{3x3}} & \mathbf{0_{3x3}} & \mathbf{0_{3x1}} & \mathbf{0_{3x1}} & \mathbf{0_{3x1}} & \\ \mathbf{0_{3x3}} & \mathbf{0_{3x3}} & \mathbf{0_{3x3}} & \mathbf{0_{3x1}} & \mathbf{0_{3x1}} & \mathbf{0_{3x1}} & \\ \mathbf{0_{1x3}} & \mathbf{0_{1x3}} & \mathbf{0_{1x3}} & \mathbf{0_{3x1}} & \mathbf{0_{3x1}} & \mathbf{0_{3x1}} & \\ \mathbf{0_{1x3}} & \mathbf{0_{1x3}} & \mathbf{0_{1x3}} & \left\{\frac{\partial^2\mathbf{T_q}}{\partial\vartheta_{\mathrm{xq}}^2}\right\}_{\mathbf{k,1:3}}\mathbf{t_{qm}^0} & \left\{\frac{\partial^2\mathbf{T_q}}{\partial\vartheta_{\mathrm{xq}}\,\partial\vartheta_{\mathrm{yq}}}\right\}_{\mathbf{k,1:3}}\mathbf{t_{qm}^0} & \left\{\frac{\partial^2\mathbf{T_q}}{\partial\vartheta_{\mathrm{xq}}\,\partial\vartheta_{\mathrm{zq}}}\right\}_{\mathbf{k,1:3}}\mathbf{t_{qm}^0} & \mathbf{0_{6x6}} \\ \mathbf{0_{1x3}} & \mathbf{0_{1x3}} & \mathbf{0_{1x3}} & \left\{\frac{\partial^2\mathbf{T_q}}{\partial\vartheta_{\mathrm{yq}}\,\partial\vartheta_{\mathrm{xq}}}\right\}_{\mathbf{k,1:3}}\mathbf{t_{qm}^0} & \left\{\frac{\partial^2\mathbf{T_q}}{\partial\vartheta_{\mathrm{yq}}^2}\right\}_{\mathbf{k,1:3}}\mathbf{t_{qm}^0} & \left\{\frac{\partial^2\mathbf{T_q}}{\partial\vartheta_{\mathrm{yq}}\,\partial\vartheta_{\mathrm{zq}}}\right\}_{\mathbf{k,1:3}}\mathbf{t_{qm}^0} & \\ \mathbf{0_{1x3}} & \mathbf{0_{1x3}} & \mathbf{0_{1x3}} & \left\{\frac{\partial^2\mathbf{T_q}}{\partial\vartheta_{\mathrm{zq}}\,\partial\vartheta_{\mathrm{xq}}}\right\}_{\mathbf{k,1:3}}\mathbf{t_{qm}^0} & \left\{\frac{\partial^2\mathbf{T_q}}{\partial\vartheta_{\mathrm{zq}}\,\partial\vartheta_{\mathrm{yq}}}\right\}_{\mathbf{k,1:3}}\mathbf{t_{qm}^0} & \left\{\frac{\partial^2\mathbf{T_q}}{\partial\vartheta_{\mathrm{zq}}^2}\right\}_{\mathbf{k,1:3}}\mathbf{t_{qm}^0} & \\ & & & \mathbf{0_{6x6}} & & & \mathbf{I_{6x6}} \end{bmatrix} \tag{3.201}$$

$$\frac{\partial^2 \mathrm{t_{qpk}}}{\partial^2 \mathbf{p_{gpq}}} = \begin{bmatrix} \mathbf{0_{3x3}} & \mathbf{0_{3x3}} & \mathbf{0_{3x3}} & \mathbf{0_{3x1}} & \mathbf{0_{3x1}} & \mathbf{0_{3x1}} & \\ \mathbf{0_{3x3}} & \mathbf{0_{3x3}} & \mathbf{0_{3x3}} & \mathbf{0_{3x1}} & \mathbf{0_{3x1}} & \mathbf{0_{3x1}} & \\ \mathbf{0_{3x3}} & \mathbf{0_{3x3}} & \mathbf{0_{3x3}} & \mathbf{0_{3x1}} & \mathbf{0_{3x1}} & \mathbf{0_{3x1}} & \\ \mathbf{0_{3x3}} & \mathbf{0_{3x3}} & \mathbf{0_{3x3}} & \mathbf{0_{3x1}} & \mathbf{0_{3x1}} & \mathbf{0_{3x1}} & \\ \mathbf{0_{1x3}} & \mathbf{0_{1x3}} & \mathbf{0_{1x3}} & \left\{\frac{\partial^2\mathbf{T_q}}{\partial\vartheta_{\mathrm{xq}}^2}\right\}_{\boldsymbol{k},\mathbf{1:3}}\mathbf{t_{p3}^0} & \left\{\frac{\partial^2\mathbf{T_q}}{\partial\vartheta_{\mathrm{xq}}\,\partial\vartheta_{\mathrm{yq}}}\right\}_{\boldsymbol{k},\mathbf{1:3}}\mathbf{t_{p3}^0} & \left\{\frac{\partial^2\mathbf{T_q}}{\partial\vartheta_{\mathrm{xq}}\,\partial\vartheta_{\mathrm{zq}}}\right\}_{\boldsymbol{k},\mathbf{1:3}}\mathbf{t_{p3}^0} & \mathbf{0_{6x6}} \\ \mathbf{0_{1x3}} & \mathbf{0_{1x3}} & \mathbf{0_{1x3}} & \left\{\frac{\partial^2\mathbf{T_q}}{\partial\vartheta_{\mathrm{yq}}\,\partial\vartheta_{\mathrm{xq}}}\right\}_{\boldsymbol{k},\mathbf{1:3}}\mathbf{t_{p3}^0} & \left\{\frac{\partial^2\mathbf{T_q}}{\partial\vartheta_{\mathrm{yq}}^2}\right\}_{\boldsymbol{k},\mathbf{1:3}}\mathbf{t_{p3}^0} & \left\{\frac{\partial^2\mathbf{T_q}}{\partial\vartheta_{\mathrm{yq}}\,\partial\vartheta_{\mathrm{zq}}}\right\}_{\boldsymbol{k},\mathbf{1:3}}\mathbf{t_{p3}^0} & \\ \mathbf{0_{1x3}} & \mathbf{0_{1x3}} & \mathbf{0_{1x3}} & \left\{\frac{\partial^2\mathbf{T_q}}{\partial\vartheta_{\mathrm{zq}}\,\partial\vartheta_{\mathrm{xq}}}\right\}_{\boldsymbol{k},\mathbf{1:3}}\mathbf{t_{p3}^0} & \left\{\frac{\partial^2\mathbf{T_q}}{\partial\vartheta_{\mathrm{zq}}\,\partial\vartheta_{\mathrm{yq}}}\right\}_{\boldsymbol{k},\mathbf{1:3}}\mathbf{t_{p3}^0} & \left\{\frac{\partial^2\mathbf{T_q}}{\partial\vartheta_{\mathrm{zq}}^2}\right\}_{\boldsymbol{k},\mathbf{1:3}}\mathbf{t_{p3}^0} & \\ & & & \mathbf{0_{6x6}} & & & \mathbf{I_{6x6}} \end{bmatrix} \tag{3.202}$$

With:

- m = 2,3 local axis direction;
- k = 1,2,3

$$\boldsymbol{\delta B_1} = \begin{bmatrix} -\sum_{k=1}^{3}\left(\left\{\frac{\partial^2 c_{pq1k}}{\partial^2 \mathbf{p_{gpq}}}\right\}_{\mathbf{1:3,1:3}} t_{p2k}\right) & -\left\{\left(\frac{\partial \mathbf{c_{pq1}}}{\partial \mathbf{p_{gpq}}}\right)^{\mathbf{T}}\left(\frac{\partial \mathbf{t_{p2}}}{\partial \mathbf{p_{gpq}}}\right)\right\}_{\mathbf{1:3,4,6}} & -\sum_{k=1}^{3}\left(\left\{\frac{\partial^2 c_{pq1k}}{\partial^2 \mathbf{p_{gpq}}}\right\}_{\mathbf{1:3,7:9}} t_{p2k}\right) & \mathbf{0_{3x3}} & \\ -\left\{\left(\frac{\partial \mathbf{c_{pq1}}}{\partial \mathbf{p_{gpq}}}\right)^{\mathbf{T}}\left(\frac{\partial \mathbf{t_{p2}}}{\partial \mathbf{p_{gpq}}}\right)\right\}_{\mathbf{4:9,1,3}} & -\sum_{k=1}^{3}\left(\left\{\frac{\partial^2 t_{p2k}}{\partial^2 \mathbf{p_{gpq}}}\right\}_{\mathbf{4:6,4:6}} c_{pq1k}\right) & \mathbf{0_{3x3}} & \mathbf{0_{3x3}} & \mathbf{0_{6x6}} \\ -\sum_{k=1}^{3}\left(\left\{\frac{\partial^2 c_{pq1k}}{\partial^2 \mathbf{p_{gpq}}}\right\}_{\mathbf{7:9,1:3}} t_{p2k}\right) & \mathbf{0_{3x3}} & -\sum_{k=1}^{3}\left(\left\{\frac{\partial^2 c_{pq1k}}{\partial^2 \mathbf{p_{gpq}}}\right\}_{\mathbf{7:9,7:9}} t_{p2k}\right) & \mathbf{0_{3x3}} & \\ \mathbf{0_{3x3}} & \mathbf{0_{3x3}} & \mathbf{0_{3x3}} & \mathbf{0_{3x3}} & \mathbf{0_{6x6}} \end{bmatrix} \tag{3.203}$$

$$\boldsymbol{\delta B_2} = \begin{bmatrix} -\sum_{k=1}^{3}\left(\left\{\frac{\partial^2 c_{pq1k}}{\partial^2 \mathbf{p_{gpq}}}\right\}_{\mathbf{1:3,1:3}} t_{p3k}\right) & -\left\{\left(\frac{\partial \mathbf{c_{pq1}}}{\partial \mathbf{p_{gpq}}}\right)^{\mathbf{T}}\left(\frac{\partial \mathbf{t_{p3}}}{\partial \mathbf{p_{gpq}}}\right)\right\}_{\mathbf{1:3,4,6}} & -\sum_{k=1}^{3}\left(\left\{\frac{\partial^2 c_{pq11}}{\partial^2 \mathbf{p_{gpq}}}\right\}_{\mathbf{1:3,7:9}} t_{p3k}\right) & \mathbf{0_{3x3}} & \\ -\left\{\left(\frac{\partial \mathbf{c_{pq1}}}{\partial \mathbf{p_{gpq}}}\right)^{\mathbf{T}}\left(\frac{\partial \mathbf{t_{p3}}}{\partial \mathbf{p_{gpq}}}\right)\right\}_{\mathbf{4:9,1,3}} & -\sum_{k=1}^{3}\left(c_{pq1k}\left\{\frac{\partial^2 t_{p3k}}{\partial^2 \mathbf{p_{gpq}}}\right\}_{\mathbf{4:6,4:6}}\right) & \mathbf{0_{3x3}} & \mathbf{0_{3x3}} & \mathbf{0_{6x6}} \\ -\sum_{k=1}^{3}\left(\left\{\frac{\partial^2 c_{pq1k}}{\partial^2 \mathbf{p_{gpq}}}\right\}_{\mathbf{7:9,1:3}} t_{p3k}\right) & \mathbf{0_{3x3}} & -\sum_{k=1}^{3}\left(\left\{\frac{\partial^2 c_{pq11}}{\partial^2 \mathbf{p_{gpq}}}\right\}_{\mathbf{7:9,7:9}} t_{p3k}\right) & \mathbf{0_{3x3}} & \\ \mathbf{0_{3x3}} & \mathbf{0_{3x3}} & \mathbf{0_{3x3}} & \mathbf{0_{3x3}} & \mathbf{0_{6x6}} \end{bmatrix} \tag{3.204}$$

$$\boldsymbol{\delta B_3} = \begin{bmatrix} -\sum_{k=1}^{3}\left(\left\{\frac{\partial^2 c_{pq1k}}{\partial^2 \mathbf{p_{gpq}}}\right\}_{\mathbf{1:3,1:3}} t_{q2k}\right) & \mathbf{0_{3x3}} & -\sum_{k=1}^{3}\left(\left\{\frac{\partial^2 c_{pq11}}{\partial^2 \mathbf{p_{gpq}}}\right\}_{\mathbf{1:3,7:9}} t_{q2k}\right) & -\left\{\left(\frac{\partial \mathbf{c_{pq1}}}{\partial \mathbf{p_{gpq}}}\right)^{\mathbf{T}}\left(\frac{\partial \mathbf{t_{q2}}}{\partial \mathbf{p_{gpq}}}\right)\right\}_{\mathbf{1:3,10,12}} & \\ \mathbf{0_{3x3}} & \mathbf{0_{3x3}} & \mathbf{0_{3x3}} & \mathbf{0_{3x3}} & \\ -\sum_{k=1}^{3}\left(\left\{\frac{\partial^2 c_{pq1k}}{\partial^2 \mathbf{p_{gpq}}}\right\}_{\mathbf{7:9,1:3}} t_{q2k}\right) & \mathbf{0_{3x3}} & -\sum_{k=1}^{3}\left(\left\{\frac{\partial^2 c_{pq1k}}{\partial^2 \mathbf{p_{gpq}}}\right\}_{\mathbf{7:9,7:9}} t_{q2k}\right) & \mathbf{0_{3x3}} & \mathbf{0_{6x6}} \\ -\left\{\left(\frac{\partial \mathbf{c_{pq1}}}{\partial \mathbf{p_{gpq}}}\right)^{\mathbf{T}}\left(\frac{\partial \mathbf{t_{q2}}}{\partial \mathbf{p_{gpq}}}\right)\right\}_{\mathbf{10:12,1,3}} & \mathbf{0_{3x3}} & \mathbf{0_{3x3}} & -\sum_{k=1}^{3}\left(c_{pq1k}\left\{\frac{\partial^2 t_{q2k}}{\partial^2 \mathbf{p_{gpq}}}\right\}_{\mathbf{10:12,10:12}}\right) & \\ \mathbf{0_{6x6}} & & & & \mathbf{0_{6x6}} \end{bmatrix} \tag{3.205}$$

$$\boldsymbol{\delta B_4} = \begin{bmatrix} -\sum_{k=1}^{3}\left(\left\{\frac{\partial^2 c_{pq1k}}{\partial^2 \mathbf{p_{gpq}}}\right\}_{\mathbf{1:3,1:3}} t_{q3k}\right) & \mathbf{0_{3x3}} & -\sum_{k=1}^{3}\left(\left\{\frac{\partial^2 c_{pq11}}{\partial^2 \mathbf{p_{gpq}}}\right\}_{\mathbf{1:3,7:9}} t_{q3k}\right) & -\left\{\left(\frac{\partial \mathbf{c_{pq1}}}{\partial \mathbf{p_{gpq}}}\right)^{\mathbf{T}}\left(\frac{\partial \mathbf{t_{q3}}}{\partial \mathbf{p_{gpq}}}\right)\right\}_{\mathbf{1:3,10,12}} & \\ \mathbf{0_{3x3}} & \mathbf{0_{3x3}} & \mathbf{0_{3x3}} & \mathbf{0_{3x3}} & \\ -\sum_{k=1}^{3}\left(\left\{\frac{\partial^2 c_{pq1k}}{\partial^2 \mathbf{p_{gpq}}}\right\}_{\mathbf{7:9,1:3}} t_{q3k}\right) & \mathbf{0_{3x3}} & -\sum_{k=1}^{3}\left(\left\{\frac{\partial^2 c_{pq1k}}{\partial^2 \mathbf{p_{gpq}}}\right\}_{\mathbf{7:9,7:9}} t_{q3k}\right) & \mathbf{0_{3x3}} & \mathbf{0_{6x6}} \\ -\left\{\left(\frac{\partial \mathbf{c_{pq1}}}{\partial \mathbf{p_{gpq}}}\right)^{\mathbf{T}}\left(\frac{\partial \mathbf{t_{q3}}}{\partial \mathbf{p_{gpq}}}\right)\right\}_{\mathbf{10:12,1,3}} & \mathbf{0_{3x3}} & \mathbf{0_{3x3}} & -\sum_{k=1}^{3}\left(c_{pq1k}\left\{\frac{\partial^2 t_{q3k}}{\partial^2 \mathbf{p_{gpq}}}\right\}_{\mathbf{10:12,10:12}}\right) & \\ \mathbf{0_{6x6}} & & & & \mathbf{0_{6x6}} \end{bmatrix} \tag{3.206}$$

$$\boldsymbol{\delta B_5} = \begin{bmatrix} -\left\{\frac{\partial \mathbf{c_{pq1}}}{\partial \mathbf{p_{gpq}}}\right\}_{\mathbf{1:3,1:3}} & \mathbf{0_{3x3}} & -\left\{\frac{\partial \mathbf{c_{pq1}}}{\partial \mathbf{p_{gpq}}}\right\}_{\mathbf{1:3,7:9}} & \mathbf{0_{3x3}} & \\ \mathbf{0_{3x3}} & \mathbf{0_{3x3}} & \mathbf{0_{3x3}} & \mathbf{0_{3x3}} & \\ -\left\{\frac{\partial \mathbf{c_{pq1}}}{\partial \mathbf{p_{gpq}}}\right\}_{\mathbf{7:9,1:3}} & \mathbf{0_{3x3}} & -\left\{\frac{\partial \mathbf{c_{pq1}}}{\partial \mathbf{p_{gpq}}}\right\}_{\mathbf{7:9,7:9}} & \mathbf{0_{3x3}} & \mathbf{0_{6x6}} \\ \mathbf{0_{3x3}} & \mathbf{0_{3x3}} & \mathbf{0_{3x3}} & \mathbf{0_{3x3}} & \\ \mathbf{0_{6x6}} & & & & \mathbf{0_{6x6}} \end{bmatrix} \tag{3.207}$$

$$\boldsymbol{\delta B_6} = \begin{bmatrix} \mathbf{0_{3x3}} & \mathbf{0_{3x3}} & \mathbf{0_{3x3}} & \mathbf{0_{3x3}} & \\ \mathbf{0_{3x3}} & \sum_{k=1}^{3}\left(\left\{\frac{\partial^2 t_{p3k}}{\partial^2 \mathbf{p_{gpq}}}\right\}_{\mathbf{4:6,4:6}} t_{pqk}\right) & \mathbf{0_{3x3}} & \left\{\left(\frac{\partial \mathbf{t_{p3}}}{\partial \mathbf{p_{gpq}}}\right)^{\mathbf{T}}\left(\frac{\partial \mathbf{t_{pq}}}{\partial \mathbf{p_{gpq}}}\right)\right\}_{\mathbf{4:6,10,12}} & \mathbf{0_{6x6}} \\ \mathbf{0_{3x3}} & \mathbf{0_{3x3}} & \mathbf{0_{3x3}} & \mathbf{0_{3x3}} & \\ \mathbf{0_{3x3}} & \left\{\left(\frac{\partial \mathbf{t_{p3}}}{\partial \mathbf{p_{gpq}}}\right)^{\mathbf{T}}\left(\frac{\partial \mathbf{t_{pq}}}{\partial \mathbf{p_{gpq}}}\right)\right\}_{\mathbf{10:12,4,6}} & \mathbf{0_{3x3}} & \sum_{k=1}^{3}\left(\left\{\frac{\partial^2 \mathbf{t}_{pqk}}{\partial^2 \mathbf{p_{gpq}}}\right\}_{\mathbf{10:12,10:12}} t_{p3k}\right) & \\ \mathbf{0_{6x6}} & & & & \mathbf{0_{6x6}} \end{bmatrix} \tag{3.208}$$

It is important to note that matrices $\boldsymbol{\delta}\mathbf{B}_\mathbf{n}$ are symmetric because of the way in which the co-rotational degrees of freedom were defined.

3.5 Comparison between Approach I and Approach II

The two co-rotational framework adopted in this thesis do not produce differences in terms of results, both lead to accurate results as better specified in Chapter 4 reporting some numerical applications.

The first approach is based on the Rodriguez formula and no kinematic approximation is adopted. The rotational degrees of freedom are the spatial form of the pseudo-rotational vector $\boldsymbol{\vartheta}$. If the convergence is possible, each step of the analysis can be arbitrarily large ($\|\delta\boldsymbol{\vartheta}\| < 2\pi$) without introducing errors, however the step has to be maintained small enough if constitutive nonlinearities have taken into account. It is also possible to transform the non-additive spatial pseudo rotational vector $\boldsymbol{\vartheta}$ to the additive pseudo vector $\boldsymbol{\psi}$ using the connection $T_s(\psi)$ (A.22) and modifying the geometrical stiffness matrix. However, this possibility has not been investigated in this thesis because it is not needed to evaluate a unique transformation $\mathbf{R} = \exp(\boldsymbol{\psi})$ that moves the body from the initial to the final point. Due to the nature of the rotations and the kinematic formulation without approximation, the geometric stiffness matrix is not symmetric.

In the second approach an incremental strategy is used to model the effect of large rotations, an improved rotational transformation matrix is adopted in order to reduce spurious lengthening of vectors upon rotation. The calculation of rotations in the system is performed incrementally using element-based vectors. This approach leads to a symmetric stiffness matrix.

Since the non-linearity of the material of the masonry structures imposes the use of an incremental numerical procedure this strategy appears particularly advantageous when both material and geometrical

nonlinearities have to be taken into account the second approach is computationally less demanding in a single step.

3.6 Virtual Work Principle

The internal Virtual Work under the assumption of small deformation can be written in the following form:

$$\begin{aligned} L_i^{element} + L_i^{interface} \\ = \iiint_V \boldsymbol{\delta}\mathbf{u}^{\mathrm{T}} \rho \mathbf{b} dV + \iint_\Gamma \boldsymbol{\delta}\mathbf{u}^{\mathrm{T}} \mathbf{t_n} \, d\Gamma \\ - \iiint_V \boldsymbol{\delta}\mathbf{u}^{\mathrm{T}} \rho \ddot{\mathbf{u}} dV \end{aligned} \tag{3.209}$$

Where:

- $\boldsymbol{\delta}$ symbol means virtual.
- $\mathbf{b}$ is a field of mass forces;
- $\ddot{\mathbf{u}}$ is the acceleration field;

$\mathbf{t_n}$ is a field of forces that are applied on the boundary;

3.6.1 The internal virtual work and stiffness matrix of the element

In this paragraph, the stiffness matrix of the macro-element is obtained. The main idea is that the element is treated as a continuum that can only perform pure shear deformations. Differently with the classical formulation of the DMEM discussed in Chapter 2, the proposed

formulation assumes that all the point of the element is subjected to a transformation that is a "pure" shear deformation (3.12):

$$L_i^{element} = \iiint_V tr\left(\mathbf{T} \bullet \widetilde{\mathbf{E}}\right) dV = \iiint_V \tau_{12}\widetilde{\gamma_{12}} + \tau_{13}\widetilde{\gamma_{13}} + \tau_{23}\widetilde{\gamma_{23}} dV \tag{3.210}$$

The constitutive law for the linear elastic isotropic material is:

$$\mathbf{T} = \lambda(tr\mathbf{E})\mathbf{I} + 2\mu\mathbf{E} \tag{3.211}$$

where:

- $\lambda = \frac{E\upsilon}{2(1+2\upsilon)}$
- $\mu = G = \frac{E}{2(1+\upsilon)}$
- υ is the Poisson ratio
- E is the Young modulus
- G is the shear modulus

Using the (3.12) the equation (3.211) is equal to:

$$\mathbf{T} = 2G\mathbf{E} = \begin{bmatrix} 0 & G\gamma_{12} & G\gamma_{13} \\ G\gamma_{12} & 0 & G\gamma_{23} \\ G\gamma_{13} & G\gamma_{23} & 0 \end{bmatrix} \tag{3.212}$$

Defining the following vectors:

$$\boldsymbol{\tau}^T = [\tau_{12} \quad \tau_{13} \quad \tau_{23}] \tag{3.213}$$

$$\boldsymbol{\gamma}^T = [\gamma_{12} \quad \gamma_{13} \quad \gamma_{23}] \tag{3.214}$$

The equation (3.212) can be written as:

$$\boldsymbol{\tau} = G\boldsymbol{\gamma} \tag{3.215}$$

The internal virtual work with the hypothesis of homogeneous linearized strain is equal to:

$$L_i^{element} = \iiint_V \boldsymbol{\delta\gamma}^{\mathbf{T}}\boldsymbol{\tau}\, dV = \iiint_V \boldsymbol{\delta\gamma}^{\mathbf{T}}\mathrm{G}\boldsymbol{\gamma} dV = \boldsymbol{\delta\gamma}^{\mathbf{T}}\mathrm{G}V\boldsymbol{\gamma} \tag{3.216}$$

Using global degrees of freedom $\boldsymbol{\delta\mathbf{p}_g}$ the internal virtual work is equal to:

$$L_i^{element} = \boldsymbol{\delta\mathbf{p}_g}^{\mathbf{T}} \begin{bmatrix} \mathbf{0}_{6x6} & \mathbf{0}_{6x1} & \mathbf{0}_{6x1} & \mathbf{0}_{6x1} \\ \mathbf{0}_{1x6} & \mathrm{G}V & 0 & 0 \\ \mathbf{0}_{1x6} & 0 & \mathrm{G}V & 0 \\ \mathbf{0}_{1x6} & 0 & 0 & \mathrm{G}V \end{bmatrix} \mathbf{p_g} = \boldsymbol{\delta\mathbf{p}_g}^{\mathbf{T}}\mathbf{q_g} \tag{3.217}$$

$$\boldsymbol{\delta\mathbf{q}_g} = \mathbf{K}^{\boldsymbol{el}}\boldsymbol{\delta\mathbf{p}_g} \quad \mathbf{K}^{\boldsymbol{el}} = \begin{bmatrix} \mathbf{0}_{6x6} & \mathbf{0}_{6x1} & \mathbf{0}_{6x1} & \mathbf{0}_{6x1} \\ \mathbf{0}_{1x6} & \mathrm{G}V & 0 & 0 \\ \mathbf{0}_{1x6} & 0 & \mathrm{G}V & 0 \\ \mathbf{0}_{1x6} & 0 & 0 & \mathrm{G}V \end{bmatrix} \tag{3.218}$$

The quantity $\mathbf{K}^{\boldsymbol{el}}$ is related to the stiffness matrix contribution of the element related to its shear deformability. Note that the matrix here obtained is valid for the isotropic elastic material. Following the same approach, it is possible to obtain the stiffness matrix for the orthotropic elastic material. According to the DMEM the material non-linearity is managed using a variable G shear modulus.

3.6.2 The internal virtual work contribution and stiffness matrix of the interface

The internal virtual work is evaluated in the paragraph 3.2. The equation (3.6) and (3.8) reports respectively the internal virtual work and the stiffness matrices.

Geometric stiffness matrix: $\delta\mathbf{B}^{\mathbf{T}}\mathbf{q_c} = \mathbf{K}_{\mathbf{g}}^{\boldsymbol{int}}\delta\mathbf{p_{gpq}}$ (3.219)

Material stiffness matrix: $\mathbf{B}^{\mathbf{T}}\mathbf{K_c}\mathbf{B}\delta\mathbf{p_{gpq}} = \mathbf{K}_{\mathbf{m}}^{\boldsymbol{int}}\delta\mathbf{p_{gpq}}$ (3.220)

3.6.3 External Virtual Work

$$L_{ve} = \iiint_V \boldsymbol{\delta}\mathbf{u}^{\mathrm{T}} \rho \mathbf{b} dV + \iint_\Gamma \boldsymbol{\delta}\mathbf{u}^{\mathrm{T}} \mathbf{t_n}\, d\Gamma - \iiint_V \boldsymbol{\delta}\mathbf{u}^{\mathrm{T}} \rho \ddot{\mathbf{u}} dV + \sum_{j=1}^{m} \boldsymbol{\delta}\mathbf{u}_{\mathbf{j}}^{\mathrm{T}} \left(\mathrm{x_j}, \mathrm{y_j}, \mathrm{z_j}\right) \mathbf{F_j}(\mathrm{x_j}, \mathrm{y_j}, \mathrm{z_j}) \tag{3.221}$$

The first integral is related to the volume forces, the second one is related to the boundary forces the third is related to the kinematic energy, last term is related to the concentrated forces directly applied to the element. As descripted before, the vector $\boldsymbol{\delta}\mathbf{u}^{\mathrm{T}}$ is a displacement field and it is dependent from the coordinates $\boldsymbol{\delta}\mathbf{u}^{\mathrm{T}}(\mathrm{x}, \mathrm{y}, \mathrm{z})$. Using the intrisic reference system, the first integral is equal to:

$$L_{ve} = \boldsymbol{\delta}\mathbf{p_\ell}^{\mathrm{T}} \iiint_{-1}^{1} \boldsymbol{\Psi}^{\mathbf{T}} \rho \mathbf{b}\, \det(\mathrm{J}) d\xi\, d\eta\, d\zeta \tag{3.222}$$

$\mathbf{p_\ell}$ is a vector that contains nodal displacement referred to the global reference system.

Using the equation (3.14) the following equation is obtained:

$$\delta \mathbf{p_\ell} = \begin{bmatrix} \mathbf{B_{\ell 1}} \\ \mathbf{B_{\ell 2}} \\ \mathbf{B_{\ell 3}} \\ \mathbf{B_{\ell 4}} \\ \mathbf{B_{\ell 5}} \\ \mathbf{B_{\ell 6}} \\ \mathbf{B_{\ell 7}} \\ \mathbf{B_{\ell 8}} \end{bmatrix} \delta\boldsymbol{\gamma} = \mathbf{B_\ell} \delta\boldsymbol{\gamma} \rightarrow \delta \mathbf{p_\ell} = \mathbf{D}\ \boldsymbol{\delta}\mathbf{p_g} \tag{3.223}$$

Using the (3.223) and (3.222) the external virtual work in terms of global degrees of freedom is obtained:

$$L_{ve} = \boldsymbol{\delta}\mathbf{p_g^T} \mathbf{D^T} \iiint_{-1}^{1} \boldsymbol{\Psi}^{\mathbf{T}} \rho \mathbf{b}\, \det(\mathrm{J}) d\xi\, d\eta\, d\zeta \tag{3.224}$$

In order to obtain the external virtual work related to concentrated forces it is important to apply the force $\mathbf{F_j}(\mathrm{x_j}, \mathrm{y_j}, \mathrm{z_j})$ in the intrinsic reference system. So, the coordinates of points $\mathbf{P_j} = \{\mathrm{x_j}, \mathrm{y_j}, \mathrm{z_j}\}$ in the intrinsic reference system are needed $\{\xi_j, \eta_j, \zeta_j\}$.

$$L_{ve} = \boldsymbol{\delta \mathbf{p}_{\boldsymbol{\ell}}}^{\mathrm{T}} \sum_{j=1}^{m} \boldsymbol{\Psi}^{\mathbf{T}} \mathbf{F_j}(\xi_j, \eta_j, \zeta_j) \tag{3.225}$$

with:

$$\begin{aligned} \mathrm{x_j} &= \sum_{\mathrm{i}=1}^{8} \Psi_{\mathrm{i}}\{\xi_j, \eta_j, \zeta_j\}\mathrm{x_i} \\ \mathrm{y_j} &= \sum_{\mathrm{i}=1}^{8} \Psi_{\mathrm{i}}\{\xi_j, \eta_j, \zeta_j\}\mathrm{y_i} \\ \mathrm{z_j} &= \sum_{\mathrm{i}=1}^{8} \Psi_{\mathrm{i}}\{\xi_j, \eta_j, \zeta_j\}\mathrm{z_i} \end{aligned} \tag{3.226}$$

In this case $\{\xi_j, \eta_j, \zeta_j\}$ are the unknown quantities of the (3.226). Solving the previous equation, and, using the (3.223),(3.225) the external virtual work in terms of global degrees of freedom is obtained:

$$L_{ve} = \boldsymbol{\delta \mathbf{p}_{\mathbf{g}}^{\mathbf{T}}} \mathbf{D}^{\mathbf{T}} \sum_{j=1}^{m} \boldsymbol{\Psi}^{\mathbf{T}} \mathbf{F_j}(\xi_j, \eta_j, \zeta_j) \tag{3.227}$$

3.7 Mechanical characterization of the model

This subsection describes the mechanical characterised of the that follows the same strategy described in paragraph 2.5 with reference to the discrete macro-elements already proposed in the context of the DMEM.

3.7.1 Linear Elastic Calibration

The proposed model solid element has a lot of capabilities and the mechanical calibration procedures differ according to the particular problem under investigation. Differently from the spatial macro-elements already introduced, the solid element here proposed has been formulated considered continuous distributed interfaces which inherit and concentrate the mechanical properties of the related structure macro-portion. As better specified in the following, the solid element can be also successfully used for model different structural typologies such as steel and concrete structures.

The homogenization technique is based on a straightforward fiber approach. Each interface is a 2D continuous surface having a three-dimensional stiffness matrix (3.62) that synthetize the mechanical behaviour of the adjacent elements that connects. The properties of the zero-thickness interface are directly related to the adjacent element material characteristics and their integration follows a Gauss quadrature strategy.

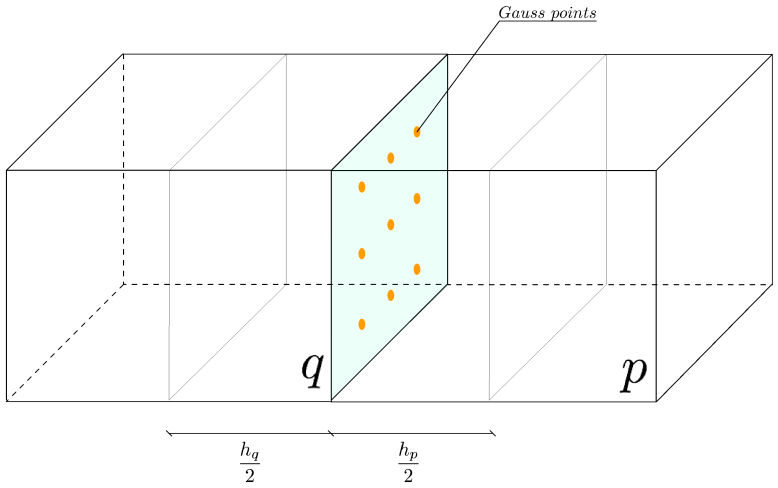

Figure 29 - Interface Gauss Points

By following the same approach already considered for the previously introduced methods, paragraph 2.5, in the application reported in chapter 4 the flexural mechanism has been assumed to be uncoupled to the sliding behaviour. However the sliding failure response is influenced by the axial force distribution on the interface owing to the adoption of Coulomb type constitutive laws. ..

3.7.2 The shear deformability

As previously discussed in Chapter 2, the DMEM is able to catch the main failure mechanisms of a masonry structure by considering an assemblage of macro-element. Flexural behaviour, slide behaviour along mortar bed, and shear element behaviour or a combination of them are captured by the interface and elements' deformability. Figure 30

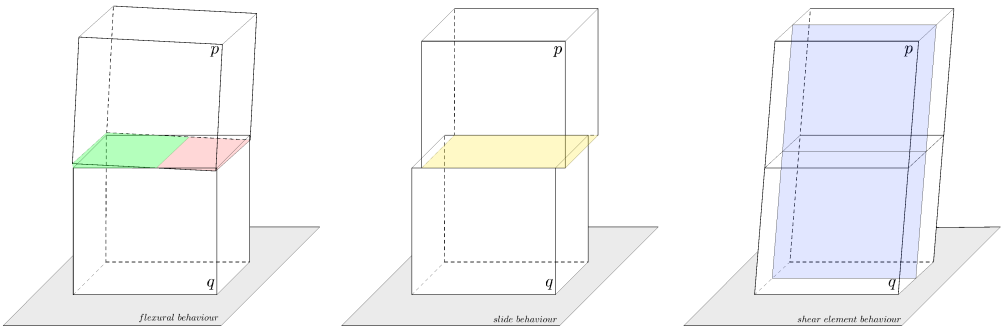

Figure 30 – Mechanical behaviour of masonry

The overall elastic shear deformation of a masonry infill, discretised by several macro-elements, is partly related to the shear deformability of the elements and partly attributed to the sliding deformability along the interfaces. The element shear failure is ruled according to suitable constitutive laws able to account for the shear-diagonal response of unreinforced masonry structures [34]. The shear sliding behaviour, ruled by the interfaces, is related to the shear-sliding failure mechanism generally governed by appropriate Mohr Coulomb constitutive laws. More details on the general calibration strategy can be found in [39].

As reported in Table 3, a series of mechanical parameters are needed in order to model a masonry structure using the DMEM proposed. In the applications reported in the following, the flexural mechanism is modelled using fracture energy constitutive laws, sliding mechanism is modelled

using Mohr-Coulomb failure mechanisms and the shear element deformability is modelled using three Turnsek-Cacovic constitutive laws.

Flexural mechanism (Fracture Energy constitutive law)	Sliding mechanism (Mohr-Coulomb yieldning criterion)	3 Shear diagonal mechanism (Turnsek-Cacovic constitutive law)
E, Young's modulus	G, Shear modulus;	G, Shear modulus;
f_c, Compression Strength;	c, cohesion;	τ_0, tangential strength;
$G_{f,C}$ Compression fracture Energy	$tan\phi$, friction coefficient;	
f_t, Tensile Strength;	$G_{f,II}$ shear fracturalas Energy (MODE II)	
$G_{f,I}$ Tensile fracture Energy (MODE I)		

Table 3 – Mechanical parameters

These parameters are needed for each macro element.

3.7.2.1 Sliding mechanism

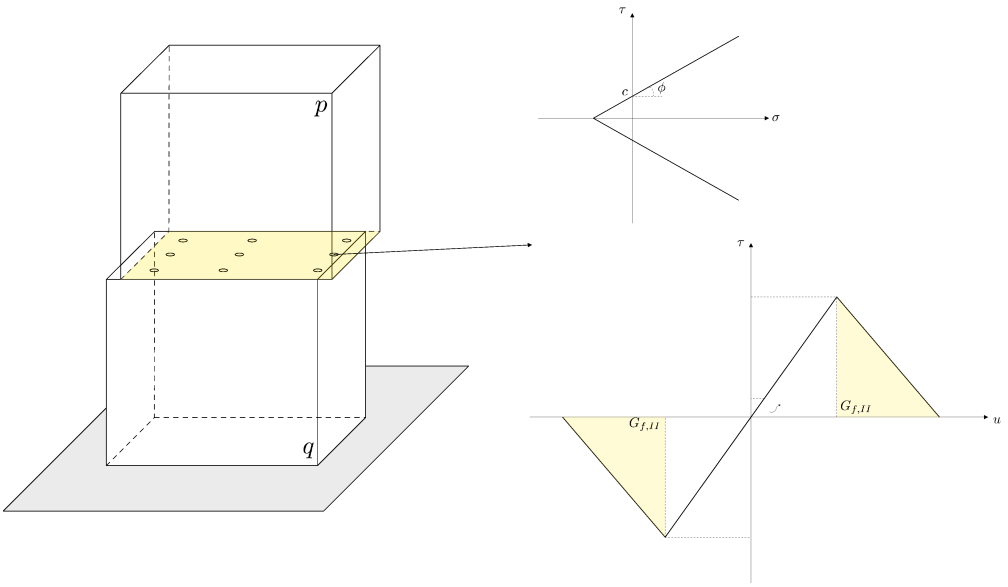

Figure 31 - Slide behavior

The sliding mechanism is concentrated on the deformation of the interfaces. The stiffness equivalent parameters $k_{//1}$ and $k_{//2}$ are obtained with the same procedure descript in **Errore. L'origine riferimento non è stata trovata.**, following a Mohr-Coulomb constitutive law. Equivalent strengths and Fractural energy are evaluated using the **Errore. L'origine riferimento non è stata trovata.**

3.7.2.2 The Shear diagonal mechanism (Turnsek-Cacovic constitutive law)

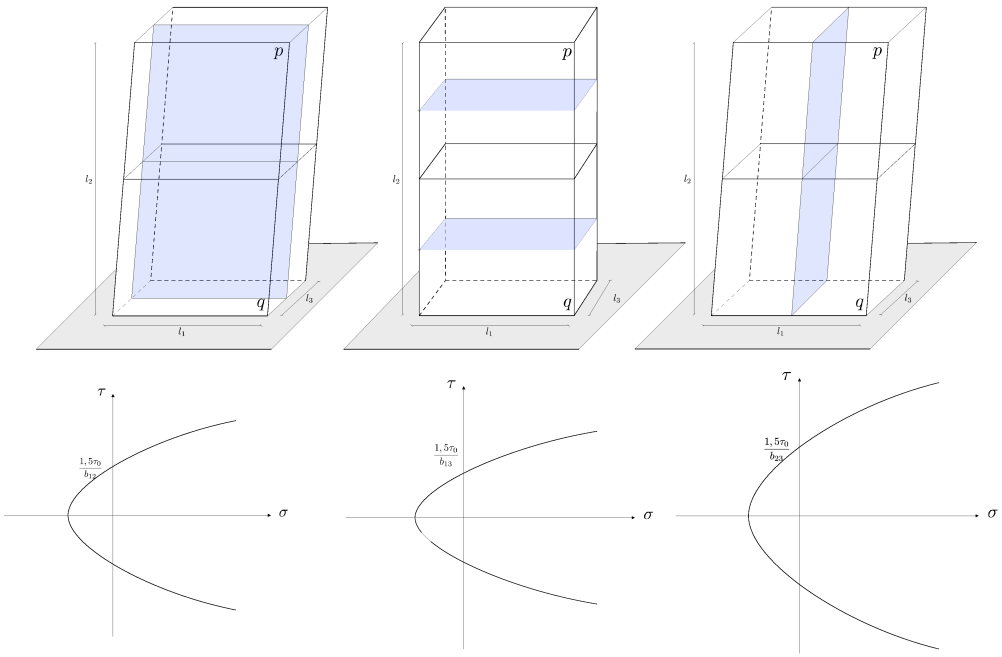

Figure 32 - Shear diagonal mechanism

For masonry structure, the element shear deformability can be described according to the Turnsek-Cacovic or Mohr-Coulomb yielding criterion. The Turnsek-Cacovic criterion can be described according to the following well known equation:

$$\tau_{\mathrm{u}} = \frac{1{,}5\ \tau_0}{b} \sqrt{1 + \frac{\sigma}{1{,}5\ \tau_0}} \tag{3.228}$$

It is worth to notice that this particular criterion has been conceived for modelling the shear diagonal mechanism of masonry walls. With reference to the solid macro-element three shear-diagonal parameters have to be defined for characterising the nonlinear shear behaviour in the space, Figure 32.

3.7.3 The axial-flexural behaviour

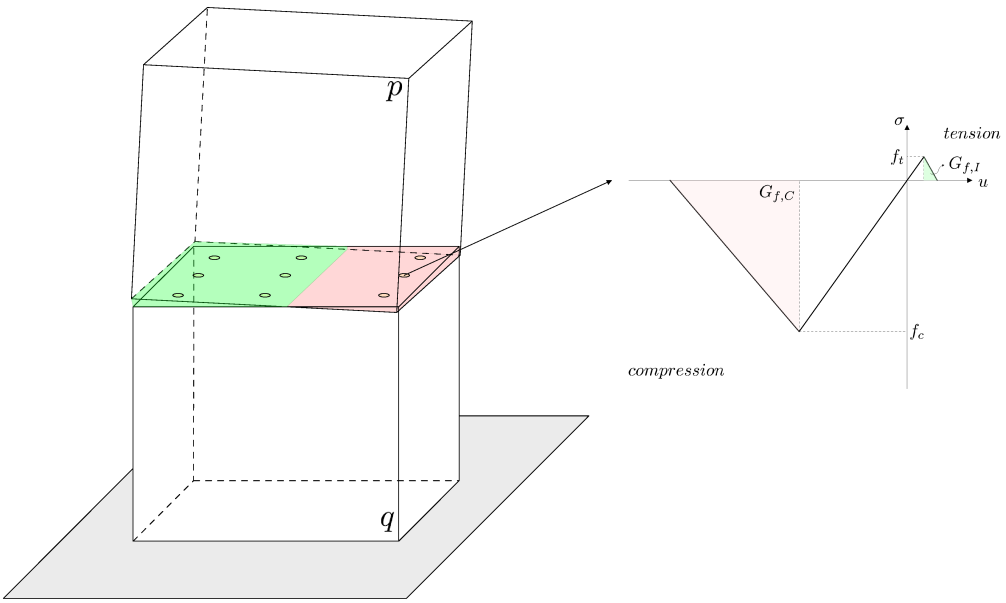

Figure 33 - Flexural behavior

As already discussed in Chapter 2, The flexural mechanism is lamped on the deformation of the interfaces.

The orthogonal stiffness of the interface encompasses the mechanical properties of the adjacent elements assuming the masonry as an orthotropic homogeneous media. If the interface discretization follows a fiber calibration approach, the evaluation of the contribution of the j-th fiber to the tangent stiffness component in the direction orthogonal to the interface, is performed by considering the corresponding influence volume. These are calibrated from the masonry mechanical properties for each direction of orthotropic. The interface is conceived to incorporate the nonlinear response of two adjacent elements, as reported in paragraph 2.5.1 the stiffness properties of the interface are obtained by considering two inelastic nonlinear springs in series leading to a unique uniaxial constitutive law. With reference to the fracture energy, it has been

assumed to make reference to the fracture related to the minimum value of strength. This assumption is justified by the consideration that if a fiber reaches his limit first, it starts to flow plastically and the other fiber cannot reach the softening branch. It is clear that this assumption is a simplification of more complex behaviour however it allows to contains the degrees of freedom to be considered and provides sufficiently accurate results as shown in the next chapter.

It is worth to notice that more complex constitutive laws can attributed to the nonlinear two-dimensional zero-thickness interfaces and to the shear element deformability.

3.8 Updated Lagrangian Formulation and Newton Raphson Method

In the previous paragraphs the global tangent stiffness matrices of elements and interfaces have been evaluated. Standard procedures have been used for assembling the global stiffness matrix of the entire structure. The geometrical and constitutive non-linearity imposes the use of an iterative method to solve the problem. Standard Newton Rapson based iterative methods have been implemented for validating the model, as briefly summarized in what follows.

The equation to solve is:

$$ {}^{n}\mathbf{K}_{\mathbf{Global}}(\boldsymbol{u})\,{}^{n}\boldsymbol{\Delta u} = {}^{n}\boldsymbol{\Delta F} \tag{3.229} $$

where:

- ${}^{n}\mathbf{K}_{\mathbf{Global}}$ is the global tangent stiffness matrix of the entire structure;
- ${}^{n}\boldsymbol{\Delta u}$ is the unknown increment of the displacement vector;
- ${}^{n}\boldsymbol{\Delta F}$ is the increment of the force vector;

All these quantities are evaluated at the step $\boldsymbol{n}$ of the analysis;

The iterative procedure used in this thesis is the Newton Raphson Method. In particular Newton Raphson Classical/Modified Force Control, Displacement Control and Arc Length were used[28,40] following the basic scheme reported in Figure 34.

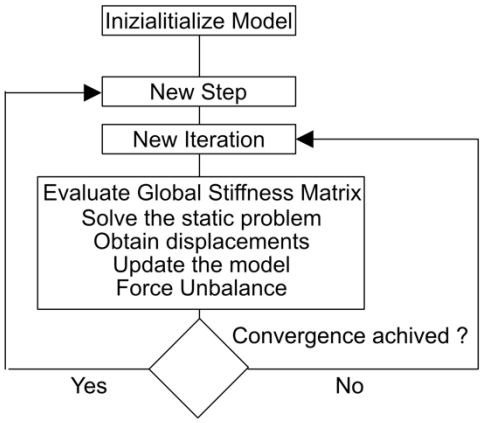

Figure 34 - Solution procedure

3.8.1 Main functions

3.8.1.1 Initialize Model

This function initializes the model, in particular using the nodal coordinates, each element is instantiated. Also, the three mono dimensional non-linear constitutive laws related to the element are instantiated. Furthermore, the program automatically calculates a series of parameters necessary for the analysis such as:

- Initial Reference system;
- Centroid;
- Initial reference system of each interface;
- Initial Stiffness Matrix of the element;

After the creation of each element, an automatically procedure check the coincidence the faces of each element and it identifies interfaces. Even for the interfaces a lot of parameters are automatically evaluated. For example:

- Local and co-rotational reference system;

- Geometrically local matrices discussed in previous paragraphs;
- Initial Stiffness Matrix of the interface;
- Constitutive laws related to the Gauss Points are also instantiated.
- After the creation of each element and each interface of the model, degrees of freedom, with a proper numeration, are saved inside a matrix. It is needed to assemble properly each degree of freedom to obtain global matrices.

3.8.1.2 Evaluate global stiffness matrix and solve the static problem

Assembling each stiffness matrices of each computational object of the model, the global stiffness matrix of the model ${}^{n}\mathbf{K}_{\boldsymbol{Global}}$ is obtained.

In this way it is possible to do the linear prediction in order to obtain global displacements:

$$ {}^{n}\boldsymbol{\Delta u} = {}^{n}\mathbf{K}_{\boldsymbol{Global}}{}^{-1}\,{}^{n}\boldsymbol{\Delta F} \tag{3.230}$$

3.8.1.3 Obtain local displacements

${}^{n}\boldsymbol{\Delta u}$ is a vector that contains all displacements, rotation angles and deformations of the model. So, it is possible to divide this vector and assign the correct parameters to each element.

For each element the following vector that is the trial solution is obtained:

$$ {}^{\mathbf{trial}}\mathbf{p}_{\mathrm{gq}}^{\mathrm{T}} = [\mathbf{u}_{\mathbf{gq}}^{\mathbf{T}} \quad \boldsymbol{\vartheta}_{\mathbf{gq}}^{\mathbf{T}} \quad \boldsymbol{\Gamma}_{\mathbf{q}}^{\mathbf{T}}] \tag{3.231}$$

$\boldsymbol{\vartheta}_{\mathbf{gq}}^{\mathbf{T}}$ is a vector that contains three rotation parameters. This vector is different for the Battini and Izzuddin parametrization:

- *approach I:* $\boldsymbol{\vartheta}^{\mathbf{T}}_{\mathbf{gq}}$ it is a rotational vector obtained from the linear prediction (3.230) so $\boldsymbol{\vartheta}^{\mathbf{T}}_{\mathbf{gq}} \in so(3)$, To obtain the correct rotational matrix in $SO(3)$ an exponential mapping is needed so it is possible to use the Rodriguez Formula (A.8).

$$\mathbf{R}_{\mathbf{rotq}} = \mathbf{exp}[{}^{\mathbf{trial}}\boldsymbol{\vartheta}^{\mathbf{T}}_{\mathbf{gq}}] \tag{3.232}$$

- *approach II:* $\boldsymbol{\vartheta}^{\mathbf{T}}_{\mathbf{gq}}$ contains component of rotation in the Euler parametrization, using this formulation as previously discussed the rotational matrix is obtained from the (A.24) or (A.25).

$$\mathbf{R}_{\mathbf{rotq}} = \mathbf{Tr}({}^{\mathbf{trial}}\boldsymbol{\vartheta}^{\mathbf{T}}_{\mathbf{gq}}) \tag{3.233}$$

Once the correct transformational matrix $\boldsymbol{R_{rot}}$ is obtained it is possible to obtain the vertex displacements of the element:

$$\mathbf{u}^{\mathbf{T}}_{\mathbf{vq}} = \mathbf{u}^{\mathbf{T}}_{\mathbf{gq}} + (\mathbf{R}_{\mathbf{rotq}} - \mathbf{I})(\mathbf{X}_{\mathbf{vq}} - \mathbf{X}_{\mathbf{gq}}) + \mathbf{R}_{\mathbf{q}}\mathbf{E}\mathbf{R}^{\mathbf{T}}_{\mathbf{q}}(\mathbf{X}_{\mathbf{vq}} - \mathbf{X}_{\mathbf{gq}}) \tag{3.234}$$

Where:

- $\mathbf{E} = f(\boldsymbol{\Gamma}^{\mathbf{T}}_{\mathbf{q}})$ is reported in (3.12);
- $\mathbf{R}_{\mathbf{q}}$ is the rotational matrix that contains the current reference system of the element;

As previously discussed only small deformations of the elements are allowed, in this way is possible to add the rigid and the deformational part of the motion.

3.8.1.4 Update model

Ones each vertex displacement of each element is evaluated it is possible to update quantities. In particular the following parameter are update starting from the previously committed configuration:

- Centroid;
- Nodal Coordinates;
- Local reference system;
- Cumulative deformations: for each gauss point the current increment of displacement is added to the committed stored value. In this way, the constitutive law is questioned, and the current stiffness and load level is obtained.
- Internal forces;

Note that those quantities are trial, and they are saved only when convergence is achieved.

3.8.1.5 Force Unbalance

In this function the internal forces are evaluated, assembled and compared with external ones. In particular for each element the internal forces are evaluated as follows:

The displacement of each gauss point is evaluated using the following formula:

$$\boldsymbol{\delta\Delta\hat{u}_i}(\boldsymbol{\xi_i},\boldsymbol{\eta_i}) = \mathbf{N}(\boldsymbol{\xi_i},\boldsymbol{\eta_i})\mathbf{A_1}\mathbf{A_2}\mathbf{A_3}\mathbf{B}\ \boldsymbol{\delta p_g^T} \tag{3.235}$$

With $\boldsymbol{\delta\Delta\hat{u}_i}(\boldsymbol{\xi_i},\boldsymbol{\eta_i})$ and the cumulative value of displacement it is possible to obtain from each fiber a value of stiffness and force.

$$\Delta\hat{\mathbf{q}}_\ell = \sum \Delta\hat{\mathbf{q}}_{\ell \mathrm{i}}(\boldsymbol{\xi_i},\boldsymbol{\eta_i}) \tag{3.236}$$

$$\mathbf{q}_\mathrm{g} = \mathbf{B^T}\mathbf{A_3^T}\mathbf{A_2^T}\mathbf{A_1^T}\Delta\hat{\mathbf{q}}_\ell \tag{3.237}$$

From the (3.237) is possible to obtain the global vector $\boldsymbol{f}_{int}$ that contains internal forces.

$$tollerance < \ norm(f_{int} - f_{ext}) \rightarrow convergence\ is\ achieved \tag{3.238}$$

If the comparison between internal forces and external forces is more than the tolerance the iteration continues alternatively the convergence is achieved and it is possibly going to the next step.

4 Numerical applications

4.1 Buckling and post-buckling analysis

In this section the proposed approach is validated against well-known theoretical solutions of simple structures, which undergo buckling phenomena. Both the buckling load and the post-buckling behaviour are investigated.

The reported applications, which are conducted considering in all cases constitutive linear field, aim at validating and discussing the capability of the proposed approach to follow the structural response when large displacements are involved.

Specifically, in Section 4.1.1 a cantilever beam subjected to an axial load is considered and in Section 4.1.2 a simple L-frame subjected to a concentrated load is studied.

4.1.1 Cantilever beam

The first benchmark buckling and post-buckling analysis of a cantilever beam. The beam has a rectangular cross section 3 m x 4 m and its length is equal to 43,5 m. A vertical compression load is applied to the free end.

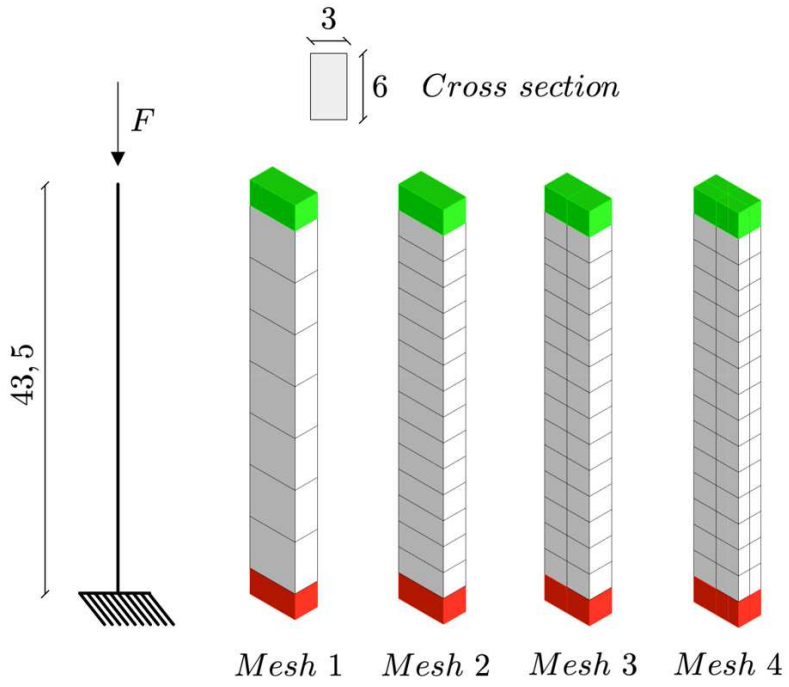

Figure 35 – Homogeneous Beam fixed at bottom, different meshes

Four models with different mesh size were arranged. The four models adopt different mesh refinements non only along the length of the beam, but also within its cross section; details on the adopted discretization are reported in Table 4.

Mesh	*Cross-section mesh*	*Discretization along the beam*	*Number of elements*	*Degrees of freedom*
1	1x1	8	8	72
2	1x1	15	15	135
3	2x1	15	30	270
4	2x2	15	60	540

Table 4 - Cantilever beam discretization

Each interface between elements has 5x5 Gaussian points. The material is elastic linear with Young's modulus and Poisson ratio are equal to $E = 21$ GPa and 0,3, respectively.

The flexural buckling load P_{cr} for the homogeneous cantilever beam [77] is:

$$\mathrm{P_{cr}} = \frac{\pi^2 EI}{4l^2} \tag{4.1}$$

which, for the considered configuration correspond to: $P_{cr} =$ 369,6701 MN

The first buckling load, obtained with the proposed approach, is reported in Table 5 for the four considered models. In the Figure 36 the post-bucking behaviour in terms of vertical and lateral displacement of the free end. It may be noticed that, as expected, the post-critical behaviour for the considered case is stable.

Mesh	*(MN)*
1	370,7417
2	368,7368
3	369,0076
4	368,1068

Table 5 – Buckling Load Cantilever beam

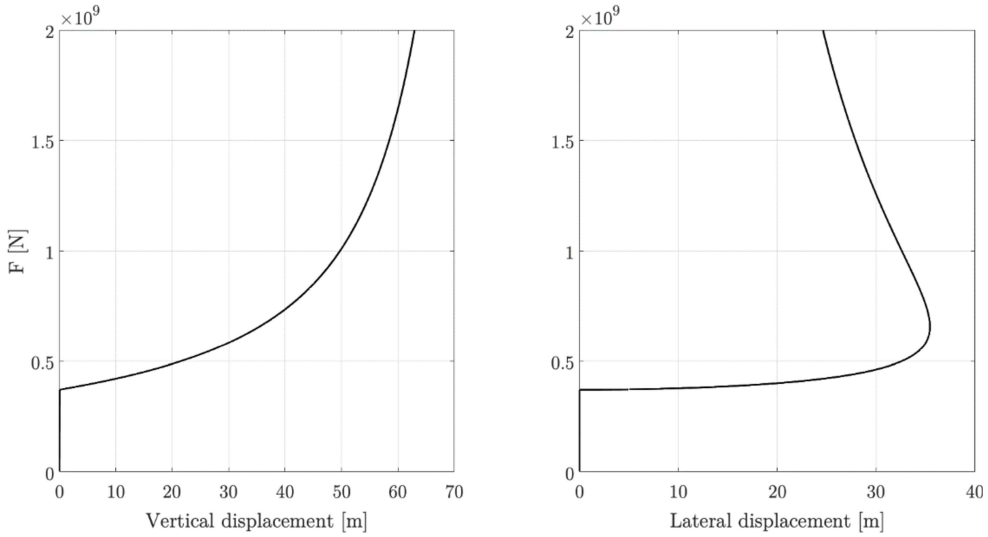

Figure 36 - Post-Critical behaviour

4.1.2 L-bracket beam

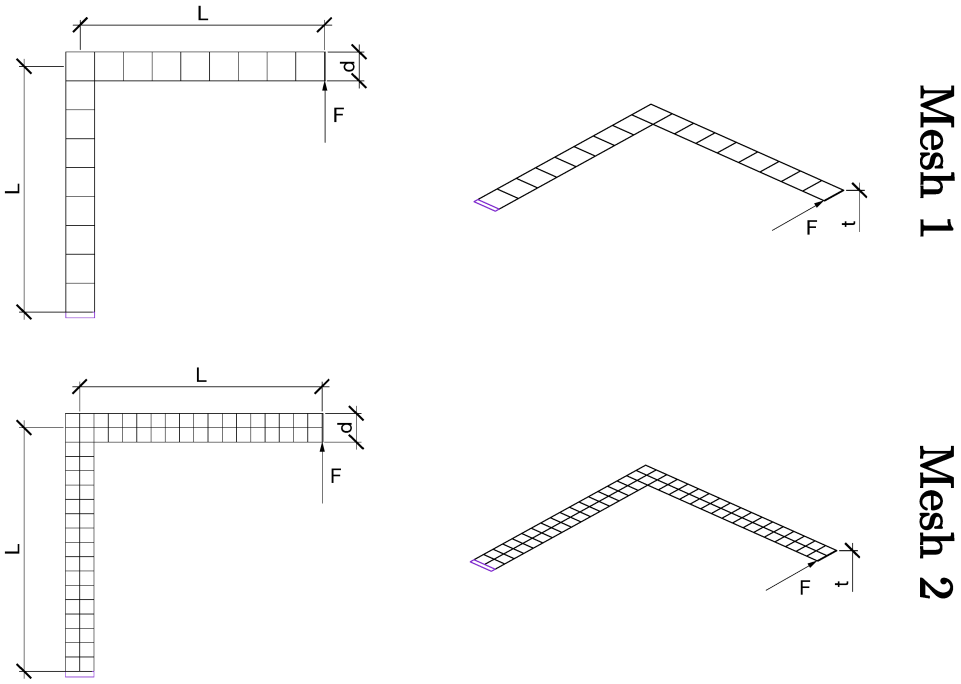

Figure 37 – L-bracket beam

The bucking load of the model reported in Figure 37 was studied in [68].

The structure is a very thin cantilever beam having a L-shape. The beams have length $L = 240\ mm$, cross section height $d = 30\ mm$, width $t = 0{,}6\ mm$, and the adopted meshes have a total amount of 68 and 272 elements. The constitutive law is elastic linear with $E = 7{,}124\ 10^4 Pa$ and Poisson ratio $\nu = 0{,}3$. The L-bracket beam is loaded in his own plane as shown in Figure 37.

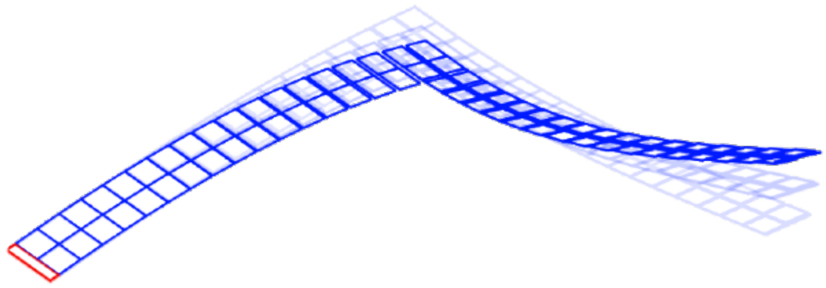

Figure 38 – Non trivial equilibrium path

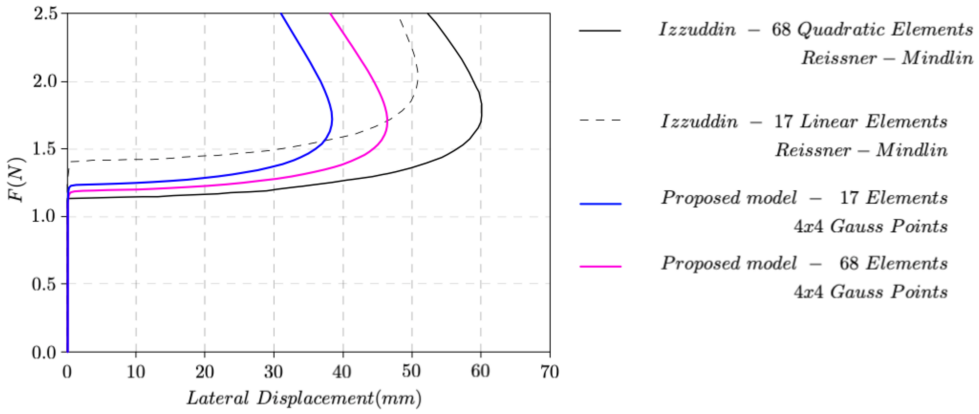

Figure 39 – Post buckling behaviour

As the force F is increased and the bucking load is reached, the structure starts to bend out of its plane. In particular, the free end and the corner move out of plane in opposite directions with a complex out of plane flexural behaviour, Figure 38. Figure 39 reports the post bucking behaviour obtained with the proposed model, compared to the co-rotational FEM linear and quadratic Reissner-Mindlin element reported in [68]. The buckling load obtained is almost coincident with the 17 Linear Elements Reissner – Mindlin but the two curves are different for higher values of the applied force.

4.2 Non-linear material behaviour

Aiming to further validated the proposed approach, in this section several applications are reported, considering nonlinear constitutive behaviour as well as geometry nonlinearities. The reported applications are of increasing complexity and gradually uncover the features of the proposed approach.

Precisely, in subsections 4.2.1 and 4.2.2 two applications relative the beams are considered, validating the numerical results with other well-known numerical solutions. In subsections 4.2.3 and 4.2.4 applications relative to masonry walls subjected to in-plane and out-of-plane loadings, respectively, are presented, comparing the results both with theoretical and experimental data available in the literature. Finally, in subsection 4.2.5, a masonry wall, subjected to out-of-plane loading and exhibiting a complex response, is investigated comparing the obtained results both with the experimental ones and those obtained with other numerical models.

4.2.1 Cantilever Beam

The following benchmark is an elastoplastic cantilever beam. Two different mesh size are adopted, namely considering 17 and 49 elements, respectively, Figure 40 and Figure 41. Correspondingly, the degrees of freedom associated to the two models are equal to 153 and 441, respectively. The distance between the centroids of the first and the last element is 4 m. The cross section is rectangular with width and height equal to 0,3 m and 0,4 m, respectively. The first element is fixed and the last has a vertical incremental force applied in his centroid. Each interface

has 8 x 8 Gauss points and the adopted constitutive law is elastic perfectly plastic with $\sigma_0 = 300\ Mpa$, Young's modulus equal to $E = 210000\ Mpa$ and Poison ratio equal to $\nu = 0{,}3$. In this example internal shear degrees of freedom of the elements are inhibited and the constitutive laws of sliding fibers are considered elastic.

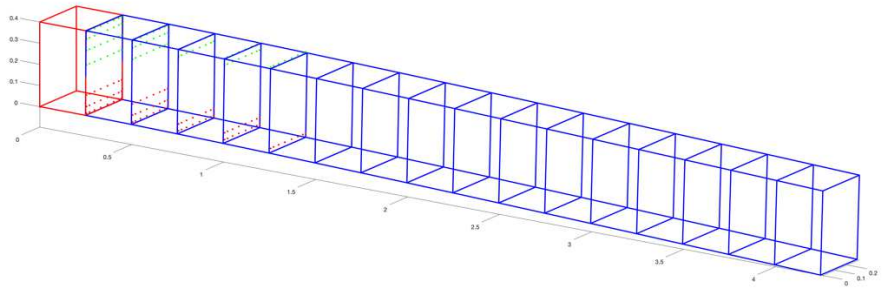

Figure 40 – Cantilever non linear beam Mesh 1

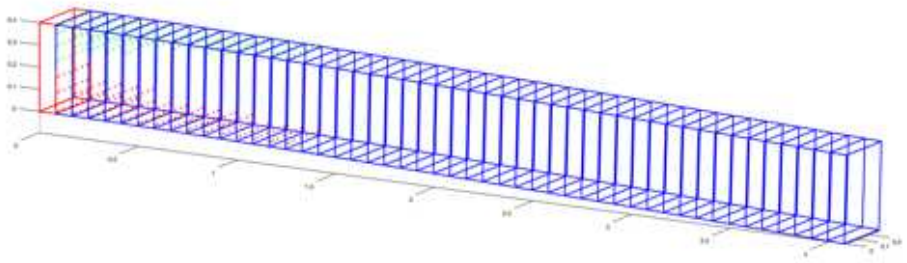

Figure 41 – Cantilever non linear beam Mesh 2

Figure 40 and Figure 41 reports the damage configuration at collapse of the beams. The red and green dots represent the Gauss points which are subjected to compressive and tensile plasticity, respectively. It possible to note that in the first section almost all the Gauss points reached their elastic limits, and that the plasticity diffusion decreases along the beam.

The Figure 42 reports the vertical force versus the displacement of the centroid of the last element. The dot line is the theoretical resisting

force of the elasto-plastic beam equal to F=900 kN. Results are very close to the theoretical value also considering the less refined used.

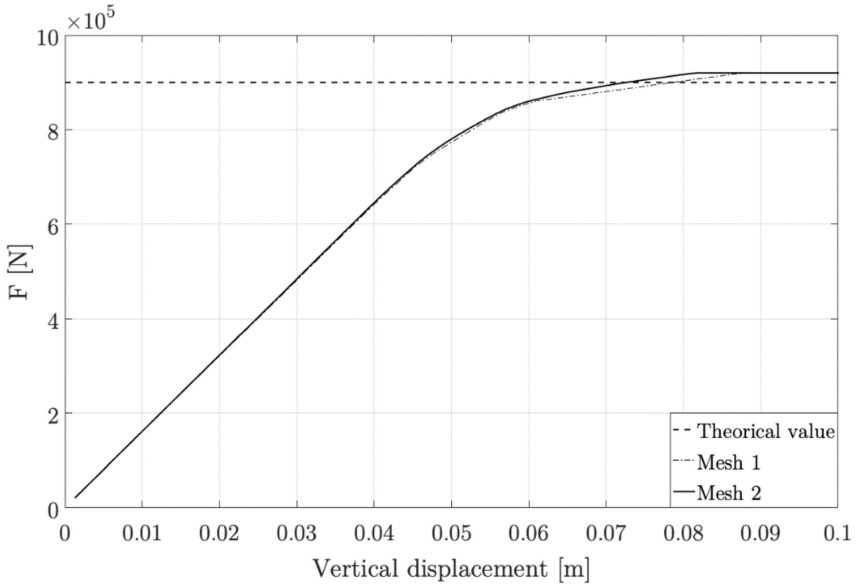

Figure 42 – Vertical Force-Displacement curve

4.2.2 Simply supported beam

The simply supported overhanging beam reported in Figure 43 was proposed by Stok and Halilovic [78]. The beam has a rectangular cross section with width $0{,}2m$ and height $0{,}4m$, $L_1 = 2m$ and $L_2 = 1m$. The material is elastic perfectly plastic with $\sigma_0 = 300\ Mpa$, Young's modulus equal to $E = 210000\ Mpa$ and a Poison ratio equal to $\nu = 0{,}3$

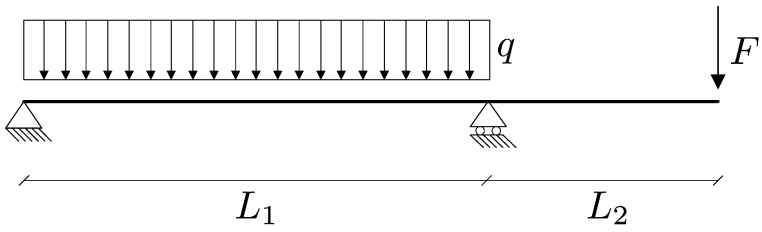

Figure 43 – Stok Halilovic beam

The beam is subjected to a concentrated force F at its free end and a uniformly distributed load q between the supports. Stok and Halilovic studied the diffusion of plasticity for different values of the ratio $\psi = \frac{F}{qL_1}$ between the external loads.

In the applications hereafter reported, the following two values of the external load ratio will be considered: *case 1* $\psi = 0{,}127$, inducing plastic yielding between the two supports; *case 2* $\psi = 0{,}225$ leading to yielding at the right support.

In Figure 44 and Figure 45 the incremental analysis in terms of total vertical load $V = F + qL_1$ versus the vertical displacement at the position of the maximum bending moment is reported. For *case 1* the control point is located at $L_1/2$ from the left support, in *case 2* the control point is located at the free end.

The theoretical ultimate vertical loads are equal to $V_p = 14200\ kN$ and $V_p = 13066\ kN$ for case 1 and case 2, respectively. The implemented model to conduct the numerical simulations is characterized by 40 elements and a total amount of 360 degrees of freedom, as depicted in Figure 46 and Figure 47; each interface has 8 x 8 Gauss points

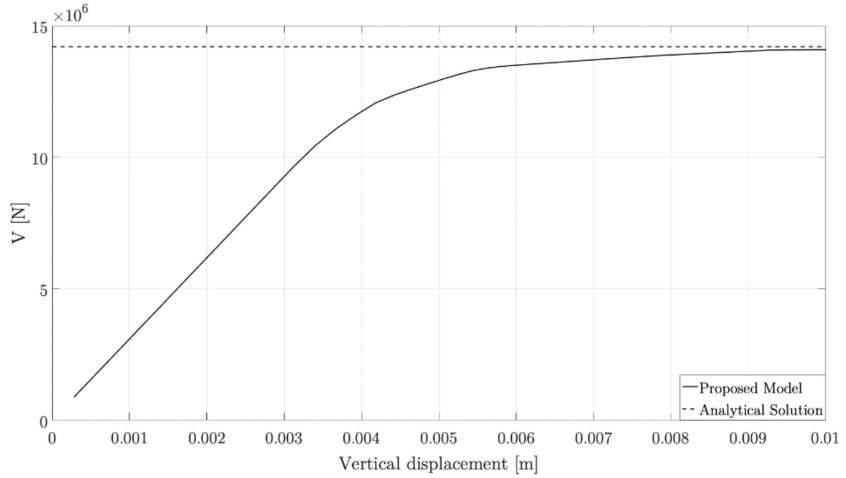

Figure 44 - case 1 $\psi = 0{,}127$- Dispacement control analisys

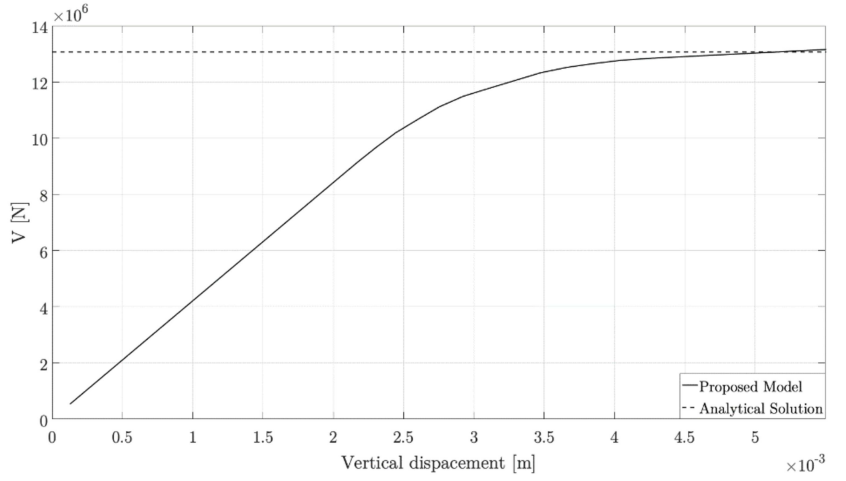

Figure 45 - case 2 $\psi = 0{,}225$ - Dispacement control analisys

Figure 46 and Figure 47 reports the different spread of the plasticity in the two cases, in particular red dots describe plastic compression behaviour and with green dots describe plastic traction behaviour.

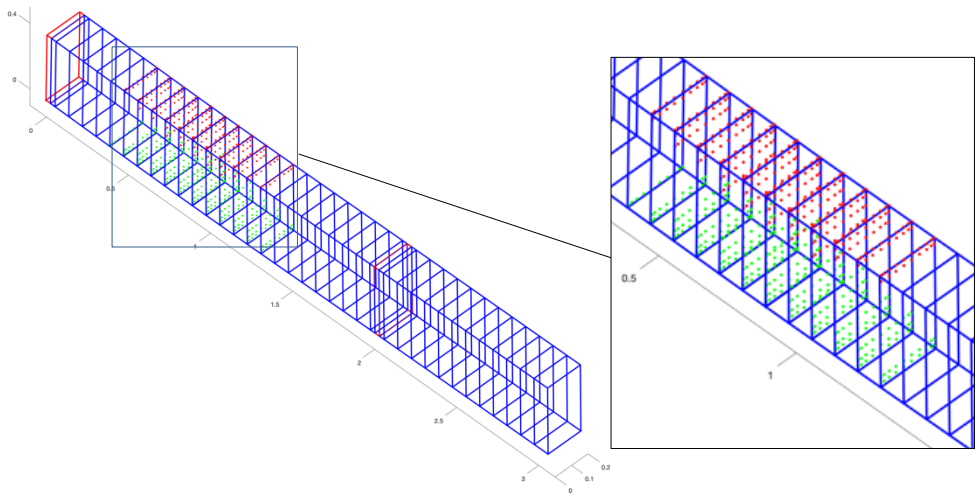

Figure 46 – case 1 $\psi = 0{,}127$ *– spread of the plasticity*

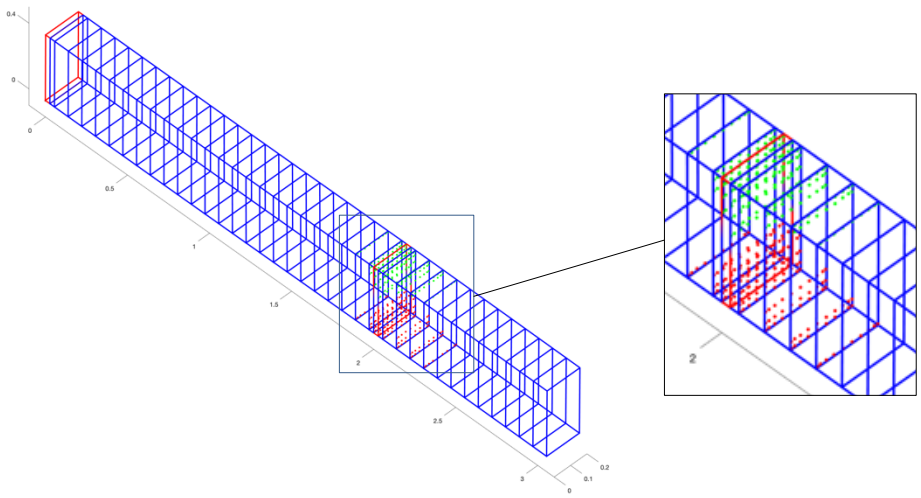

Figure 47 - case 2 $\psi = 0{,}225$ *spread of the plasticity*

4.2.3 Wall – In plane behaviour

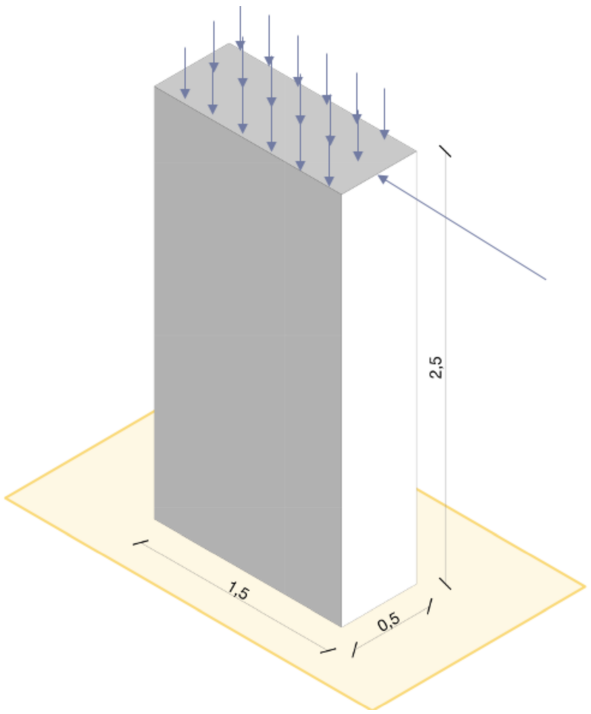

Figure 48 – Wall: in plane behaviour

This benchmark aims at validating more complicated constitutive laws, involving low (or no) tensile materials.

The comparisons here reported are made with the theoretical resistance domain of masonry panels provided in the Italian code [79]. Each panel is considered clamped at the base and free at the top, and is subjected to a vertical compression and to an increasing horizontal concentrated load applied to the top of the wall. Such a domain account for three possible failure modes, namely rocking, diagonal shear cracking and sliding. The sliding mechanism is here ignored since it can occur only in very rare loading conditions. The in-plane bending mechanism is governed by the following expression:

$$M_u = \left(\frac{l^2 t\sigma}{2}\right)\left(1 - \frac{\sigma}{0{,}85\ f}\right) \tag{4.2}$$

where:

- M_u is the ultimate bending moment;
- l is the length of the wall;
- h is the height of the wall;
- t is the thickness of the wall
- $\sigma = \frac{N}{lt}$ is the average compression stress with N axial compression force;
- f is the compressive resisting strength of the masonry;

The relationship between ultimate bending moment at the base of the panel and applied horizontal force is $M_u = V_u h$.

The shear résistance of a masonry panel is provided by the following formula consistent with the Turnsek and Cacovic [57] yielding criterion:

$$V_u = l\ t\frac{1{,}5\ \tau}{b}\sqrt{1 + \frac{\sigma}{1{,}5\ \tau}} \tag{4.3}$$

where:

- V_u is the shear resistance associated to the diagonal shear collapse failure mode;
- l is the length of the wall;
- t is the thickness of the wall;
- h is the height of the wall;
- $b = h/l$;
- $\sigma = \frac{N}{lt}$ is the everage compression stress, with N axial compression force;
- τ is the masonry shear strength;

The model studied is a panel with a rectangular cross section 0,5 m x 1,25 m with height equal to 2,5 m. A single element was employed to perform the analyses.

The adopted constitutive law for the shear behaviour is elastic perfectly plastic with yielding domain associated to the well-known Turnsek and Cacovic formula **Errore. L'origine riferimento non è stata trovata.** [57], while the constitutive law for the interfaces is elastic perfectly plastic. All the adopted parameters are reported in Table 6.

Parameters	
Young's modulus E (MPa)	1740
Poisson ratio ν	0,2
Compressive strength f_c *(MPa)*	3,264
Shear strength τ_0 *(MPa)*	0,054

Table 6 – In plane wall mechanical parameters

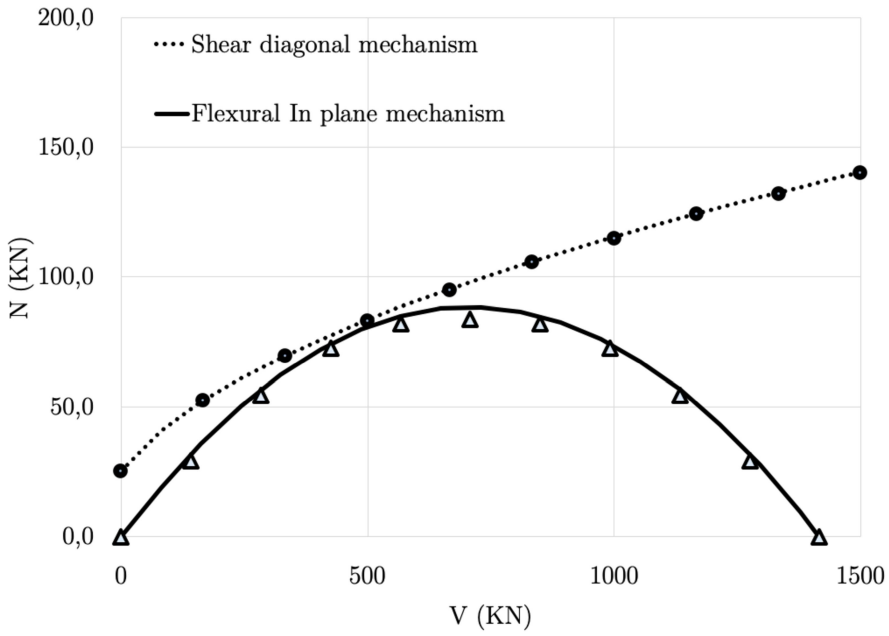

Figure 49 – In plane flexural and shear diagonal behaviour

Figure 49 reports the results in terms of ultimate load for different levels of compression acting on the panel. The two domains, which are associated to the two different mechanisms, are reconstructed alternatively keeping the shear and the flexural behaviours elastic. The black and the dot lines, are obtained by means of equations (4.2) and (4.3), respectively. On the other hand the markers refer to the ultimate loads obtained with the proposed approach.

4.2.4 Slender wall

The present benchmark refers to the experimental campaign conduct by Sandoval, Roca in [80]. They performed several tests on masonry walls with different slenderness, with scale factor 1:4, subjected to an increasing eccentric vertical load, Figure 50, which lead to a pronounced out-of-plane response. The numerical simulations here reported refer to one of those panels,

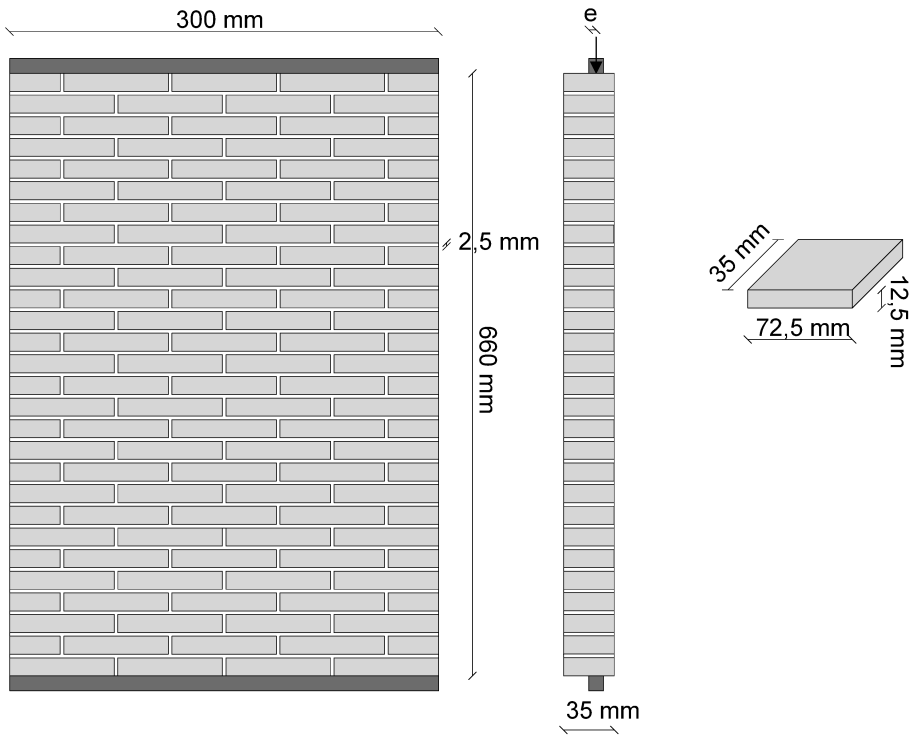

Figure 50 – Wall tested.

The vertical load is applied with an eccentricity $e = t/6$ as shown in Figure 50. Figure 51 reports the adopted mesh to perform the numerical simulations which are characterized by 4 and 16 elements, respectively, corresponding to 36 and 144 degrees of freedom.

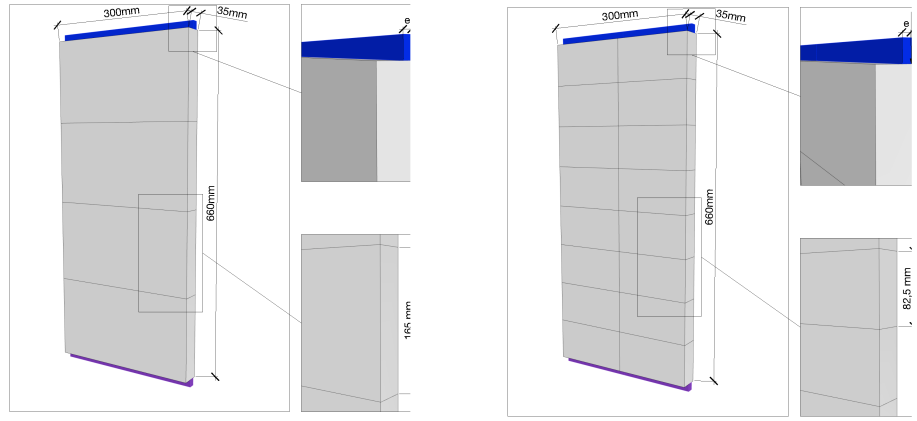

(a) (b)

Figure 51 - (a) Mesh 1, (b) Mesh 2

Parameters	
Young Modulus E(MPa)	3480 or 4000 or 4500
Poisson ratio ν	0,15
Compression Strength f_c (MPa)	14,2
Tensile Strength f_t (MPa)	0,55
Compression fractural energy $G_{f,C}$ (N/m)	20380
Traction fractural energy $G_{f,I}$ (N/m)	50
Coesion c (MPa)	0,45
Angle of internal friction tanϕ	0,812
Slide fractural energy $G_{f,II}$ (N/m)	45

Table 7 - Mechanical parameters - Slender wall

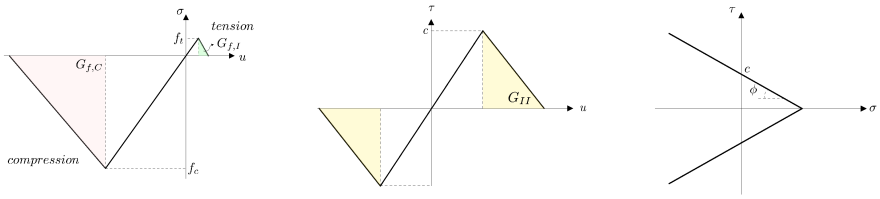

(a) (b) (c)

Figure 52 - (a) Flexural constitutive law - (b) Shear constitutive law - (c) Mohr – Coulomb failure Criterion

The adopted mechanical properties, reported in Table 7, are relative to the constitutive laws depicted in Figure 52.

Figure 53, Figure 54 and Figure 55 report a parametric study to evaluate the influence of mesh, Gauss points and Young's modulus in the proposed model. The variability is computed with respect to a reference modulus with $E = [3480,4000,4500]\ MPa$, number of Gauss points at the interfaces equal to $[5x5,10x10]$ and adopting mesh [Mesh 1, Mesh 2]. The vertical stress (evaluated as the vertical applied forces divided by the area of the cross section of the wall) is reported, versus the lateral displacement of middle point of the panel.

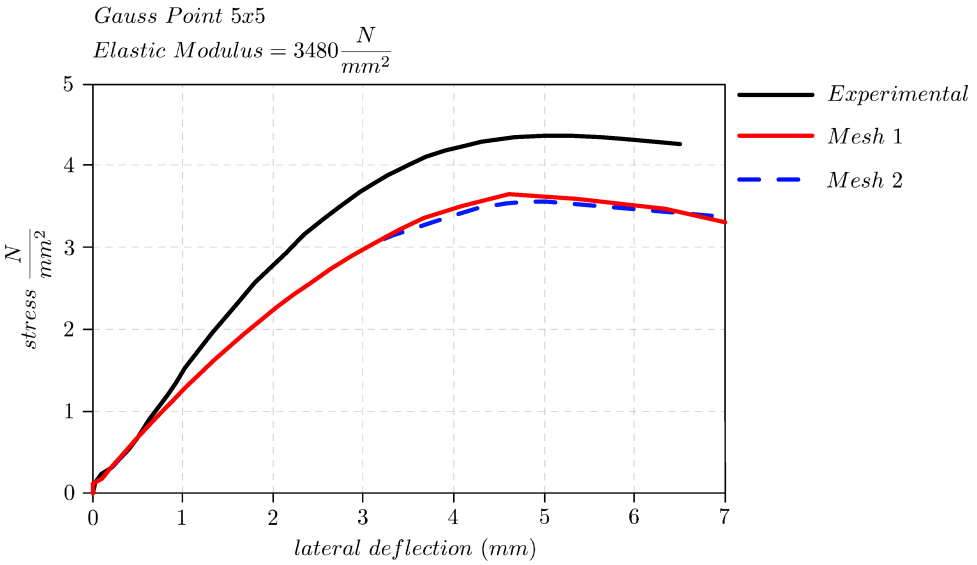

Figure 53 – Mesh influence

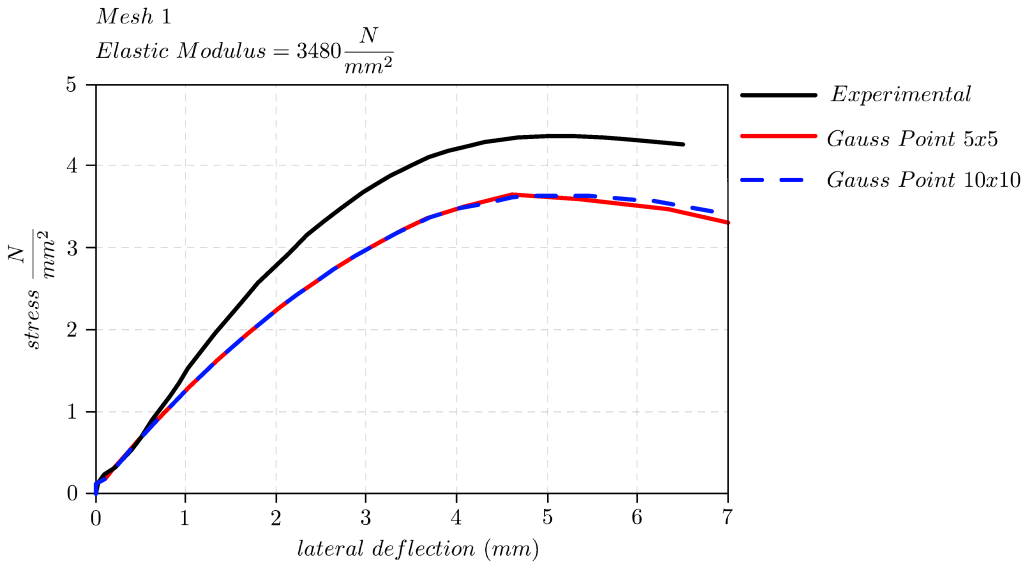

Figure 54 - Influence of the number of Gauss points

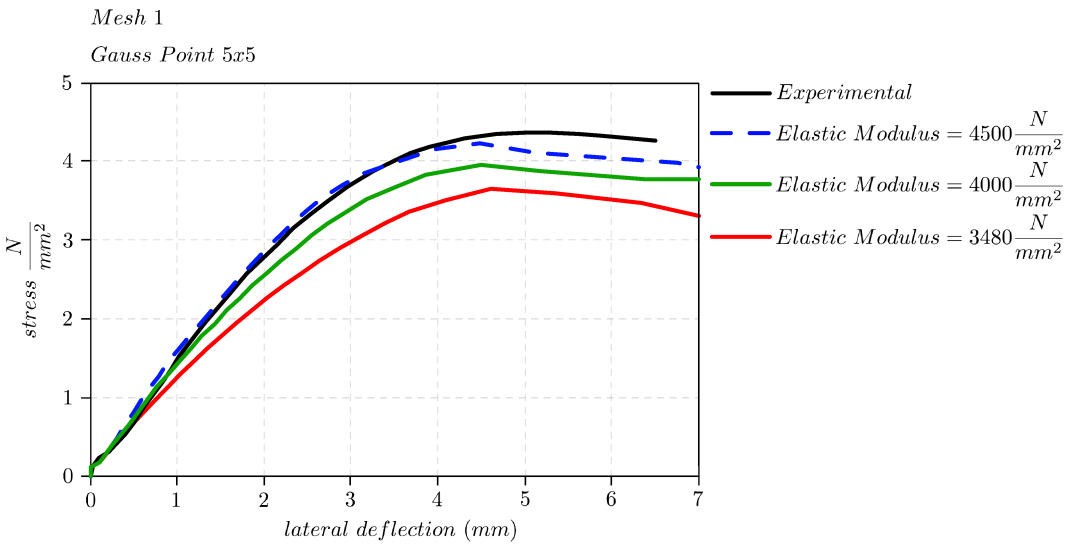

Figure 55 - Young's modulus influence

Figure 53 and Figure 54 show that the response of the model is not significantly affected by the mesh size and the number of employed Gauss points. Figure 55 reports the variability in terms of Young's modulus. It

is important to consider that the elasticity modulus, suggested by Sandoval et al. and experimentally obtained, is defined as '*secant*'. However, is a progressive loss of stiffness can be accounted for, it is reasonable to adopt higher values of the Young's modulus. By adopting a Young's modulus equal to 4500 *Mpa* the obtained results are very close to the experimental curve.

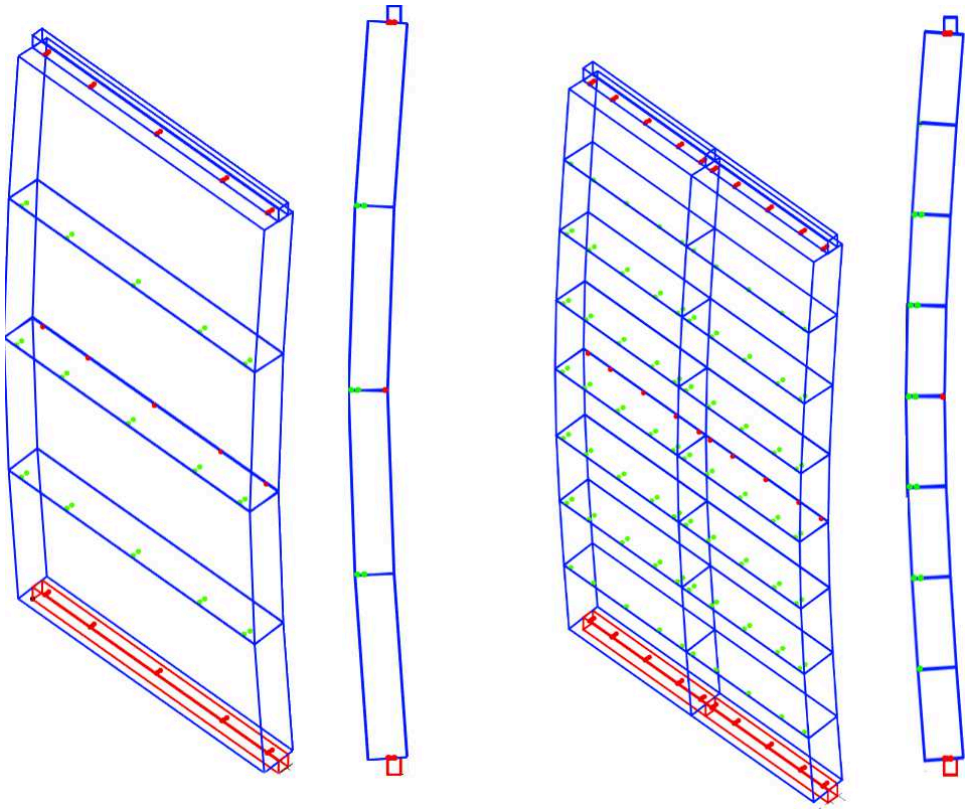

Figure 56 – Collapse mechanisms for different mehes.

Figure 56 reports the collapse mechanism for different mesh size which is characterized by the opening of three cylindrical horizontal hinges, in accordance to the experimental outcome.

4.2.5 Mesoscale wall

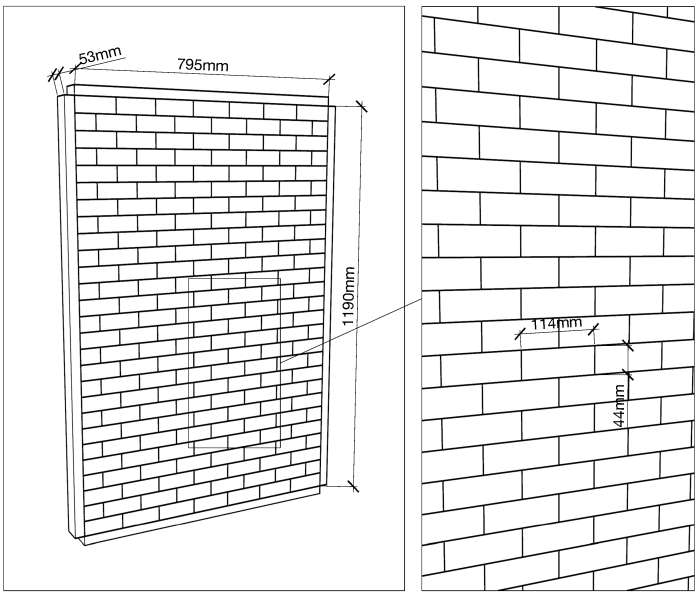

Figure 57 – Wall 8, Mesoscale Macro Element mesh

This benchmark here investigate refers to the experimental tests conduct by Chee Liang Ng [81] on two identical specimen called wall 8 and wall 12, and afterwards studied by Milani [56], with a limit analysis approach, and Macorini & Izzuddin in [17], who employed an advanced nonlinear FEM approach applied at the mesoscale.

The specimen is characterized by a height, width and thickness equal to 1190 mm 795 mm and 53 mm, respectively. Each brick is 112×53×36 mm and the mortar joints are 10 mm thick. In [81] the specimens were loaded up to collapse by applying a uniform out-of-plane load. The four sides of the walls are simply supported.

The adopted mesh is consistent with the units' arrangement and is reported in Figure 57. The proposed method is here used at the meso scale, also to explore the possibility to adopt it according to different modelling strategies. According to the adopted modelling strategy the

explicit modelling of the mortar joints is not required since their mechanical properties is embedded in the interfaces. As a consequence, the elements are a bit larger than bricks in order to embed the mortar thickness. In the following table are reported mechanical parameters used in this benchmark and suggested in [17].

Parameters	
Young's modulus E (MPa)	7200
Compressive strength f_c (MPa)	-6
Tensile strength f_t (MPa)	0,35
Compressive fracture energy $G_{f,C}$ (N/m)	5000
Traction frecture energy $G_{f,I}$ (N/m)	18
Cohesion c (N/mm)	0,42
Angle of internal angle tanϕ	0,52
Sliding fracture energy $G_{f,II}$ (N/m)	125

Table 8 – Mechanical parameters - Mesoscale wall

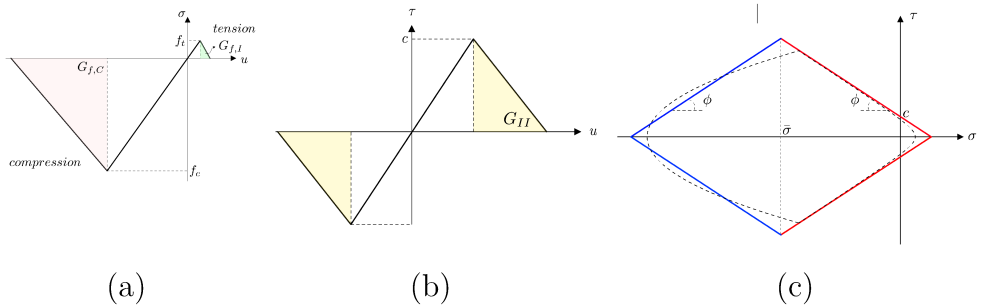

(a) (b) (c)

Figure 58 – (a) Flexural constitutive law - (b) Shear constitutive law - (c) Mohr – Coulomb failure Criterion with cap in compression

The adopted mechanical properties adopted to simulate the experimental test are reported in Table 8 and are consistent with the constitutive laws depicted in Figure 58. The flexural constitutive law is bilinear with linear softening associated to tensile and compressive fracture energies. A simplified version of the yielding criterion proposed

in [17] is here adopted to simulate the possibility of the units to slide. Specifically, the Mohr coulomb criterion (red line) is associated to a cap in compression (blue line). The domain is obtained using the parameters reported in Figure 58(c) with a value of $\overline{\sigma} = \frac{f_t + f_c}{2}$, in this way the failure slide criterion is very close to the one used in [17] (dot line in Figure 58(c)).

The adopted Young's modulus was suggest by Chee Liang Ng in [81] although not obtained experimentally. The other parameters are consistent with those adopted in the numerical simulations conducted in [17] and [56]. The collapse mechanism is governed by the cracks at the joints and by the relative sliding among the units. The compressive strength associated to the cap of the sliding yielding domain plays an important role to limit the sliding strength.

Figure 59 reports the comparison among the proposed model, using several number of Gauss points, with the experimental results and other numerical approaches. The pressure applied on the panel is reported versus the horizontal displacement in the middle of the panel.

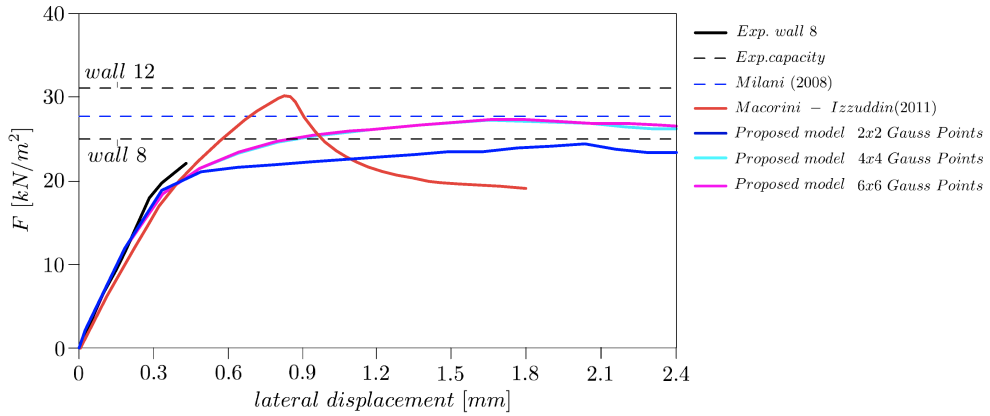

Figure 59 – Comparison between proposed model and other results in literature

As the number Gauss points increases, the response of the structure changes. However, when 4x4 Gauss points the is quite stable, and increasing the number of Gauss points does not lead to significant changes in the numerical response.

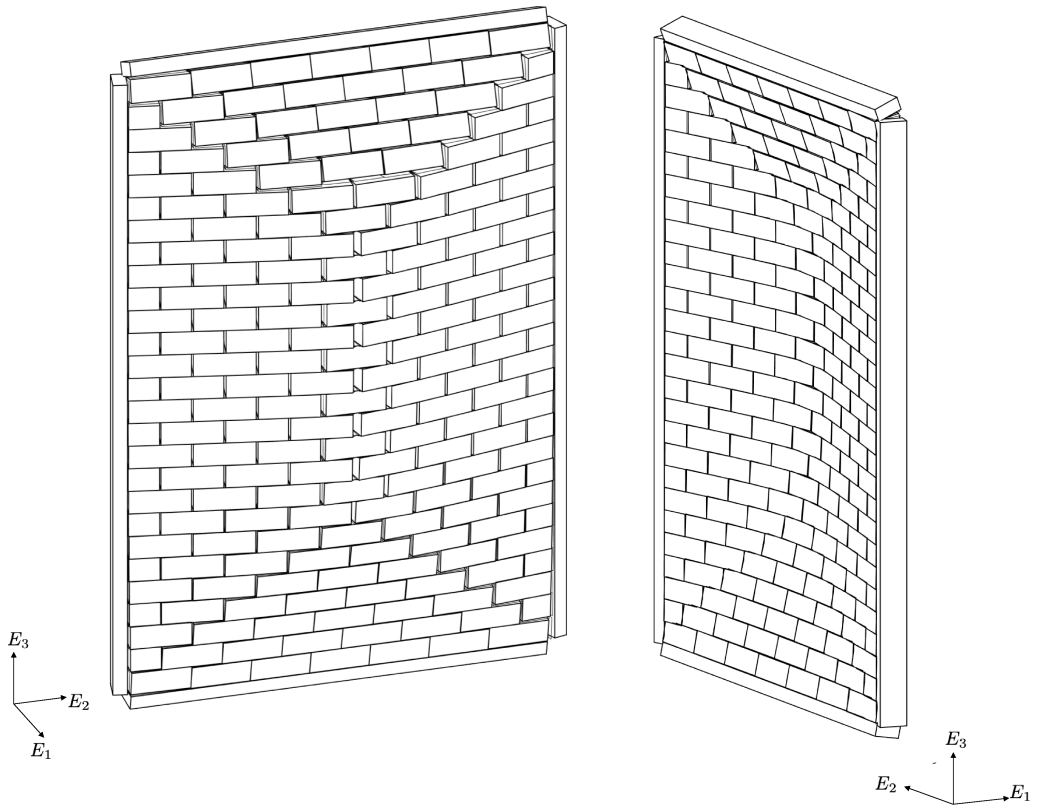

Figure 60 – Collapse mechanism: scale of displacement is 100x

Figure 60 reports the collapse mechanism associated to a magnification factor of the displacements equal to 30. It is worth to note that the number of elements adopted for the present simulations, thanks to the capability of the model to simulate the occurrence of not coincident interfaces among the elements, is lower than those needed according to the numerical approaches proposed by the other authors. Precisely, in [56] each brick is divided in several tetrahedral elements, and in [17] each

brick is divided into two elements, thus guaranteeing the coincidence of the nodes between adjacent elements consistently with a FE approach. With respect to such approaches the mentioned feature represents an undeniable advantage.

5 Conclusions

In the present thesis an original solid discrete element, for the study of masonry structures, is developed. It is based on DMEM and introduces some important innovations: a solid element, three different shears local degree of freedom inside the element, the possibility to create a continuum interface in all his faces and the capability to study second-order phenomena. This is possible using the co-rotational approach that uncouples the small deformations with the large rigid motions. Two different approaches were developed which differ in the way in which the rotations are parametrized. The DME model is based on the use of solid element characterised by only 9 degrees of freedom for each element and it can be used at the macro-scale or at the micro scale. A software, called Macro_Ex has been implemented in MatLab code environment. It embeds a lot of numerical procedures that allow studying elastic and plastic non-linear static problems.

Several benchmarks have been considered for the model validation. Some benchmarks have been chosen with the purpose to study post-buckling problems and others with the purpose to compare the proposed model with an experimental test on masonry walls. Results fit very well with other methods present in literature as well as with the experimental results. The introduction of a solid element accounting for large displacement formulation within the context of the DMEM open to a large number of applications in different engineering fields. Second-order phenomena in tall or slender structures (towers, facades), multi-leaf masonry walls and geotechnical problems are only three possible

interesting applications that can be investigated using this model particular model. The element kinematics together with appropriate calibration procedure suggest the use of this model in several different context from progressive collapse of structure to nonlinear soil-structure interaction problems. The research is ongoing and a series of future improvements could be performed. The element geometrical irregularity, the adoption of more sophisticated constitutive laws and the extension to the dynamic context will allow the nonlinear modelling of complex structure subjected to seismic or extreme loadings in presence of geometrical and material nonlinearities.

Appendix A: Large Rotations

A.1 Introduction

A central issue in the development of a co-rotational approach is the treatment of finite 3D rotations. According to Euler Theorem, in a 3-Dimensional space any displacement of a rigid body having a fixed point, is equivalent to a single rotation about some axis that runs through the fixed point. It also means that any composition of rotations is also a rotation. The main difficulty related to the large rotations is that they cannot be treated as vectors. So, large rotations depend on the order in which they are applied. In literature a lot of parametrizations of rotation can be found, the most used in computational mechanics are those based on the Rodriguez Formula or related to Euler parameters. In the present work, for the parametrization of large rotations, both approaches are used.

A.2 Rodriguez Formula

As descripted in [82] a rotation group $SO(3)$, called manifold, is a group of transformations in $\mathbb{R}^3$ respecting the following condition:

$$SO(3) := \{\boldsymbol{\Lambda}: \mathbb{R}^3 \rightarrow \mathbb{R}^3 | \boldsymbol{\Lambda^T} = \boldsymbol{\Lambda^{-1}} \ \& \ \det(\boldsymbol{\Lambda}) = +1\} \tag{A.1}$$

So, it is possible to describe a rotation in a 3-Dimensional space as a matrix 3x3 with the following properties:

- It is defined in $\mathbb{R}^3$ and convert element in $\mathbb{R}^3$;
- the inverse is equal to the transpose;

- the determinant is equal to +1

The tangent space to $SO(3)$ at the initial configuration is called $so(3)$ or $T_I SO(3)$ and it is defined as:

$$so(3) := \{\tilde{\boldsymbol{\omega}}: \mathbb{R}^3 \to \mathbb{R}^3 | \tilde{\boldsymbol{\omega}} + \tilde{\boldsymbol{\omega}}^{\boldsymbol{T}} = \mathbf{0}\} \tag{A.2}$$

In this case, the transformation $\tilde{\omega}$ has the following properties:

- It is defined in $\mathbb{R}^3$ and convert element in $\mathbb{R}^3$;
- It is a skew-symmetric tensor so $\tilde{\boldsymbol{\omega}} + \tilde{\boldsymbol{\omega}}^{\boldsymbol{T}} = \mathbf{0}$
- It has an eigenvector $\omega \in \mathbb{R}^3$such that $\tilde{\boldsymbol{\omega}}\ \boldsymbol{\omega} = \mathbf{0}$

The matrix representation of this kind of transformation is:

$$\tilde{\boldsymbol{\omega}} = \begin{bmatrix} 0 & -\omega_3 & \omega_2 \\ \omega_3 & 0 & -\omega_1 \\ -\omega_2 & \omega_1 & 0 \end{bmatrix} \qquad \boldsymbol{\omega} = \begin{bmatrix} \omega_1 \\ \omega_2 \\ \omega_3 \end{bmatrix} \tag{A.3}$$

It represents an infinitesimal transformation around the fixed axis $\boldsymbol{\omega}$.

The tangent space at any $\boldsymbol{\Lambda} \in SO(3)$ is defined as:

$$T_{\boldsymbol{\Lambda}} SO(3) := \left\{ \boldsymbol{\Lambda}\tilde{\boldsymbol{\omega}} \equiv \tilde{\boldsymbol{\vartheta}}\boldsymbol{\Lambda} \ \mid \ \tilde{\boldsymbol{\omega}} \in so(3)\ \&\ \tilde{\boldsymbol{\vartheta}} = \boldsymbol{\Lambda}\tilde{\boldsymbol{\omega}}\boldsymbol{\Lambda}^{\boldsymbol{T}} \in so(3) \right\} \tag{A.4}$$

So $\tilde{\boldsymbol{\vartheta}}\boldsymbol{\Lambda} \in TSO(3)$ and $\boldsymbol{\Lambda}\tilde{\boldsymbol{\omega}} \in TSO(3)$ are the right (spatial) and the left (material) representation of the same tangent space $TSO(3)$ at $\boldsymbol{\Lambda}$.

The $\tilde{\boldsymbol{\vartheta}}\boldsymbol{\Lambda} \in TSO(3)$ can be thought as an infinitesimal rotation $\tilde{\boldsymbol{\vartheta}}$ superposed to the finite rotation $\boldsymbol{\Lambda}$ and $\boldsymbol{\Lambda}\tilde{\boldsymbol{\omega}} \in TSO(3)$ can be thought as a finite rotation $\boldsymbol{\Lambda}$ superposed to the infinitesimal rotation $\tilde{\boldsymbol{\vartheta}}$.

The equation (A.4) means that two different transformation $\tilde{\boldsymbol{\vartheta}} \in so(3)$ and $\tilde{\boldsymbol{\omega}} \in so(3)$ applied to $\boldsymbol{\Lambda}$ depending belong to the same tangent space $T_{\boldsymbol{\Lambda}} SO(3)$

This topic is crucial in the three-dimensional mechanical analysis because the variation of a rotational matrix $\in T_{\Lambda} SO(3)$.

It is possible to transform infinitesimal rotation $so(3)$ to finite rotations $SO(3)$ using the exponential map:

$$\exp[\tilde{\boldsymbol{\omega}}] := \sum_{k=0}^{\infty} \frac{1}{k!} \tilde{\boldsymbol{\omega}}^k \in SO(3) \tag{A.5}$$

The pseudo-vector $\boldsymbol{\omega}$ defined in (A.3) is also equal to:

$$\boldsymbol{\omega} = \|\boldsymbol{\omega}\| \boldsymbol{n} \tag{A.6}$$

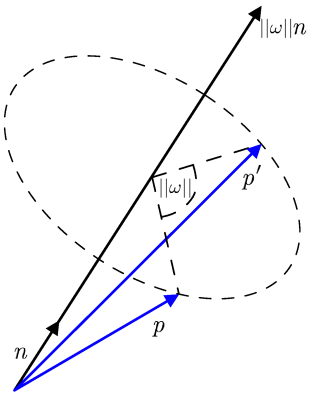

Figure 61 – Rotational vector

The equation (A.5) has also two different closed form:

$$\mathbf{R} = \exp[\tilde{\boldsymbol{\omega}}] = \mathbf{I} + \frac{\sin\|\boldsymbol{\omega}\|}{\|\boldsymbol{\omega}\|} \tilde{\boldsymbol{\omega}} + \frac{1}{2} \frac{\sin^2(\frac{1}{2}\|\boldsymbol{\omega}\|)}{(\frac{1}{2}\|\boldsymbol{\omega}\|)^2} \tilde{\boldsymbol{\omega}}^2 \tag{A.7}$$

and

$$\mathbf{R} = \exp[\tilde{\boldsymbol{\omega}}] = \cos(\|\boldsymbol{\omega}\|)\, \mathbf{I} + \sin\|\boldsymbol{\omega}\|\, \tilde{\boldsymbol{n}} + [1 - \cos(\|\boldsymbol{\omega}\|)] \boldsymbol{n} \otimes \boldsymbol{n} \tag{A.8}$$

Where $\tilde{\boldsymbol{n}}$ is the skew-antisymmetric matrix based on $\boldsymbol{n}$.

The equations (A.7) and (A.8) are called to Rodriguez formulas and they are valid also for the pseudo-spatial vector $\boldsymbol{\vartheta}$.

So, the rotated vector of p about the axis ω is equal to:

$$p' = \mathbf{R} p \tag{A.9}$$

A.2.1 Compound rotation

Considering a rotation operator $\mathbf{R_0} \in \mathrm{SO}(3)$ which maps the orthogonal cartesian reference system $\mathbf{e}_i$ into the triad $\mathbf{t}'_i$

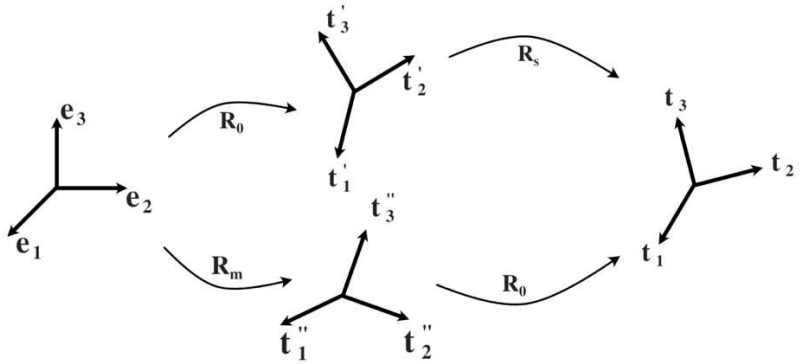

Figure 62 Compound rotation

$$\mathbf{t}'_i = \mathbf{R_0}\mathbf{e_i} \tag{A.10}$$

Likewise, in the (A.4) an incremental finite rotation $\mathbf{R_s} \in SO(3)$ is applied to the triad $\mathbf{t}'_i$. The final triad $\mathbf{t}_i$ is obtained.

$$\mathbf{t_i} = \mathbf{R_s}\mathbf{R_0}\mathbf{e_i} \tag{A.11}$$

The same result is obtained applying the incremental finite rotation $\mathbf{R_m}$ to the initial triad:

$$\mathbf{t}''_i = \mathbf{R_m}\mathbf{e_i} \tag{A.12}$$

And later applying the rotation $\mathbf{R_0}$ to the obtained triad $\mathbf{t}''_i$

$$\mathbf{t_i} = \mathbf{R_0}\mathbf{R_m}\mathbf{e_i} \tag{A.13}$$

The composed final rotation is equal to:

$$\mathbf{R} = \mathbf{R_0}\mathbf{R_m} = \mathbf{R_s}\mathbf{R_0} \tag{A.14}$$

With:

$$\begin{aligned}
&\mathbf{R_m} = exp[\tilde{\boldsymbol{\omega}}] \text{ material rotation} \\
&\mathbf{R_s} = exp\left[\tilde{\boldsymbol{\vartheta}}\right] \text{ spatial rotation} \\
&\qquad \mathbf{R_\epsilon} = \ \mathbf{R}\ \exp[\epsilon\tilde{\boldsymbol{\omega}}] = \ \exp\left[\epsilon\tilde{\boldsymbol{\vartheta}}\right]\ \mathbf{R} \in SO(3)
\end{aligned} \tag{A.15}$$

$$\begin{aligned}
\delta\mathbf{R} &= \left(\frac{\mathrm{d}(\mathbf{R}\ \exp[\epsilon\tilde{\boldsymbol{\omega}}])}{\mathrm{d}\epsilon}\right)_{\epsilon=0} = \left(\frac{\mathrm{d}\left(\exp\left[\epsilon\tilde{\boldsymbol{\vartheta}}\right]\ \mathbf{R}\right)}{\mathrm{d}\epsilon}\right)_{\epsilon=0} \\
&\delta\mathbf{R} = \mathbf{R}\delta\tilde{\boldsymbol{\omega}} = \delta\tilde{\boldsymbol{\vartheta}}\mathbf{R} \in T_R SO(3)
\end{aligned} \tag{A.16}$$

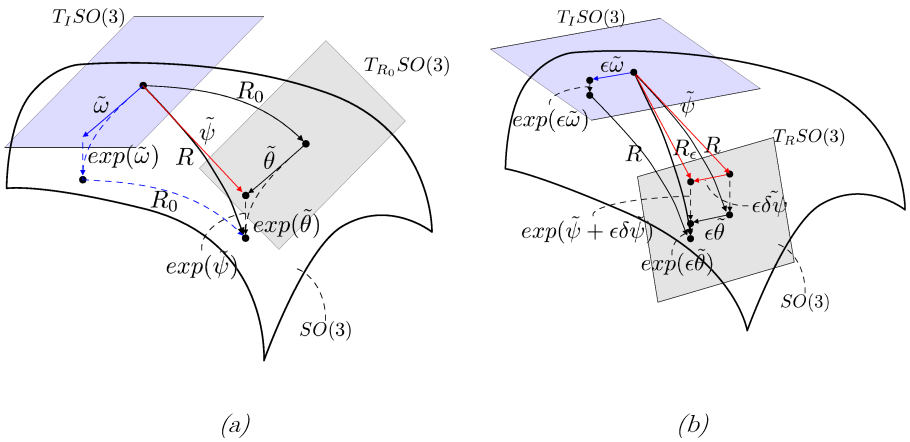

Figure 63 – Geometric interpretation of rotations (a) Compound finite rotation in material and spatial description; (b) Variation of rotation in material and spatial description;

$\delta\mathbf{R}$ is the variation of the matrix $\mathbf{R}$ and it belong to $T_R SO(3)$.

As report in Figure 63a, the rotational matrix $\mathbf{R}$ is also equal to:

$$\mathbf{R} = exp\left[\tilde{\boldsymbol{\psi}}\right] \tag{A.17}$$

Considering an infinitesimal variation of rotation $\tilde{\boldsymbol{\psi}}$ the following equation is obtained:

$$\mathbf{R}_\epsilon = \exp\left[\tilde{\boldsymbol{\psi}} + \epsilon\delta\tilde{\boldsymbol{\psi}}\right] \tag{A.18}$$

Using the (A.16) and (A.17) the (A.18) is also equal to: (Figure 63b)

$$\begin{aligned} \exp\left[\tilde{\boldsymbol{\psi}} + \epsilon\delta\tilde{\boldsymbol{\psi}}\right] &= \exp\left[\epsilon\tilde{\boldsymbol{\vartheta}}\right]\ \exp\left[\tilde{\boldsymbol{\psi}}\right] \\ \exp\left[\epsilon\tilde{\boldsymbol{\vartheta}}\right] &= \exp\left[\tilde{\boldsymbol{\psi}} + \epsilon\delta\tilde{\boldsymbol{\psi}}\right]\ \exp\left[-\tilde{\boldsymbol{\psi}}\right] \end{aligned} \tag{A.19}$$

$$\left(\frac{\mathrm{d}\left(\exp\left[\epsilon\tilde{\boldsymbol{\vartheta}}\right]\right)}{\mathrm{d}\epsilon}\right)_{\epsilon=0} = \left(\frac{\mathrm{d}\left(\exp\left[\tilde{\boldsymbol{\psi}} + \epsilon\delta\tilde{\boldsymbol{\psi}}\right]\right)\ \exp\left[\tilde{\boldsymbol{\psi}}\right]}{\mathrm{d}\epsilon}\right)_{\epsilon=0} \tag{A.20}$$

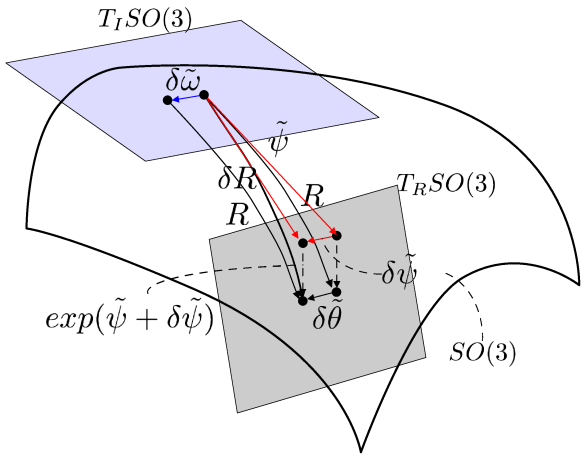

Figure 64 – Infinitesimal variation o of rotation in material and spatial description;

Using the (A.20) and (A.7) the following equation is obtained:

$$\begin{aligned} \delta\tilde{\boldsymbol{\vartheta}} &= T_s(\psi)\delta\tilde{\boldsymbol{\psi}} \\ \delta\tilde{\boldsymbol{\psi}} &= T_s^{-1}(\psi)\delta\tilde{\boldsymbol{\vartheta}} \end{aligned} \tag{A.21}$$

Where:

$$T_s(\psi) = \frac{\sin\psi}{\psi}\boldsymbol{I} + \left(1 - \frac{\sin\psi}{\psi}\right)\boldsymbol{m}\boldsymbol{m}^{\boldsymbol{T}} + \frac{1}{2}\left(\frac{\sin\frac{\psi}{2}}{\frac{\psi}{2}}\right)^2\tilde{\boldsymbol{\psi}} \tag{A.22}$$

And $\boldsymbol{\psi} = \|\psi\|\boldsymbol{m}$

Is important to note that $\tilde{\boldsymbol{\psi}} \in T_I SO(3)$ and $\tilde{\boldsymbol{\vartheta}} \in T_R SO(3)$ so the equation (A.22) is the connection between these two group of parameters.

Equation (A.16) is crucial in the evaluation of the stiffness matrix, it will be used in Chapter 3 the of this document. In this thesis, the *Approach 1* used to define the interface kinematic, is formulated using Rodriguez Formula [63].

A.3 Euler and Tait - Bryan Angles

Another description for large rotations is related to Euler Angles or Tait-Bryan Angles, they describe the body rotation with a combination of three main rotations according to the Euler theorem. The main idea is that a complete rotation in three dimensions can be achieved by a combination of three different rotation around a specified axis. In this method the order of the rotation is fundamental.

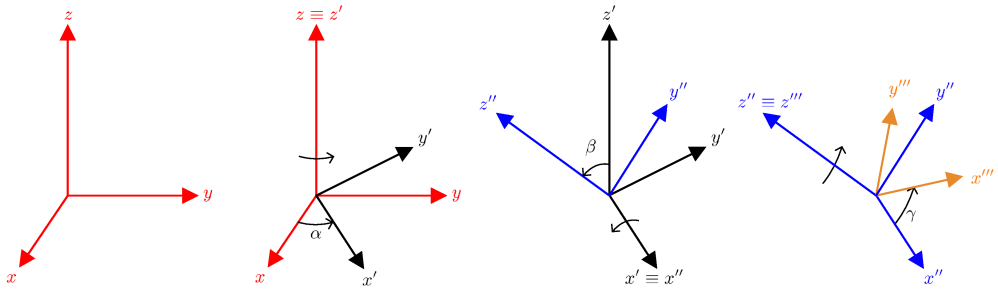

Figure 65 – Intrinsic Euler Rotations

Using this notation, it is possible to have an intrinsic or extrinsic rotation.

Intrinsic rotations are elemental rotations that occur about the axes of a coordinate system XYZ attached to a moving body.

Extrinsic rotations are elemental rotations that occur about the axes of the fixed coordinate system xyz.

The difference between Euler and Tait-Bryan Angles is that Tait–Bryan angles represent rotations about three distinct axes (e.g. $x-y-z$, or $x-y'-z''$), while proper Euler angles use the same axis for both the first and third elemental rotations (e.g., $z-x-z$, or $z-x'-z''$).

Without considering the possibility of using two different conventions for the definition of the rotation axes (intrinsic or extrinsic),

there exist twelve possible sequences of rotation axes, divided in two groups:

- Euler angles (z-x-z, x-y-x, y-z-y, z-y-z, x-z-x, y-x-y)
- Tait–Bryan angles (x-y-z, y-z-x, z-x-y, x-z-y, z-y-x, y-x-z).

For example, the Figure 65 is a three-dimensional rotation using Euler intrinsic angles. The three rotations are compound in the following way:

- Rotation about z of α
- The new x is N and it is the intersection between xy and XY planes;
- Rotation about N of β;
- Rotation about Z of γ;

The rotational matrix can be written as follow (intrinsic):

$$\mathbf{T} = \mathbf{R}_{\gamma}^{\mathbf{z}''}\mathbf{R}_{\beta}^{\mathbf{x}'}\mathbf{R}_{\alpha}^{\mathbf{z}} \tag{A.23}$$

It is important to note that in the Euler Angle rotation the same axis for both first and third elemental rotation is used $\mathrm{z}'' - \mathrm{x}' - \mathrm{z}$;

Instead, Tait-Bryan angles descript a rotation about three distinct axes $\mathrm{x} - \mathrm{y} - \mathrm{z}$; Figure 66

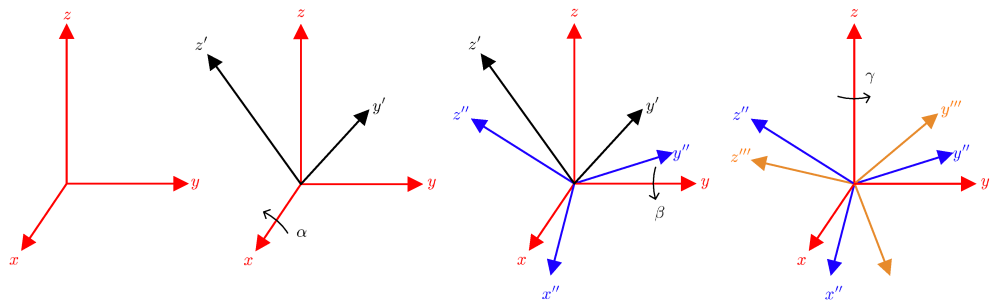

Figure 66 – Extrinsic Tait-Bryan rotations

In this example the transformation is extrinsic because it is about the initial axes, with the following scheme:

- Rotation about x of α;
- Rotation about y of β;
- Rotation about z of γ;

$$\mathbf{T_r} = \mathbf{R^z_\gamma R^y_\beta R^x_\alpha} = \begin{bmatrix} \mathrm{c_\gamma c_\beta} & -\mathrm{s_\gamma c_\alpha} + \mathrm{c_\gamma s_\beta s_\alpha} & \mathrm{s_\gamma s_\alpha} + \mathrm{c_\gamma s_\beta c_\alpha} \\ \mathrm{s_\gamma c_\beta} & \mathrm{c_\gamma c_\alpha} + \mathrm{s_\gamma s_\beta s_\alpha} & -\mathrm{c_\gamma s_\alpha} + \mathrm{s_\gamma s_\beta c_\alpha} \\ -\mathrm{s_\beta} & \mathrm{c_\beta s_\alpha} & \mathrm{c_\beta c_\alpha} \end{bmatrix} \tag{A.24}$$

In which:

- $\mathrm{c_a} = \cos a$
- $s_\mathrm{a} = \sin a$

Using the formula reported in the equation (A.24) or similar one's, no error is performed [67]. In general, in order to perform a complete non-linear structural analysis an incremental approach is used, so, in this case it is possible to approximate the rotational matrix as follow:

$$\mathbf{T_r} = \begin{bmatrix} 1 - \dfrac{(\beta^2 + \gamma^2)}{2} & -\gamma + \dfrac{\beta\alpha}{2} & \beta + \dfrac{\alpha\gamma}{2} \\ \gamma + \dfrac{\alpha\beta}{2} & 1 - \dfrac{(\alpha^2 + \gamma^2)}{2} & -\alpha + \dfrac{\beta\gamma}{2} \\ -\beta + \dfrac{\alpha\gamma}{2} & \alpha + \dfrac{\beta\gamma}{2} & 1 - \dfrac{(\alpha^2 + \beta^2)}{2} \end{bmatrix} \tag{A.25}$$

This is a second order approximation of the matrix (A.24) [65].

The variation on the matrix $\delta\mathbf{T_r}$ is obtained as follow:

$$\frac{\delta\mathbf{T_r}}{\delta\alpha} = \begin{bmatrix} 0 & \dfrac{\beta}{2} & \dfrac{\gamma}{2} \\ \dfrac{\beta}{2} & -\alpha & -1 \\ \dfrac{\gamma}{2} & 1 & -\alpha \end{bmatrix} \quad \frac{\delta\mathbf{T_r}}{\delta\beta} = \begin{bmatrix} -\beta & \dfrac{\alpha}{2} & 1 \\ \dfrac{\alpha}{2} & 0 & \dfrac{\gamma}{2} \\ -1 & \dfrac{\gamma}{2} & -\beta \end{bmatrix} \quad \frac{\delta\mathbf{T_r}}{\delta\gamma} = \begin{bmatrix} -\gamma & -1 & \dfrac{\alpha}{2} \\ 1 & -\gamma & \dfrac{\beta}{2} \\ \dfrac{\alpha}{2} & \dfrac{\beta}{2} & 0 \end{bmatrix} \tag{5.26}$$

The second variation of $d$the matrix $\mathbf{T_r}$ is equal to:

$$\frac{\delta \mathbf{T}_\mathbf{r}^2}{\delta\alpha^2} = \begin{bmatrix} 0 & 0 & 0 \\ 0 & -1 & 0 \\ 0 & 0 & -1 \end{bmatrix} \quad \frac{\delta \mathbf{T}_\mathbf{r}^2}{\delta\beta\delta\alpha} = \begin{bmatrix} 0 & \frac{1}{2} & 0 \\ \frac{1}{2} & 0 & 0 \\ 0 & 0 & 0 \end{bmatrix} \quad \frac{\delta \mathbf{T}_\mathbf{r}^2}{\delta\gamma\delta\alpha} = \begin{bmatrix} 0 & 0 & \frac{1}{2} \\ 0 & 0 & 0 \\ \frac{1}{2} & 0 & 0 \end{bmatrix}$$

$$\frac{\delta \mathbf{T}_\mathbf{r}}{\delta\alpha\delta\beta} = \begin{bmatrix} 0 & \frac{1}{2} & 0 \\ \frac{1}{2} & 0 & 0 \\ 0 & 0 & 0 \end{bmatrix} \quad \frac{\delta \mathbf{T}_\mathbf{r}^2}{\delta\beta^2} = \begin{bmatrix} -1 & 0 & 0 \\ 0 & 0 & 0 \\ 0 & 0 & -1 \end{bmatrix} \quad \frac{\delta \mathbf{T}_\mathbf{r}^2}{\delta\gamma\delta\beta} = \begin{bmatrix} 0 & 0 & 0 \\ 0 & 0 & \frac{1}{2} \\ 0 & \frac{1}{2} & 0 \end{bmatrix} \tag{A.27}$$

$$\frac{\delta \mathbf{T}_\mathbf{r}^2}{\delta\alpha\delta\gamma} = \begin{bmatrix} 0 & 0 & \frac{1}{2} \\ 0 & 0 & 0 \\ \frac{1}{2} & 0 & 0 \end{bmatrix} \quad \frac{\delta \mathbf{T}_\mathbf{r}^2}{\delta\beta\delta\gamma} = \begin{bmatrix} 0 & 0 & 0 \\ 0 & 0 & \frac{1}{2} \\ 0 & \frac{1}{2} & 0 \end{bmatrix} \quad \frac{\delta \mathbf{T}_\mathbf{r}^2}{\delta\gamma^2} = \begin{bmatrix} -1 & 0 & 0 \\ 0 & -1 & 0 \\ 0 & 0 & 0 \end{bmatrix}$$

The same matrices can be easily calculated in relation to the Tiat – Brian transformation (A.24). In this thesis, the *Approach 2* (descripted in the Chapter 3) used to define the interface kinematic, is formulated using the extrinsic Tait-Bryan rotations or the approximated transformation matrix.

6 Bibliography

[1] H. Hilsdorf, «Investigation into the failure mechanism of brick masonry loaded in axial compression.,» 1969.

[2] P. Lourenco, J. Rots e J. Blaauwendraad, «Continuum model for masonry: parameter estimation and validation.,» *J. Struct. Eng.,* vol. 124, pp. 642-652, 1998.

[3] P. Asteris, M. Chronopoulos, C. Chrysostomou, H. Varum, V. Plevrisa, N. Kyriakidesc e S. V., «Seismic vulnerability assessment of historical masonry structural systems,» *Engineering Structures,* vol. 62–63, pp. 118-134, 2014.

[4] E. Minga, L. Macorini, B. A. Izzuddin e I. Calio', Numerical Modeling of Masonry and Historical Structures, Woodhead Publishing 263-294, 2019.

[5] M. Betti e A. Vignoli, «Numerical assessment of the static and seismic behaviour of the basilca of Santa Maria all'Impruneta (Italy),» *Contr. Build. Mater.,* vol. 25, pp. 4308-4324, 2011.

[6] M. Betti e A. Vignoli, «Assessment of seismic resistance of a basilica-type church under earthquake loading: modelling and analysis.,» *Adv. Eng. Soft.,* vol. 39, pp. 258-283, 2008.

[7] E. Mele, A. De Luca e A. Giordano, «Modelling and analysis of a basilica under earthquake loading,» *Journal of Cultural Heritage,* vol. Vol. 4, n. Issue 4, pp. 355-367, 2003.

[8] A. Araujo, P. Lourenco, D. Oliveira e J. Leite, «Seismic assessment of St James Church by means of push over analysis - before and after New Zeland earthquake.,» *Open Civil Eng. J.,* vol. 6, n. 160-172, 2012.

[9] P. Lourenco, A. Nuno Mendes e L. Ramos, «Seismic performance of the St. George of the Latins church: lessons learned from studying masonry ruins.,» *Eng. Struct.,* vol. 40, pp. 501-518, 2012.

[10] G. Barbieri, L. Biolzi, M. Bocciarelli, L. Fragonese e A. Frigeri, «Assessing the seismic vulnerability of a historical building,» *Eng. Struct.,* vol. 57, pp. 523-535, 2013.

[11] G. Milani e M. Valente, «Comparative pushover and limit analysis on seven masonry churches damaged by the 2012 Emilia-Romagna (Italy) seismic events: possibilities of non linear finite elements compared with pre-assigned

failure mechanisms.,» *Engineering Failure Analysis,* vol. 47, pp. 129-161, 2014.

[12] H. Lotfi e P. Shing, «Interface Model Applied to Fracture of Masonry Structures,» *Journal of the Structural Engineering Division, American Society of Civil Engineers, New York,* vol. 120, n. 1, 1994.

[13] A. Anthonie, «Homogenisation of periodic masonry: plane stress, generalised plane strain or 3D modelling?,» *Commun. Numer. Methods Eng.,* vol. 13, pp. 319-326, 1997.

[14] L. Gambarotta e S. Lagomarsino, «Damage models for the seismic response of brick masonry shear walls. Part II: the continuum model and its applications,» *Earthq. Eng. Struct. Dyn.,* vol. 26, pp. 441-462, 1997.

[15] P. B. Lourenco e J. G. Rots, «Continuum model for masonry:parameter estimation and validation,» *J. Struct. Eng.,* vol. 124, n. (6), pp. 642-652, 1998.

[16] L. Berto, A. Saetta, R. Scotta e R. Vitaliani, «Orthotropic damage model for masonry structures.,» *Int. J. Numer. Methods Eng.,* vol. 55, pp. 127-157, 2002.

[17] L. Macorini e B. Izzuddin, «A non-linear interface element for 3D mesoscale analysis of brick-masonry structures,» *International Journal for Numerical Methods in Engineering,* vol. 85, n. 12, pp. 1584-1608, 2011.

[18] C. Chisari, L. Macorini, C. Amadio e B. Izzuddin, «Identification of mesoscale model parameters for brickmasonry,» *International Journal of Solids and Structures,* vol. 146, pp. 224-240, 2018.

[19] G. Brenchich, L. Gambarotta e S. Lagomarsino, «A macro-element approach to the three-dimensional seismic analysis of masonry buildings.,» in *Proceedings of 11th European Conference of Earthquake Engineering*, Balkema,Paris,Rotterdam, 602.

[20] G. Megenes e A. Della Fontana, «Simplified nonlinear seismic analysis of masonry buildings.,» *Br. Mason Soc. Proc.,* vol. 8, pp. 190-195, 1998.

[21] A. Kappos, G. Penelis e C. Drakopoulos, «Evaluation of simplified models for lateral load analysis of unreiforced masonry buildings,» *J. Struct. Eng. ,* vol. 128, pp. 890-897, 2002.

[22] I. Caliò, M. Marletta e B. Pantò, «A semplified model for the evaluation of the seismic behaviour of masonry buildings.,» in *Topping, B.H.V. (Ed.) Proceeding of the Tenth International Conference on Civil, Structural and*

Environment Engineering Computing, Civil-Comp Press, Stirlingshire, 195, 2005.

[23] S. Chen, F. Moon e T. Yi, «A macroelement for the nonlinear analysis of in-plane unreinforced masonry piers.,» *Eng. Struct.,* vol. 30, n. 8, pp. 2242-2252, 2008.

[24] R. Marques e P. Lourenco, «Possibilities and comparison of structural component model for the seismic assessment of modern unreinforced masonry buildings,» *Computer and Structures,* vol. 89, pp. 2079-2091, 2011.

[25] S. Lagomarsino, S. Penna, A. Galasco e S. Cattari, «TREMURI program: an equivalent frame model for the nonlinear seismic analysis of masonry buildings.,» *Eng. Struct.,* vol. 56, pp. 1787-1799, 2013.

[26] E. Raka, E. Spacone, V. Sepe e G. Camata, «Advanced frame element for seismic analysis of masonry structures: model formulation and validation,» *Earthquake engineering structural dynamics,* vol. 44, n. 14, pp. 2489-2506, 2015.

[27] S. Casolo e F. Peña, «Rigid Element model for in-plane dynamics of masonry walls considering hysteretic behaviour and damage.,» *Earthq. Eng. Struct. Dyn.,* vol. 36, pp. 1029-1048, 2007.

[28] S. Casolo e C. Sanjust, «Seismic analysis and strengthening design of a masonry monument by a rigid body spring model: the "Maniace Castle" of Syracuse,» *Eng. Struct.,* vol. 31, pp. 1447-1459, 2009.

[29] M. Valente e G. Milani, «Non-linear dynamic and static analyses on eight historical masonry towers in the North-East of Italy,» *Engineering Structures,* vol. 114, pp. 241-270, 2016.

[30] I. Caliò, M. Marletta e B. Pantò, «A new discrete element model for the evaluation of the seismic behaviour of unreinforced masonry buildings,» *Engineering Structures,* n. 40, pp. 327-338, 2012a.

[31] I. Caliò, M. Marletta e B. Pantò, «Un semplice macro-elemento per la valutazione della vulnerabilità sismica di edifici in muratura,» 2004.

[32] B. Pantò, E. Raka, F. Cannizzaro, G. Camata, S. Caddemi e E. Spacone, «Numerical macro-modeling of unreinforced masonry structures: a critical appraisal,,» in *Proceedings of the Fifteenth International Conference on Civil, Structural and Environmental Engineering Computing, eds B. H. V. Topping and P. Iványi (Stirlingshire: Civil-Comp Press).*, 2015.

[33] I. Caliò, F. Cannizzaro, E. D'Amore, M. Marletta, B. Pantò, A. Santini e N. Moraci, «A new discrete-element approach for the assessment of the seismic resistance of composite reinforced concrete-masonry buildings,» 2008.

[34] S. Caddemi, I. Caliò, F. Cannizzaro e B. Pantò, «A new computational strategy for the seismic assessment of infilled frame structures,» 2013.

[35] I. Caliò e B. Pantò, «A macro-element modeling approach of infilled frame structures.,» *Comput.Struct.,* vol. 143, pp. 91-107, 2014.

[36] R. Marques e P. Lourenco, «Unreinforced and confined masonry buildings in seismic regions:validation of macro-element models and cost analysis.,» *Eng.Struct.,* vol. 64, pp. 52-67, 2014.

[37] B. Pantò, L. Giresini, M. Sassu e I. Caliò, «Non-Linear modeling of masonry churches throught a discrete macro-element approach,» *Earthquake and Structures,* vol. 12, n. (2), pp. 223-236, 2017.

[38] B. Pantò, The Seismic Modeling of Masonry Structure, An Innovative Macro-Element Approach, PhD Thesis in Structural Engineering, in Italian. Catania: University of Catania, 2007.

[39] S. Caddemi, I. Caliò, F. Cannizzaro e B. Pantò, «The Seismic Assessment of Historical Masonry Structures,» 2014.

[40] I. Caliò, F. Cannizzaro e M. Marletta, «A discrete element for modeling masonry vaults.,» *Adv. Meter. Res.,* pp. 133-134, 447.452, 2010.

[41] F. Cannizzaro, Artist, *The seismic behaviour of Historical Buildings: A Macro-Element Approach.* [Art]. Phd Thesis Structural Engineering. University of Catania (in Italian), 2010.

[42] S. Caddemi, I. Caliò, F. Cannizzaro, G. Occhipinti e B. Pantò, «A parsimonious discrete model for the seismic assessment of monumental structures.,» Stirlingshire, 2015.

[43] F. Cannizzaro, B. Pantò, S. Caddemi e I. Caliò, «A Discrete Macro-Element Method (DMEM) for the nonlinear structural assessment of masonry arches,» *Eng. Struct. ,* vol. 168, pp. 243-256, 2018.

[44] S. A. Pietruszczak e R. P. Ushaksaraei, «Description of inelastic behaviour of structural masonry VL,» Vol. %1 di %24003 EP - 4019 T1, n. 10.1016/S0020-7683(03)00174-4 JO, 2003.

[45] G. Milani, M. Pizzolato e A. Tralli, «Simple numerical model with second order effects for out-of-plane loaded masonry walls,» *Engineering Structures,* n. 48, pp. 98-120, 2013.

[46] P. Cundall, «A computer model for simulating progressive large scale movements in blocky rock systems.,» *Proc. Symp. Rock Fracture (ISRM), Nancy.,* 1971.

[47] D. Mamolo, M. DeJong e A. Penna, «Distinct Element modelling of the in-plane failure mechanisms of URM walls,» Milan, Italy, 2018.

[48] 3DEC, «3DEC: 3-Dimensional Distinct Element Code, Theory and Background. Itasca Consulting Group, Minneapolis, Minnesota. Inc.». 1998.

[49] C. Papantonopoulos, I. Psycharis, D. Papastamatiou, J. Lemos e H. Mouzakis, «Numerical prediction of the earthquake response of classical columns using the distinct element method,» *Earthquake Engineering & Structural Dynamics,* vol. 31, p. 1699–1717, 2002.

[50] M. DeJong e C. Vibert, «Seismic response of stone masonry spires,» *Computational and experimental modeling, Engineering Structures,* vol. 40, p. 566–574, 2012.

[51] E. Çaktı, Ö. Saygılı, J. Lemos e C. Oliveira, «Discrete element modeling of a scaled masonry structure and its validation,» *Engineering Structures,* vol. 126, p. 224–236, 2016.

[52] T. Kawai, «New discrete models and their application to seismic response analysis of structures,» *Nuclear Engineering and Design,* vol. 48, p. 207–229, 1978.

[53] S. Casolo e G. Uva, «Nonlinear analysis of out-of-plane masonry façades: full dynamic versus pushover methods by rigid body and spring model: FULL DYNAMIC AND PUSHOVER ANALYSIS OF OUT-OF-PLANE MASONRY,» *Earthquake Engineering & Structural Dynamics,* vol. 42, p. 499–521, 2013.

[54] K. Meguro e H. Tagel-Din, «Applied Element Method Used for Large Displacement Structural Analysis,» *Journal of Natural Disaster Science,* vol. 24, pp. 25-34, 2002.

[55] C. Casapulla e D. D'Ayala, «Lower bound approach to the limit analysis of 3D vaulted block masonry structures.,» in *Computer methods in Structural Masonry*, Swansea, 2001.

[56] G. Milani, «3D upper bound limit analysis of multi-leaf masonry walls, International Journal of Mechanical Sciences. 50 (2008),» *International Journal of Mechanical Sciences,* vol. 50, p. 817–836, 2008.

[57] V. Turnsek e F. Cacovic, «Some Experimental Results on the Strength of Brick Masonry Walls,» 1971.

[58] I. Caliò, F. Cannizzaro, M. Marletta e B. Pantò, «A 3D Computer Program for the Seismic Assessment of Masonry Buildings Catania, Italy,» *Gruppo Sismica S.R.L.,* 2012b.

[59] B. Pantò, F. Cannizzaro, I. Caliò e L. P.B., «Numerical and Experimental Validation of a 3D Macro-Model for the In-Plane and Out-Of-Plane Behavior of Unreinforced Masonry Walls,» *International Journal of Architectural Heritage,* vol. 11, p. 946–964, 2017.

[60] B. Pantò, I. Caliò e P. Lourenco, «A 3D discrete macro-element for modelling the out-of-plane behaviour of infilled frame structures.,» *Engineering Structures,* vol. 175, pp. 371-385, 2018.

[61] C. Chácara, F. Cannizzaro, B. Pantò, I. Caliò e P. Lourenço, «Assessment of the dynamic response of unreinforced masonry structures using a macroelement modeling approach,» *Earthquake Engng Struct Dyn.,* 2018.

[62] S. Caddemi, I. Caliò, F. Cannizzaro e B. Pantò, «New Frontiers on Seismic Modeling of Masonry Structures,» *Frontiers in Built Environment,* vol. 3, 2017.

[63] J. Battini, Artist, *Co-rotational beam elements in instability problems.* [Art]. Phd Thesis, 2002.

[64] T.-N. Le, J. Battini e M. Hjiaj, «A consistent 3D corotational beam element for nonlinear dynamic analysis of flexible structures,» vol. 269, n. 538-565, 2014.

[65] B. Izzuddin, Artist, *Nonlinear dynamic analysis of framed structures.* [Art]. Phd Thesis, 1991.

[66] B. Izzuddin e A. Elnashai, «Eulerian formularion for Large-Displacement Analysis of Space Frames,» vol. 119, 1993.

[67] B. Izzuddin, «Conceptual issues in geometrically nonlinear analysus of 3D framed structures,» vol. 191, 2001.

[68] B. Izzuddin, «An enhanced co-rotational approach for large displacement analysis of plates,» vol. 64, 2005.

[69] M. Crisfield, Advanced Topics, Volume 2, Non-Linear Finite Element Analysis of Solids and Structures, Volume 2 edition a cura di, Wiley, 1997.

[70] C. Felippa e B. Haugen, «Unified Formulation of Small-Strain Corotational Finite Elements: I. Theory,» 2005.

[71] B. Izzuddin, Artist, *Software ADAPTIC.* [Art]. Imperial College of London.

[72] A. Ibrahimbegovic, «On the choice of finite rotation parameters.,» vol. 149, n. 49-71, 1997.

[73] C. Pacoste, «Co-rotational flat facet triangular elements for shell instability analysis.,» vol. 156, n. 75-110, 1998.

[74] C. Pacoste e A. Eriksson, «Element behaviour in post-critical plane frame analysis,» vol. 319–343, n. 125, 1995.

[75] C. Pacoste e A. Eriksson, «Element formulation and numerical techniques for stability problems in shells,» *Comput. Methods Appl. Mech. Engrg.,* vol. 191, n. 35, pp. 3775-3810, 2002.

[76] C. Oran, «Tangent Stiffness in Plane Frames,» *Journal of Structural Division,* vol. 99, pp. 1350-1374, 1973.

[77] S. Timoshenko e J. Gere, Theory of elastic stability, New York: McGraw-Hill, 1961.

[78] B. Štok e M. Halilovič, «Analytical solutions in elasto-plastic bending of beams with rectangular cross section,» *Applied Mathematical Modelling,* vol. 33, pp. 1749-1760, 2009.

[79] Italian Code:NTC 2018, Artist, *Norme tecniche per le costruzioni 2018 (NTC 2018),https://www.gazzettaufficiale.it/eli/gu/2018/02/20/42/so/8/sg/pdf..* [Art]. 2018.

[80] C. Sandoval, P. Roca, E. Bernat e L. Gil, «Testing and numerical modelling of buckling failure of masonry walls,» *Construction and Building Materials,* vol. 25, p. 4394–4402, 2011.

[81] C. Ng, Artist, *Experimental and Theorethical Investigation of the beaviour of Brickwork cladding panel subjected to lateral loadings.* [Art]. Phd. Thesis, University of Edinburgh, 1996.

[82] J. Simo e D. Fox, «On a stress resultant geometrically exact shell model. Part I: Formulation and optimal parametrization,» *Computer Methods in Applied Mechanics and Engineering,* vol. 72, p. 267–304, 1989.

[83] A. B. Izzudin , A. G. Vlassis e A. Y. Elghazouli, «Progressive collapse of multi-storey buildings due to sudden column loss — Part I: Simplified assessment framework,» *Engineering Structures,* vol. 30, pp. 1308-1318, 2008.

[84] B. A. Izzudin, A. G. Vlassis e A. Y. Elghazouli, «"Progressive collapse of multi-storey buildings due to sudden column loss—Part II: Application,» *Engineering Structures,* vol. 30, p. 1424–1438, 2008.

[85] K. Khandelwal e S. El-Tawil, «Pushdown resistance as a measure of robustness in progressive collapse analysis,» *Engineering Structures ,* vol. 33 , p. 2653–2661, 2011.

[86] B. A. Izzuddin, ADAPTIC User Manual, Department o Civil and Environmental Engineering, Revision Jannuary 2012.